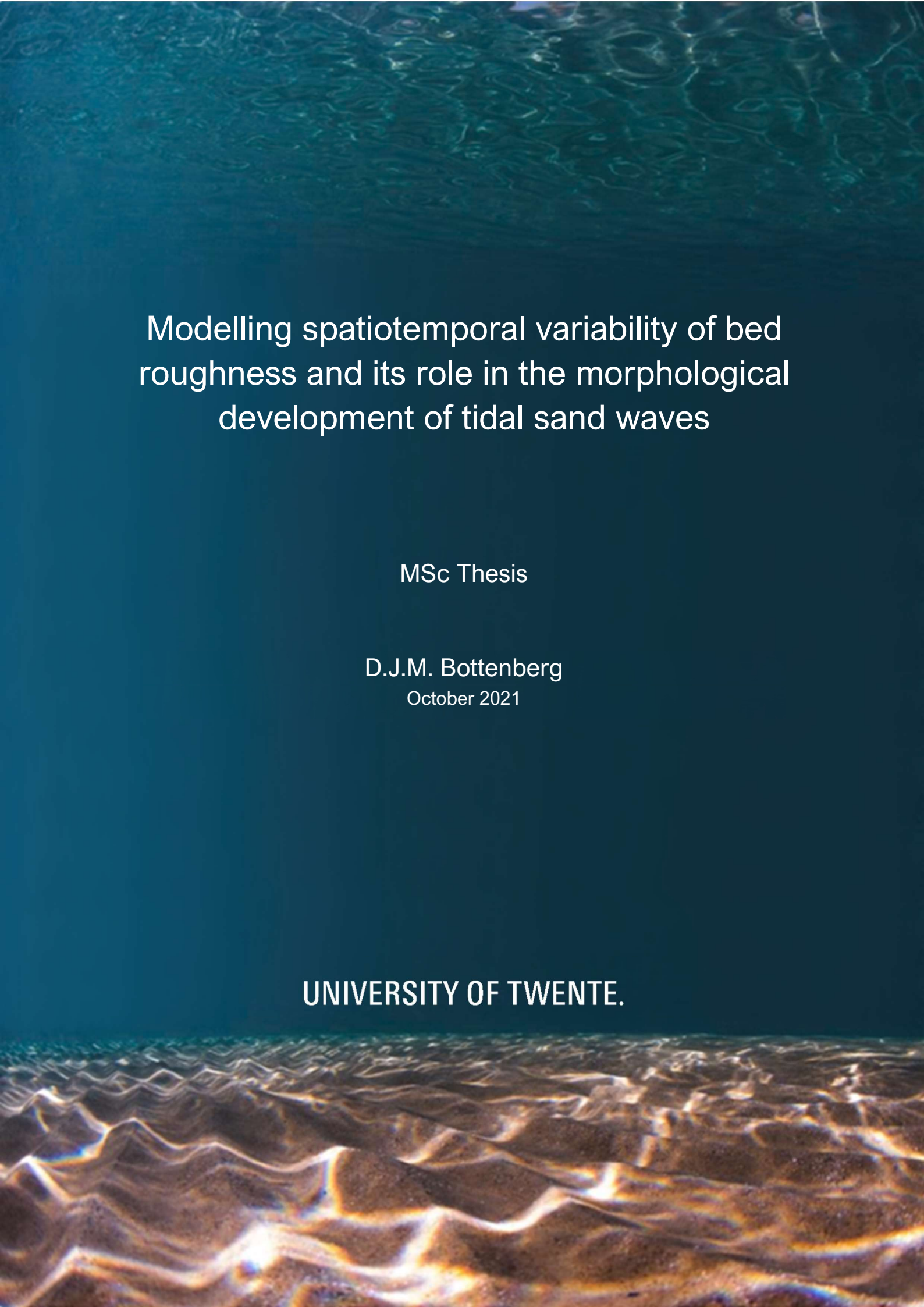

Modelling spatiotemporal variability of bed roughness and its role in the morphological development of tidal sand waves

MSc Thesis

D.J.M. Bottenberg

October 2021

UNIVERSITY OF TWENTE.

Modelling spatiotemporal variability of bed roughness and its role in the morphological development of tidal sand waves

A Master thesis

By
D.J.M. Bottenberg (Dennis)

To obtain
the degree of Master of Science
in Civil Engineering and Management
Specializing in River and Coastal Engineering

At

UNIVERSITY OF TWENTE.
Faculty of Engineering Technology

Graduation Committee

Head of committee:	Dr. Ir. B.W. Borsje
Daily supervisor:	Dr. Ir. J.H. Damveld

Preface

This thesis marks the end of my master programme Civil Engineering and Management at the Water Engineering and Management department of University of Twente. The previous months have consisted of working on modelling the effects of bed roughness on tidal sand waves. Despite some hurdles on the way, I enjoyed the process and gained a lot of new knowledge regarding processes controlling sand wave behavior and specifically bed roughness.

I would like to thank the members of my graduation committee for their supervision and support during this research. First of all, I want to thank my daily supervisor Johan Damveld for always making time to give me valuable feedback, your motivational words guided me in the right direction and made this thesis a success. Additionally, I would like to thank Bas Borsje for his critical view on increasing the academic level of this research.

Finally, I want to thank my family and friends who provided me with good times during my life as a student and supported me on this thesis.

I hope you enjoy reading my thesis.

Dennis Bottenberg
September 9, 2021

Summary

The sandy seabed of many coastal seas consists of a variety of rhythmic bed patterns. Among the largest are sand waves with dimensions that cover a significant portion of the water depth and have considerable migration rates. Coastal seas are generally busy areas to which sand waves could pose a serious threat. Morphological models can predict sand wave evolution and migration for many years in the future. To study the morphological behaviour of sand waves in tidal environments, process-based models are set-up. However, some physical processes, such as the bed roughness, remain simplified. It is often assumed uniform while observations show distinct variations in bed patterns over sand waves. Modelling these variations may lead to an increase in the accuracy of the process-based morphological models for long-term sand wave development.

This study uses the 3D process-based morphological model Delft3D in the 2DV mode. The roughness predictor VRIJN07 and sediment transport model TR2004 is used to estimate dynamic bed roughness based on hydrodynamic conditions and sediment properties. The reference case consists of a uniform Chézy coefficient of 75 $m^{0.5}s^{-1}$ (C75) combined with sediment transport model TR1993. The aim is to understand how spatiotemporal variable bed roughness influences the hydro-morphodynamic processes that govern sand wave development and improve long term simulation results of the reference case. To achieve this, firstly a flat bed is used to focus on the temporal variability in bed roughness and its effect on hydro-morphodynamics. Fastest growing mode (FGM) simulations have been performed that estimate the bedform wavelength with the largest growth rate of a given parameter setup. This wavelength is therefore most likely to emerge on the long term. Secondly, by using FGM simulations the initial topography is extended to a low-amplitude 0.5-meter sand wave to introduce spatial variation to the bed roughness estimates. Thirdly, the amplitude is increased to 1.5-meters and spatial variability of bed roughness is forced by linearly interpolating a Chézy coefficient of 50 $m^{0.5}s^{-1}$ at the sand wave crest and 80 $m^{0.5}s^{-1}$ at the trough (Cspatial). Finally, long term simulations have been conducted for C75/TR1993, Cspatial/TR1993 and VRIJN07/TR2004.

The results show that the bed roughness has a large influence on the strength of circulation cells, caused by decreasing flow velocities as flow passes over the sand wave. Generally, this gives rise to faster growth rates but shorter preferred wavelengths. VRIJN07 estimates larger bed roughness than C75 which is mainly caused by the contribution of megaripple roughness height and is highly dynamic temporally. This leads to VRIJN07 having larger sand wave growth rates than C75. However, the transport model greatly influences the sediment transport rates. TR1993 has transport rates several times larger than TR2004, meaning TR1993 combinations lead to fast growing short wavelength sand waves while TR2004 leads to very slow growth for large wavelengths. Furthermore, VRIJN07 estimates negligible spatial variation due to a mechanism limiting the maximum attainable megaripple roughness height being reached at all parts of the sand wave. This means that VRIJN07 is only temporally variable which limits the sand wave growth rate more by effectively reducing bed shear stress and sediment transport rates. Spatially averaged, Cspatial is rougher than C75 but smoother than VRIJN07. Linear interpolation of bed roughness causes local areas with increased erosion at the crest, while decreasing it at the trough. Long term, this limits the equilibrium height of sand waves to 6.2 meters. Compared to C75/TR1993 with 8.8 meters, this is a large improvement towards the average sand wave height in the North Sea that is between 2 meters for the smallest and >7 meters for the largest sand waves observed by Damen et al. (2018). VRIJN07/TR2004 severely overestimates these averages with approximately 13 meters and requires severely longer computation time.

C75/TR1993 has proven itself to give simulation results with reasonable agreement to field observations by parameterizing complex near-bed processes. Using a constant Chézy coefficient also

eliminates complex and elaborate feedback mechanisms, reducing uncertainty in the simulation results. Using VRIJN07/TR2004 for (spatio)temporal bed roughness modelling with the presented setup is not recommended. However, calibration could improve the results and increase the accuracy towards simulation results that match field conditions. Cspatial/TR1993 was introduced to force spatial variation in bed roughness and it provided a significant improvement of modelling equilibrium sand wave heights under North Sea conditions. This implies that bed roughness might have a larger influence on tidal sand waves than previously presumed. Also, modelling spatial variation rather than temporal variation has the effect on improving simulation results.

Further research should focus on extending the model with an asymmetrical tide and wind-currents and -waves, VRIJN07 might translate these hydrodynamic processes to more accurate bed roughness which C75 and Cspatial are unable to do. Also, grain sorting and the influence of bio-organisms directly influence the bed roughness leading to spatial variability. Since modelling spatial variation in bed roughness was successful in increasing the accuracy, these processes could have a large effect.

Content

1 Introduction

The sandy seabed of many coastal seas consists of a variety of rhythmic bed patterns with different spatial and temporal scales. The largest bedforms are tidal sand banks typically having wavelengths in the order of 5-10 km and reaching heights up to 30 m, which is more than half of the local water depth (Hulscher, 1996). On a smaller scale, typical sand wave wavelengths range from 100 m up to 1 km and have heights up to 10 m, i.e., a considerable portion of the local water depth (Besio et al., 2004). Also, sand waves can migrate with a rate of up to 10 m per year (Terwindt, 1971). Subsequently, mega ripples with wavelengths of 10 m and wave heights up to 0.4 m have been observed in the North Sea by Van Dijk & Kleinhans (2005). The smallest scale bed form consists of ripples with wavelengths ranging from 0.1 m up to 1 m and heights up to 0.1 m (Dodd et al., 2003). These bed forms have been found to commonly coexist with one another, sand waves may be superimposed on sand banks and the surface of sand waves may be covered with (mega) ripples (Roos, 2019). An overview of the bed forms and their characteristic spatial and temporal scales is given in table 1.

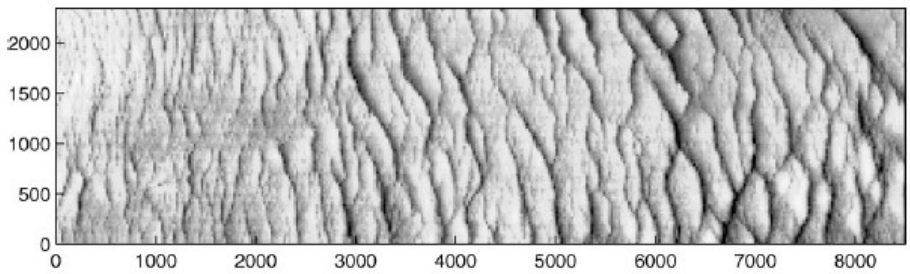

Figure 1. Bathymetry measurements in the North Sea, with horizontal coordinates specified in metres and a colorbar denoting the seabed level below mean sea level (in metres). (Németh et al., 2002)

Table 1. Characteristics of offshore sand bed forms. (Dodd et al., 2003; Besio et al., 2004; Hulscher, 1996; Terwindt, 1971; Van Dijk & Kleinhans, 2005)

Bed form	Wavelength (m)	Height (m)	Timescale	Migration rate
Sand banks	5,000-10.000	~30	Centuries	~1 m/year
Sand waves	100-1.000	~10	Years	~10 m/year
Mega ripples	1-10	~0,4	Days	~100 m/year
Ripples	0,1-1	~0,1	Hours	~1 m/day

Coastal seas in which these bed forms are found are generally busy areas for offshore industry and navigation channels for shipping. An example of such a sea is the North Sea, which is one of the most intensively used coastal seas in the world and is expected to become even busier in the next decades (Rijksoverheid, 2015). The port of Rotterdam is among the largest in the world, and its growth causes the navigation channels to become more crowded. Furthermore, climate concerns have led to an aim of reducing CO2-emissions in the Netherlands with 49% by 2030 as compared to 1990 in the Paris climate agreement. An energy transition is necessary to achieve this, so among other sustainable forms of energy, offshore wind farms are being constructed. Starting 2015, the Dutch government plans to increase the wind energy collected at sea by eleven times by 2030 (Rijksoverheid, 2019). This increase will require a major expansion of the already 3.300km vast subsea cable network. Sustainable design and maintenance of these activities and structures is crucial to keep up with these advancements.

In order to do so, insight in the seabed morphodynamics is essential as bed forms are dynamic bed features and could pose threats for these offshore activities due to their dimensions and migration rates. Although sand banks are the largest scale bed features, they are not the biggest threat due to their low migration rate and can be considered nearly static. Similar to mega(ripples), these small-scale bed forms do not pose a threat as their heights are generally neglectable as compared to the local water depth. Sand waves, however, cover a significant portion of the local water depth, and also have considerable migration rates and could therefore have the largest impact on offshore activities and structures. So far, threats have been solved by avoidance; avoid sand wave fields if possible, otherwise bury the objects deep enough to prevent exposure, or instant repairs by rock dumping. However, these solutions are expensive and regular surveys are required to evaluate possible problems before the implementation and detect any danger afterwards (Besio et al., 2008). This approach is unsustainable when also considering the expansion of the offshore wind farms in the coming decades due to the wind energy goals by 2030 (Rijksoverheid, 2019).

A sustainable approach would involve using morphological models to predict sand wave evolution and migration for many years in the future. Throughout the years, research has been conducted where the morphological behaviour of sand waves is studied to develop such models and increase the accuracy of their estimates. Sand waves were investigated by Fredsøe and Deigaard (1992), their approach was able to describe the form of sand waves. However, it was unable to explain the mechanism causing these bedforms and predict conditions which lead to their appearance. Hulscher (1996) was first to propose a fully three-dimensional model for studying the morphological behaviour of sand waves by using the three-dimensional shallow water equations. Later, this model has been extended in many respects: solution method, hydrodynamics (symmetric vs asymmetric forcing, turbulence model, wind waves), sediment transport (bed load vs suspended load, grain size sorting) and influence of benthic activity (see e.g., Roos (2019) and references therein). However, some physical processes within these models remain simplified. One of these potentially relevant processes is the seabed roughness, which is often assumed uniform while observations show distinct variations in bed patterns over sand waves (Damveld et al., 2018).

Modelling these variations may lead to an increase in the accuracy of the process-based morphological models for long-term sand wave development. Roughness predictors can be used to estimate the roughness of the bed based on hydrodynamic conditions and sediment properties. A dynamic roughness coefficient is thus obtained that potentially represents the actual roughness better than using a uniform value. However, application of these roughness predictors in tidal environments is scarce. Roughness predictors could therefore lead to better predictions of sand wave fields and help creating sustainable designs and maintenance of offshore structures and activities.

1.1 Knowledge gap

The behaviour of sand waves is often studied by applying process-based morphodynamical models to predict the long-term evolution of the seabed. However, various processes such as bed roughness are idealized or even totally neglected. It is well known that the small-scale topography of the seabed varies significantly in space and time, which inherently implies spatial and temporal variations in bed roughness. Although the general concept of bed roughness is researched quite well in literature, its potential effects on the processes governing sand waves is not fully researched. Predictors have been proposed to estimate bed roughness based on hydrodynamic and morphological conditions, but their application on sand waves is still absent in literature. Using roughness predictors may give a better understanding of the role of bed roughness in the development of sand waves and could potentially improve the accuracy of sand wave morphology simulations.

1.2 Research objective

The research is focussed at studying the effects of spatiotemporally varying bed roughness and therefore increasing the general understanding of its effect on physical processes governing sand wave morphodynamics. With this knowledge, the main research objective is to improve the process-based model estimates of sand wave dynamics by including spatiotemporal variations in bed roughness.

1.2.1 Main research question

"What is the effect of modelling spatiotemporal variations of bed roughness in process-based morphodynamic models, on sand wave morphology, and how do the results compare to field observations?"

1.2.2 Sub-questions

1) "What is the initial response of hydro-morphodynamic processes on a flat bed using constant bed roughness, a roughness predictor and different sediment transport models, and how sensitive are the results to changing parameters?"
    a) How does the roughness predictor perform compared to using uniform bed roughness?
    b) How does the sediment transport model affect the results?
    c) What parameters are the simulation results sensitive to?
2) "How does the bed roughness estimate of the roughness predictor vary, based on initial morphodynamic response over a low-amplitude wavy bed, and how do these spatial and temporal bed roughness variations affect hydrodynamics and morphodynamics?"
    a) How does the roughness predictor vary spatiotemporally?
    b) How does the sediment transport model affect the results?
    c) How does the spatiotemporally varying bed roughness affect hydrodynamics and morphodynamics compared to using uniform bed roughness?
3) "How does the roughness predictor perform against field-observation based bed roughness as an initial morphodynamic response over a large-amplitude wavy bed, and how do these spatial and temporal variations affect the morphodynamics of sand waves?"
    a) What bed roughness behaviour is commonly observed in the field?
    b) How do the morphological simulation results compare when using uniform bed roughness, a roughness predictor and field-observation based bed roughness?
    c) What is the difference in initial morphodynamic response between the low-amplitude and large-amplitude case?
4) "How does the roughness predictor perform against uniform and field-observation based bed roughness, in long term morphodynamic simulations, and what are the causes for any differences or similarities?"
    a) What is the long term morphodynamic result of using uniform bed roughness?
    b) What is the long term morphodynamic result of using field-observation based bed roughness?
    c) What is the long term morphodynamic result of using a roughness predictor?
    d) What is the cause of any differences between the morphological results of uniform bed roughness, a roughness predictor and field-observation based bed roughness?
    e) How do spatial and temporal variations in bed roughness affect the physical processes responsible for long term sand wave dynamics?

1.3 Research structure

This study uses the 3D process-based morphological model Delft3D in the 2DV mode. The roughness predictor VRIJN07 and sediment transport model TR2004 by Van Rijn (2007) is used to estimate dynamic bed roughness based on hydrodynamic conditions and sediment properties. The reference case of Van Gerwen et al. (2018) is used wherein a constant Chézy coefficient of 75 $m^{0.5}s^{-1}$ (C75) is used with sediment transport model TR1993 by Van Rijn (1993). The aim is to understand how spatiotemporally dynamic bed roughness influences the hydro-morphodynamic processes that govern sand wave development. To achieve this, firstly a flat bed is used to focus on the temporal variability in bed roughness and its effect on hydro-morphodynamics. Fastest growing mode (FGM) simulations have been performed to determine the initial wavelength. Secondly, by using FGM simulations the initial topography is extended to a low-amplitude 0.5-meter sand wave to introduce spatial variation to the bed roughness estimates. Thirdly, the amplitude is increased to 1.5-meters and spatial variability of bed roughness is forced by linearly interpolating a Chézy coefficient of 50 $m^{0.5}s^{-1}$ at the sand wave crest and 80 $m^{0.5}s^{-1}$ at the trough (Cspatial). Finally, long term simulations have been conducted for C75/TR1993, Cspatial/TR1993 and VRIJN07/TR2004. A schematic overview of the research structure is shown in figure 2 based on research question.

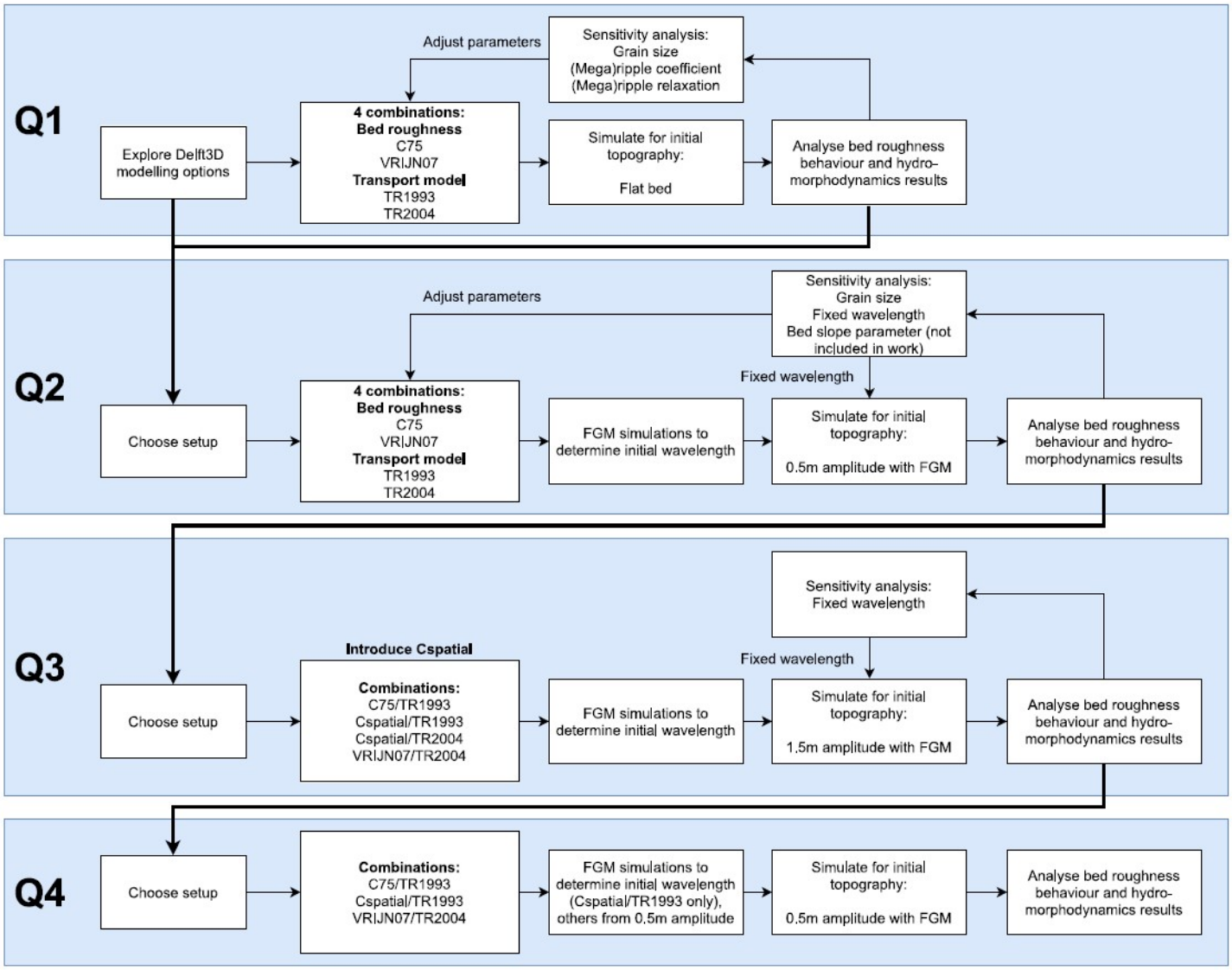

Figure 2. Schematic overview of the research structure of this thesis

2 Theoretical framework

Chapter 2 gives the theoretical framework behind processes in this thesis and consists of three parts. The first part (§2.1) describes the generic processes that are governing sand wave behaviour. The second part (§2.2) focusses on the theory behind bed roughness and its effects. The third part (§2.3) discusses modelling methods for sand waves and bed roughness that are currently often used and relevant to modelling methods in this work.

2.1 Processes governing sand waves

2.1.1 Hydrodynamics

Observational studies have shown that large-scale bedforms are commonly found in coastal seas where tidal processes dominate such as the North Sea (McCave, 1971; Terwindt, 1971; Van Dijk & Kleinhans, 2005). Hulscher (1996) studied the tide-topography interaction and found that the interaction of oscillatory tidal flow with a wavy bed gives rise to circulation cells as shown on figure 3. Within these circulation cells, steady streaming flow displaces sediment to the crest of the bottom perturbations if the flow is strong enough to overcome gravitational effects. This causes the perturbation to grow and is therefore regarded as the main growth mechanism of tidal sand waves.

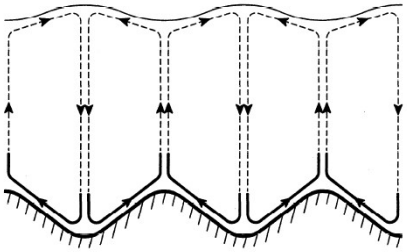

Figure 3. Strong near-bed circulation which supports the growth of bottom perturbations (Hulscher, 1996).

Oscillatory tidal currents are rarely symmetrical due to the presence of residual currents caused by multiple tidal constituents, pressure gradients or wind-driven currents. The presence of a residual current causes the circulation cells to no longer be symmetric with respect to the crests and troughs of the sand waves. This leads to sand wave asymmetry and migration in the direction of the residual current (Németh et al., 2002; Besio et al., 2004; Campmans et al., 2018a; Toodesh & Verhagen, 2018).

Furthermore, waves generate an orbital motion that extends down into the water column and are flattened to a more oscillatory motion near the bed. Waves may enhance migration induced by tidal asymmetry and wind-driven flow (Campmans et al., 2018b). However, waves strong enough to move sediment in deep water only occur during storms. Therefore, tidal currents are considered to be the dominant sediment moving process (Van Dijk and Kleinhans, 2005).

2.1.2 Sediment transport

Sediment transport processes are key in sand wave dynamics and occur when the waves and currents are sufficiently strong to erode sediment from the bottom. Subsequently, sediment transport and deposition then lead to morphological evolutions (Dodd et al., 2003). Sediment transport is a complex interplay of sediment properties and hydrodynamics. Grain size is the most important sediment

property and the interaction with hydrodynamics will determine the transport mode, which is found to have a large influence on sand wave development.

2.1.2.1 Grain size

The most influential sediment property is the grain size, even if there is significant wave and current action, sediment transport and the formation of sand waves will be limited if the dominant local grain size is coarse (Besio et al., 2003). Van der Veen et al. (2006) investigated grain size dependency and found that this phenomenon is caused by critical bed shear stress, which is the threshold for the initiation of motion. Both bed shear stress and critical bed shear stress increase of increasing grain sizes. However, the critical bed shear stress increases more rapidly than the bed shear stress, this implies a certain critical grain size which prevents sediment transport when exceeded. Model results of Van Santen et al. (2011) shows larger wavelengths when coarser sand is present. This trend is also found in the data analysis of field and flume data by Flemming (2000), the results show that the maximum potential bedform sizes are larger for coarse sediments than fine sediments.

Soil composition also influences the occurrence of sand waves, as sand waves only occur at locations where sand is the dominant bed material (Hulscher & van den Brink, 2001). Furthermore, the sediment size may not be uniformly distributed over sand waves. Simulation results of Damveld et al. (2020) show that typically, the crests of sand waves are coarser than the troughs. This is due to the difference in settling velocity between grain sizes causing larger grains to deposit on the upper lee slope, whilst smaller grains are found on the lower lee slope. Long term, the sorting processes will lead to longer wavelengths and lower wave heights.

2.1.2.2 Transport mode

Damen et al. (2018) showed that that the mode of sediment transport is a dominant factor in explaining sand wavelength, height, and asymmetry. Van Rijn (1984) defines three modes of particle motion: (1) Rolling and/or sliding motion; (2) saltation motion; and (3) suspended particle motion. Usually, rolling, sliding and saltating is defined as bed-load transport and suspended motion is suspended-load transport. The mode in which particles will move depends on the bed shear velocity and the critical value for initiation of motion (Van Rijn, 2007). When the value of the bed shear velocity just exceeds the critical value for initiation of motion, the particles will be rolling, sliding or both while remaining in continuous contact with the bed. For increasing values of the bed shear velocity, the particles will be moving along the bed by more or less regular jumps, which are called saltations. When the value of the bed-shear velocity exceeds the fall velocity of the particles, the sediment particles can be lifted to a level where upward turbulent forces exceed gravitational forces and as a result the particles may go in suspension. Due to the slower fall velocities and lower critical bed shear stress, finer sediment particles usually go into suspension while coarser sediment remains on the bed (Van Rijn, 2007).

The model by Tonnon et al. (2006) shows that sand waves tend to grow when bed-load transport is dominant and decay when suspended load is dominant. Borsje et al. (2014) found the effect of this mechanism in analysed field data, sand wave fields were only found when bed-load transport was the dominant mode. Suspended load transport was found to lead to the absence of sand waves which implies a dampening effect of suspended load transport. Furthermore, it was found that grain size in combination with suspended sediment transport has implications for the growth of sand waves. The study by Borsje et al. (2014) concluded that for relatively large grain sizes (the bed load regime) the preferred wavelength of the sand wave increased by including suspended load transport. However, for a relatively small grain size (the suspended load regime), the damping effect of suspended load transport in combination with slope-induced transport dominated over the growth mechanism due to bed load transport leading to a stable flat bed.

2.1.3 Seabed topography

The water column of oceans can be divided into three main layers where friction plays a different role: (1) the surface boundary layer, where wind induces friction forces on the ocean surface, (2) the generally frictionless ocean interior and (3) where bed roughness is relevant, the bottom boundary layer where friction between the flow and bottom dissipates energy from the ocean's interior (Salon et al., 2008). The presence of this frictional bottom boundary affects the near-bed hydrodynamics and sediment transport strongly through the vertical velocity profile and turbulent structures. The ocean layers are schematized in figure 4.

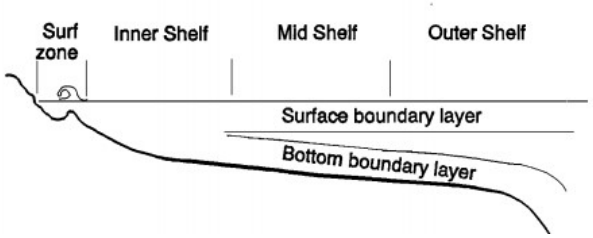

Figure 2. Spatial relationships of the major subregions of the continental shelf (Nittrouer & Wright, 1994)

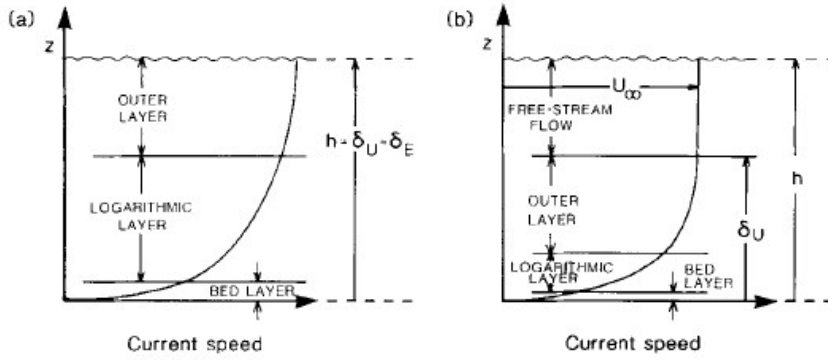

Figure 5. Components of the bottom boundary layer. (a) For a bottom boundary layer which extends over the entire water column; (b) for water which is deeper than the bottom boundary layer thickness. Layers are not to scale. (Soulsby, 1983)

The bottom boundary layer can be divided in three layers schematized in figure 5: the bed layer, logarithmic layer and outer layer. Above the outer layer, the flow does not feel the presence of the bottom boundary anymore but instead, the flow characteristics depends on its nature (e.g. tidal oscillation, earth's rotation, vertical density gradients and wind forcing). According to Soulsby (1983), it is often the case in shallow seas that the depth of water is less than the thickness which the boundary layer would otherwise attain. In this case, the vertical velocity profile and turbulent structure becomes more complex as surface boundary processes now coincide with bottom boundary processes.

2.2 Seabed roughness

Bed roughness is the physical property that describes the irregularity of a surface over which a fluid flows and the frictional effect that it exerts on the passing flow. This effect is confined within the bottom boundary layer and affects the near-bed vertical velocity profile and turbulent structures depending on the classification (§2.2.1). In case of an erodible bed consisting of sediments, the effective bed roughness consists of a sum of three components: grain roughness (§2.2.2), form roughness (§2.2.3) and transport roughness (Nikuradse, 1933; Grant & Madsen 1982; Li & Amos, 1998). Transport roughness occurs when the energy of the flow increases which transfers fluid momentum to particles (Houwman and Van Rijn, 1999). Although it is known that transport roughness affects the flow, the magnitude is still uncertain and therefore not considered further. Finally, the effects of bed roughness on the hydrodynamics and morphodynamics is discussed (§2.2.4).

2.2.1 Classification of roughness

Zooming in on the bed layer within the bottom boundary layer, Nikuradse (1933) introduced the concept of an equivalent or effective roughness height (k_s) to simulate the roughness of arbitrary roughness elements of the bottom boundary. The effective bed roughness for a given bed material size is not constant but depends on the flow conditions. Three flow regimes over rough surfaces have been identified by Nikuradse (1933) based on the magnitude of the Reynolds number. It classifies smooth turbulent, transitional and rough turbulent wherein the latter is applicable for ocean environments.

This is because the classification describes whether the roughness elements are within the laminar sublayer and thereby the extent to which they cause energy losses of the flow. The laminar sublayer only has a thickness in the order of millimetres (Chriss & Caldwell, 1984) and generally most of the ocean bottom has roughness elements with a characteristic scale exceeding that of the viscous sub-layer (Salon et al., 2008). So, the thickness of the laminar sublayer is so small that all roughness elements extend through it, causing near-bed flow to be completely within the turbulent layer. At this point, the energy losses due to vortices have attained a constant value and an increase in the Reynolds number no longer cause an increase in resistance. So, the resistance to the flow only depends on the roughness element height and the velocity profile behaves logarithmically (Nikuradse, 1993).

2.2.2 Grain roughness

In the pure form of a non-movable flat sandy bed, the bed roughness consists of grain roughness only and is the results of skin friction forces acting on the bed material (Houwman and Van Rijn, 1999). In this case, the equivalent sand grain roughness is the sand diameter of a flat bed of uniform sand packed at maximum density (Grant & Madsen, 1982). However, in nature this is rarely the case and if there is a mixture of grain sizes, the effective roughness may be very different from the median grain diameter. This is because the fine grains may fill the gaps between the large grains to give a relatively smooth surface (Soulsby, 1983). Furthermore, as discussed in §2.1.3, Damveld et al. (2020) found that sediment sorting may lead to local differences grain size variations on the sand wave. Therefore, grain roughness will likely have spatial variations. Van Rijn (1993) found the roughness due to the presence of bed material (grain roughness) generally to be about equal to $3D_{90}$.

2.2.3 Form roughness

When sediment transport occurs, bedforms begin to grow and exert form roughness (k_f) on the passing flow due to pressure gradients acting on the bedforms (Nikuradse, 1933). Soulsby (1983) describes sand (mega)ripples to be the main origin of seabed roughness. This is because the presence of the bedforms strongly affects the flow resistance because the friction factor is no longer determined only by the sediment grain size (the skin friction). Instead, bedform size and shape directly affect the roughness height. This plays a primary role in determining the flow structure and the resulting sediment transport capacity of the flow (Cataño-Lopera and García, 2006a).

2.2.3.1 Ripples

As water flows over a sand bed it exerts a shear force on the bed and if the flow is strong enough, sand grains are lifted to roll and bounce along the bed. This motion causes ripples to form on the bed surface in a process that is similar to the formation of sand waves as discussed in §2.1.1 (Besio et al., 2003). Once ripples are formed, they are generally maintained by the interaction between near-bed flow and the evolving bed roughness resulting from ripple generation. The wavelengths of ripples are controlled by grain size (Amos et al., 2019). As the energy of the flow increases then the transport rate of the sand also increases, and the bedforms change. At higher flow energy it has been observed that these bed features are washed out to produce a flat bed (Cataño-Lopera and García, 2006b).

2.2.3.2 Megaripples

Under the right conditions, ripples may even grow into megaripples. This was shown by Idier et al. (2004) who studied the formation of megaripples and found that megaripples emerge from a combined roughness enhancement of ripples and waves. Le Bot and Trentesaux (2004) observed the morphology of sand waves. Sand waves with symmetric megaripples at their crest are observed in areas where the asymmetry of the tidal peak current velocity is negligible. So, if the bedform growth mechanism described in §2.1.1 is not disrupted by asymmetric currents, the symmetric tide and flattened wave orbital motion will keep transporting sediment to the bedform crest. During this process, the growing ripples will increase the bed roughness and induce more bed shear stress which increases the sediment transport. This growth process will lead to the presence of megaripples.

2.2.4 Effect of bed roughness

As the previous section described, bed roughness is a complex physical property that is caused by the interplay of hydrodynamics, sediment characteristics and transport dynamics. Depending on the water depth, roughness effects can be confined to a thin layer near the bottom if the bed is very smooth, or extend over the entire water column in case it is very rough. Bedform development and the corresponding bed roughness directly affect the magnitude of bed shear stress, skin friction to form drag ratio, near-bed velocity structure and vertical profiles of suspended sediment concentration (Li & Amos, 1998).

The bed shear stress in a fully rough turbulent flow depends on the physical bottom roughness; a larger bottom roughness results in a larger shear stress (Glenn & Grant, 1986). This is because an increase in bed roughness causes a steeper gradient in flow velocity near the bed (Borsje, 2012), thereby directly influencing the near-bed velocity structure. The relation between bed roughness and bed shear stress is summarized by Glenn & Grant (1986); If the bed shear stress is below that required to initiate sediment motion, the bottom roughness is constant and is associated with sediment grains (grain roughness) in the bed or with pre-existing bed forms (form roughness). If the bed shear stress is increased above that required to initiate sediment motion, the bed roughness is associated with ripples (form roughness) and near-bed transport (transport roughness). As the bed shear stress increases, near-bed sediment transport increases and ripples will form if it concerns a sandy seabed. Ripples remain in equilibrium with the flow as the bed shear stress increases until a break off point is reached. As the boundary shear stress increases past the break off point, ripple heights decay until the bed is flat but covered by an intense near-bed sediment transport layer. Bed roughness also generates near-bed turbulence, which then affects the rate of deposition of suspended sediment (Wright et al., 1999). Turbulence acts as the force that keeps suspended sediment particles in the water column, when turbulence weakens, the gravitational forces acting on the particle will pull it down to the bed and cause it to settle. The generation of near-bed turbulence is greatly increased once (mega)ripples start forming. The resistance to the flow induced by bedforms is associated with the flow expansion on their lee side resulting in kinetic energy loss (Herrling et al., 2019). This phenomenon is also called flow separation and dominates the flow over (mega)ripples.

It is important to note that roughness elements are not isolated features, it is commonly found that a hierarchy of bedforms is present in areas of strong sediment transport. Thus large sand waves may have megaripples on their backs, with ripples in turn on their backs. Smith and McLean (1977) showed that each class of bedform acts as topography when the wavelength greatly exceeds the water depth, but acts as roughness elements when their wavelength is comparable to or slightly lower than the water depth.

2.3 Modelling sand waves and roughness

In this section, the main methods for studying the morphological development of sand waves and bed roughness will be discussed. Roos (2019) made an overview of recent sand wave research and found that currently the most used methods are data analysis, empirical modelling and process-based modelling. Within process-based modelling two types can be distinguished; idealised models and complex models. Idealised models gain generic insight in a specific physical mechanism and are often stability based while complex models are generally aimed at solving site-specific engineering problems. The latter is used in this work and will be described in §2.3.1. Modelling bed roughness is described in §2.3.2 and frequently used methods in complex models consist of using a Chézy coefficient (§2.3.2.1), roughness height (§2.3.2.2) and roughness predictors (§2.3.2.3).

2.3.1 Complex numerical modelling of sand waves

Complex models are being used more often in recent literature, for example the numerical model Delft3D (Borsje et al., 2014; Van Gerwen et al., 2018; Damveld et al., 2020). The model is based on the fundamental laws of physics and attempts to describe the important hydrodynamic and sedimentary processes in coastal seas. This is done through partial differential equations consisting of momentum equations, a continuity equation, a turbulence closure model, a sediment transport equation and a sediment continuity equation, supplemented with boundary conditions. The general idea of complex numerical modelling of sand waves consists of defining the initial topography, hydrodynamic properties and sediment characteristics for a default case, and solving the morphological feedback loop using the governing equations. By changing any of these aspects, it is possible to obtain insight in the effect of various hydrodynamic processes and sediment characteristics.

It is important to note that complex models are still combined with other modelling methods, some of the physical processes may be parametrized through empirical relations in order to keep the model manageable or since they are not fully understood yet. Furthermore, to develop these models, data analysis on field observations and flume experiments is crucial to determine relations between morphodynamic processes. Additionally, to apply morphological models to practical purposes, information about the local characteristics is required for model set-up and calibration. Finally, the sand wave development should be monitored to confirm the estimates of the morphological model.

2.3.2 Modelling roughness

According to Van Rijn (1984), the fundamental difficulty is that the bed characteristics (bed forms), and thus, bed roughness, depend on flow conditions (flow velocity and depth) and sediment transport rate. These flow conditions are, in turn, strongly dependent on the bed configuration and its bed roughness. For this reason, the bed roughness is often simplified and considered uniform in morphological sand wave models. In complex process-based modelling, bed roughness is often implemented as a uniform Chézy coefficient or constant roughness height. Roughness predictors are used less often but are able to estimate bedform dimensions and thereby roughness height under dynamic conditions.

2.3.2.1 Chézy coefficient

Although bottom variations in roughness elements such as (mega)ripples are readily observed (Damveld et al. 2019), bed roughness is generally characterized by a constant Chézy roughness coefficient C. According to Deltares (2014), a roughness height value k_s of $0.01m$ corresponds to very smooth surfaces and with a mean water depth of $25m$ this leads to approximately $C = 80m^{1/2}s^{-1}$. For example, $C = 50m^{1/2}s^{-1}$ would represent a quite rough surface with a roughness height (k_s) of $0.5m$. In this Chézy coefficient range, previous research is generally performed with a uniform value in the upper end of this range which implies a relatively smooth surface. For example, Van Gerwen et al.

(2018) and Damveld et al. (2020) both used a Chezy coefficient of $75m^{0.5}s^{-1}$ and Borsje et al. (2013) used $65m^{1/2}s^{-1}$, which is also the default in Delft3D (Deltares, 2014).

2.3.2.2 Roughness height

The Chézy coefficient is based on the roughness height k_s and water depth H. Rather than defining a Chézy coefficient, the roughness is also frequently modelled by defining a roughness height. For example, Besio et al. (2004) defines a constant roughness height directly. Another method is using an empirical predictor to calculate the roughness height of bedforms such as the predictor proposed by Soulsby and Whitehouse (2005). Borsje et al. (2009) uses this predictor to determine the roughness height of ripples. Van Santen et al. (2011) also uses roughness predictors but includes both roughness due to ripples and megaripples. In both cases, the roughness height for bedforms is determined and kept constant.

2.3.2.3 Roughness predictors

Although application of roughness predictors is common in fluvial studies, there are very few numerical studies in coastal setting that apply bedform predictors and deal with the effect of bedform roughness on the hydro- and morphodynamics (Herrling et al., 2019). Also, as mentioned in §2.3.3.1, even though some sand wave studies use roughness predictors, the input variables such as the bedform wavelength and height is kept constant Borsje et al. (2014). In reality, when sediment transport occurs, the bed topography evolves and leads to changes in bed roughness. This will in turn affect the hydrodynamics and consequently the morphodynamics which leads back to a change in topography to start the cycle again. Roughness predictors could be used to estimate bed roughness at every iteration of the morphological feedback loop and thus generate more accurate bed evolution. There are many roughness predictors available in literature (Soulsby and Whitehouse, 2005), so the use of roughness predictors specific to this work is elaborated further in §3.1.3.

3 Methodology

This chapter describes the methodology used to answer the sub-questions defined in §1.3.2 as a step towards answering the main research question defined in §1.3.1. Firstly, a general introduction is given regarding the numerical model Delft3D by Deltares (2014) in §3.1. The model setup and parameter choice is described in §3.2. Then, a more detailed elaboration of the roughness formulations is given in §3.3. Some processing methods are described in §3.4. The next four sections describe the methods for each sub-question consecutively.

3.1 Model description

Delft3D uses the governing hydrodynamic and sedimentary equations to complete the morphological feedback loop, which consists of topography, hydrodynamics, sediment transport and bed evolution consecutively. Once the initial topography is described, the next step is to solve the hydrodynamics which usually consists of currents, tides and waves. Depending on the hydrodynamic conditions and sediment characteristics, sediment transport may occur and change the initial topography. Once this happens, the evolved bed will replace the initial topography and the loop is calculated again for the next time step. The change in topography or hydrodynamics also implies a change in roughness, Delft3D models the interaction and feedbacks regarding bed roughness as shown in figure 6. This is an extension on the traditional morphodynamical feedback loop.

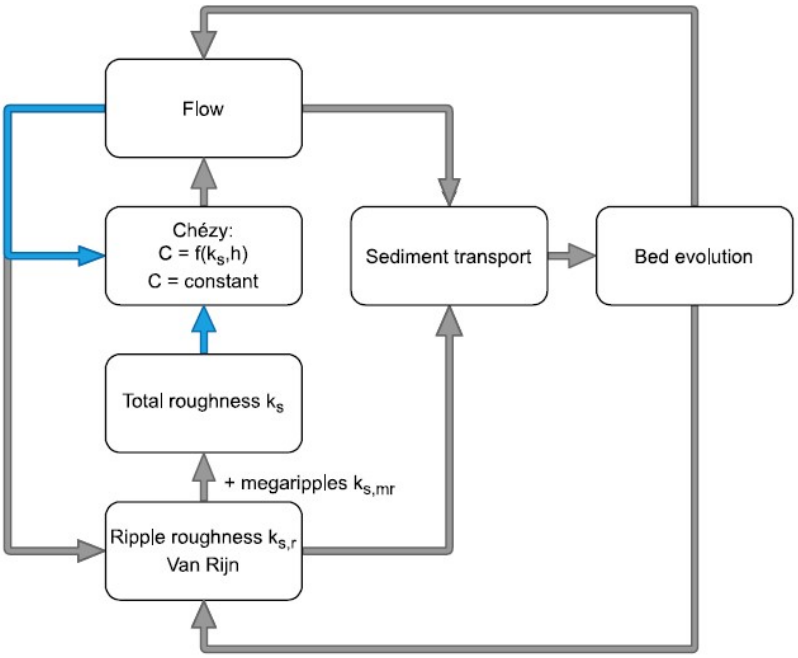

Figure 6. Schematic overview of interaction and feedbacks related to ripples and megaripples in Delft3D. Blue arrows: this connection is removed by choosing a constant Chézy value C, note that the sediment transport in this case still depends on $k_{s,r}$. Figure based on Brakenhoff et al. (2020).

The model by Van Gerwen et al. (2018) is used and the equations are only described here qualitatively. We refer to Van Gerwen et al. (2018) for a summarized model description and the Delft3D-FLOW user manual (Deltares, 2014) for a comprehensive description of the used equations.

3.1.1 Hydrodynamics

In Delft3D the system of equations consists of the Navier-Stokes equations, flow- and sediment continuity equations, sediment transport equations and a turbulence closure model. The vertical Navier-Stokes component is reduced to the hydrostatic pressure relation as vertical accelerations are assumed to be small compared to gravitational acceleration. The model is run in the two-dimensional vertical (2DV) mode, thus considering flow and variation in x- and z-direction only, while assuming zero flow and uniformity in y-direction and ignoring Coriolis effects. The vertical eddy viscosity is calculated by using the $k-\varepsilon$ turbulence model in which both the turbulent energy k and the dissipation ε are computed. The resulting vertical eddy viscosity is variable both in time and space. At the bed, a quadratic friction law is applied. At the free surface, a no-stress condition is applied. Riemann boundary conditions are imposed at the lateral boundaries to allow outgoing numerical waves to cross the boundary without reflecting back into the domain, this prevents disturbance of the circulation cells.

3.1.2 Sediment transport and bed evolution

The transport modelling of non-cohesive sediment is done by Van Rijn's 1993 or 2004 transport model by default in Delft3D (Van Rijn and Walstra, 2004). In our case, we consider Van Rijn's (1993) transport model (TR1993) as the default transport formulation since this is the default in Van Gerwen et al. (2018). In all these formulations Van Rijn distinguishes between bed load and suspended load which both have a wave-related and current-related contribution. Since a no-stress condition is applied at the free surface, wave contributions are not modelled and sediment transport due to wave effects are not described further.

Van Rijn's bed-load transport contributions are based on a quasi-steady approach, which implies that the bed-load transport contributions are based on the assumption that bed-load transport responds instantaneously to prevailing current-velocities. The current-related suspended load transport is based on variation of the suspended sand concentration field due to the effect of currents (Van Rijn and Walstra, 2004). The most important improvements from TR1993 towards TR2004 are the refinement of the predictors for the current-related bed roughness (VRIJN07) described in §3.3.3 and the suspended sediment size, which previously had to be specified by the user (Van Rijn and Walstra, 2004).

Both the Van Rijn (1993) and Van Rijn et al. (2004) sediment transport model distinguishes between three transport components that are all treated like bed or total load: 1) bedload due to currents, 2) bedload due to waves and 3) suspended load due to waves.

$$S_{total} = S_{bedload\ current} + S_{bedload\ waves} + S_{suspended\ waves} \quad (1)$$

$$\frac{dz}{dt} = S_{total\ out} - S_{total\ in} + Entrainment - Deposition \quad (2)$$

Herein $S_{bedload\ current}$, $S_{bedload\ waves}$, $S_{suspended\ waves}$, Entrainment and Deposition depend on the sediment transport formula used and will lead to change in bed level z. In our case, $S_{bedload\ waves} = 0$ and $S_{suspended\ waves} = 0$. TR1993 distinguishes between sediment transport below the reference height which is treated as bedload transport and that above the reference height is treated as suspended-load. Sediment is entrained in the water column by imposing a reference concentration at the reference height (Deltares, 2014). It is important to note that the calculation for the reference concentration is according to TR1993 in TR2004, but the calculation for the reference height is updated in TR2004. This effectively makes is lower than in TR1993.

3.1.3 Bed roughness

Both in Delft3D and similar models, roughness elements such as grains, ripples, and megaripples are smaller than the model grid (i.e., sub-grid), so they are not explicitly solved on that scale and hence need to be parameterized (Brakenhoff et al., 2020). In Delft3D using trachytopes is the functionality to solve this issue by allowing the definition of roughness on a sub-grid area based level.

Although Delft3D has five built-in roughness predictors, these are all fluvial predictors meaning that these are mainly designed for riverine conditions. Furthermore, three of these predictors require the definition of calibration parameters. Since reliable field data of bed-load transport in coastal conditions are extremely scarce (Van Rijn, 2007), it is opted not to use roughness predictors that require calibration. The two predictors that are available are Van Rijn (1984c) and Van Rijn's (2007) bedform predictor. Van Rijn (1984c) is only applicable on riverine conditions as it is only able to predict dune dimensions and is thus unusable in oscillatory flow. Therefore, only Van Rijn's (2007) bedform predictor (VRIJN07) is applicable in a coastal environment and is the only predictor that is implemented. Furthermore, a constant Chézy coefficient is applied which serves as the reference to compare the performance of VRIJN07.

3.1.3.1 Chézy coefficient

The first roughness type is described by the Chézy roughness coefficient. As described in §2.2.1, coastal beds generally have roughness elements with a characteristic scale that exceed the thickness of the viscous sublayer (Salon et al., 2008). This implies hydraulically rough conditions and the White-Colebrook equation is therefore used to calculate the Chézy roughness coefficient

$$C = 18^{10}\log\left(\frac{12H}{k_s}\right) \tag{3}$$

Where H is the water depth and k_s the equivalent geometrical roughness of Nikuradse.

By using a constant value for the Chézy coefficient, the blue arrow in figure 6 is removed. This means that the bed roughness is no longer dependent on the flow. Although there is no feedback between the Chézy coefficient and the flow anymore, the sediment transport still depends on $k_{s,r}$ determined from VRIJN07 (see §3.1.3.2). Note that this is different to k_s shown in equation 3.

Following Van Gerwen et al. (2018) and Damveld et al. (2020), a Chézy roughness coefficient of 75 $m^{0.5}s^{-1}$ is used as the reference case and shall be referred to as C75.

3.1.3.2 Van Rijn 2007 bedform predictor

The Van Rijn's (2007) bedform predictor (VRIJN07) is one of the most important improvements of the TR2004 model and estimates the current-related bed roughness. The VRIJN07 equation consists of ripple, mega-ripple and dune contributions which are combined in the following equation.

$$k_s = \min\left(\sqrt{k_{s,r}^2 + k_{s,mr}^2}, \frac{h}{2}\right) \tag{4}$$

With roughness heights of ripples k_r and mega-ripples k_{mr}. The contribution of dune roughness height k_d is omitted since these are considered to be riverine bedforms (Van Rijn and Walstra, 2004). The roughness height of ripples is determined by

$$k_{s,r} = \alpha_r \begin{cases} 20D_{silt} & if\ D_{50} < D_{silt} \\ k_{s,r}^* & otherwise. \end{cases} \tag{5}$$

Where α_r is a calibration factor that is set to 1, $D_{silt} = 32\mu m$ and $k_{s,r}^*$ is given by

$$k_{s,r}^{*} = \begin{cases} 150 f_{cs} D_{50} & if\ \psi \leq 50 \\ (182.5 - 0.65\psi) f_{cs} D_{50} & if\ 50 < \psi \leq 250 \\ 20 f_{cs} D_{50} & if\ \psi > 250 \end{cases} \quad (6)$$

With factor $f_{cs} = (0.25 D_{gravel}/D_{50})^{1.5}$ in which $D_{gravel} = 0.002m$. Furthermore, ψ is the current-wave mobility parameter defined as

$$\psi = U_{wc}^{2}/[(s-1) g D_{50}] \quad (7)$$

Using the relative density $s = \rho_s/\rho_w$ and

$$U_{wc}^{2} = U_{w}^{2} + u_{c}^{2} \quad (8)$$

With depth-averaged current velocity u_c and peak orbital velocity near bed U_w. Note that this is a wave-contribution and is equal to zero. This means that the current-wave mobility parameter is only dependent on the depth-averaged current velocity and median grain size.

Similarly, the roughness height contribution of mega-ripples k_{mr} is determined by

$$k_{s,mr} = \alpha_{mr} \begin{cases} 0 & if\ D_{50} < D_{silt} \\ k_{s,mr}^{*} & otherwise. \end{cases} \quad (9)$$

Where α_{mr} is a calibration factor that is set to 1 and $k_{s,mr}^{*}$ is given by

$$k_{s,mr}^{*} = \begin{cases} 0.0002 f_{fs} \psi H & if\ \psi \leq 50 \\ (0.011 - 0.00002\psi) f_{fs} H & if\ 50 < \psi \leq 550 \\ 0.02 & if\ \psi > 550\ and\ D_{50} \geq D_{sand} \\ 200 D_{50} & if\ \psi > 550\ and\ D_{silt} \leq D_{50} < D_{sand} \end{cases} \quad (10)$$

In which $f_{fs} = (D_{50}/1.5 D_{sand})$ and $D_{sand} = 0.000062m$. Note: the value of $k_{s,mr}$ is limited to values smaller than $0.2m$ by Delft3D. The complete equation has a third component; the contribution of dunes k_d, but since these are river bedforms their calibration component α_d is set to zero and dune contribution is not taken into consideration. Lastly, for reference, VRIJN07 also exists in linear form, then equation 3 becomes:

$$k_s = \min\left(k_{s,r} + k_{s,mr}, \frac{h}{2}\right) \quad (11)$$

In both equation 3 and 11 the $h/2$ argument will only take effect in very shallow water. As this is not the case, k_s will be determined from the ripple and mega-ripple roughness height contributions. The difference in the linear and quadratic equation is visible in figure 7 and also shows how VRIJN07 behaves under variation in the current-wave mobility parameter. The quadratic equation is applied in this work as no significant quantitative differences in results were observed.

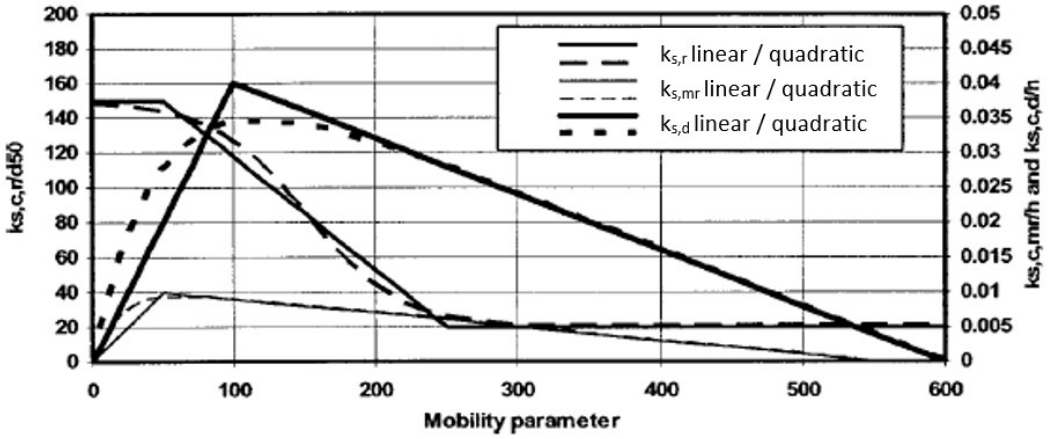

Figure 7. Linear (continuous) and quadratic (dashed) current-related roughness of ripples, megaripples, and dunes for range of current-wave mobility parameter (Van Rijn, 2007).

The VRIJN07 equations are approximations for the roughness height under equilibrium conditions. This implies that the bed roughness instantaneously adjusts to new hydrodynamic conditions. So, the bedforms that induce this roughness also develop on the same timescale as the hydrodynamics. However, this is not true as morphological development occurs at a far greater timescale than hydrodynamic processes. So, under time and spatially varying conditions, the roughness height needs time to adjust. This effect is implemented trough a relaxation option given by:

$$k_{s,r} = (1-\alpha_r)k_{(s,r,new)} + \alpha_r k_{s,r,old} \quad where\ \alpha_r = e^{-\Delta t/T_r} \tag{12}$$

$$k_{s,mr} = (1-\alpha_{mr})k_{(s,mr,new)} + \alpha_{mr} k_{s,mr,old} \quad where\ \alpha_{mr} = e^{-\Delta t/T_{mr}} \tag{13}$$

Where Δt_r is the timestep of bed roughness updating, and T_r and T_{mr} are different relaxation time scales for the two bedform types.

3.2 Model setup

3.2.1 Grid setup

The calculation grid has a variable resolution in both the x- and z-direction. The horizontal domain of the model is approximately 50 km in length. In the centre of this domain, there are evenly distributed cells such that the horizontal grid resolution is 2 m. Choosing a larger amount of such cells thus implies a wider domain to accompany sand waves with large wavelengths but comes on the expense of longer computation times. Towards the boundaries of the domain, the cell width increases to a maximum resolution of 1500 m. The vertical domain consists of 60 σ-layers, these layers have an increasing resolution towards the bed (up to 0.05% of the local water depth). Since the resolution is based on a percentage of the water depth, the layer height will vary over a sand wave having thinner layers near the sand wave crest. The grid setup is visualised in figure 8.

In the case of a flat bed (i.e. research question 1), 500 evenly distributed cells are used in the centre of the domain. In case of a wavy bed (i.e. research questions 2,3 and 4), the FGM analysis (§3.2.1.1) will determine the initial wavelength that corresponds to the model setup and initial sand wave height. When large wavelengths emerge for combinations, the amount of accurate cells is increased to 1000 such that at least three full grown sand waves are present in the initial topography. This ensures that at least one sand wave in the middle does not experience side-effects from the boundary conditions. A gradual transition from the flat bed is ensured by multiplying the sand wave field with an envelope function.

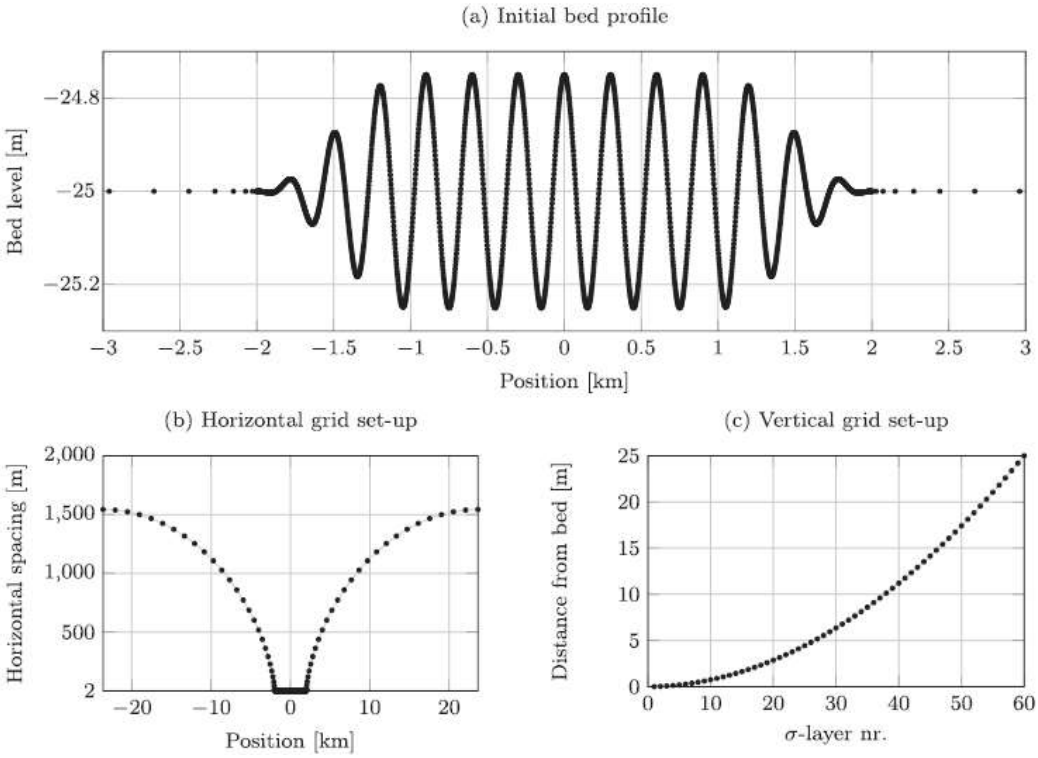

Figure 8. Calculation grid setup, with (a) an example initial bed for a wavelength of 300 m, (b) the horizontal grid distribution, using a fine grid in the center where the sand waves are calculated and a coarser grid towards the boundaries and (c) the distribution of the σ-layers over the water column, showing the distance from the bottom per layer for a mean water depth of 25 m (Van Gerwen et al., 2018).

3.2.1.1 Fastest growing mode

In order to define the initial topography, the sand wave dimensions have to be determined. Defining a flat bed with random irregularities will also lead to sand wave formation under the correct conditions, but may take decades and is therefore very computationally expensive. A faster method is determining the fastest growing mode (FGM) and is based on the assumption that sand waves will grow to a characteristic length scale based on model parameters and certain forcing. The process of simulating decades of morphological development is mimicked by simulating an initial topography of the same wave height, but various wave lengths. The initial morphodynamic response is then determined as a function of the topographic wave number $k = 2\pi/\lambda$, with wavelength λ. The initial wave number k is varied in 9 equal steps from $0.0063m^{-1}$ ($\lambda = 1000m$) to $0.063m^{-1}$ ($\lambda = 100m$).

The model is run for two tidal cycles, wherein the first tidal cycle is used for spin-up time and no morphological changes are allowed. Following Borsje et al. (2014), the growth rate γ_R for the initial bed topography is calculated by

$$\gamma_R = \frac{1}{T} Re\left\{log\left(\frac{A_1}{A_0}\right)\right\} \tag{14}$$

In which T is the tidal period, A_0 is the initial bed amplitude and A_1 is the bed amplitude of the sand wave at the end of the second tidal cycle. Both A_0 and A_1 are determined by a fast Fourier transform of the central part of the sand wave domain. Positive values of γ_R indicate growth of the bottom perturbation, whereas negative values indicate decay. Since each of the parameter setups has a characteristic length scale, the ten different wavelengths will show a certain growth rate for an equal sand wave height, water depth and tidal velocity. The wavelength with the largest growth rate γ_R after one tidal cycle is assumed to be the fastest growing mode and will serve as the initial topography for the corresponding parameter setup.

It is known that the topography has a significant effect on hydrodynamics over a sand wave. Since the FGM and thus initial topography is different for every roughness method and transport model combination, the effect of bed roughness on the hydrodynamics and morphodynamics might not be easily observable. Therefore, simulations in research question 2 and 3 have also been performed with a fixed wavelenght. The chosen fixed wavelength is the average of the preferred wavelengths. The fixed wavelength enables isolation of the effects of roughness method as an initial response on the same topography.

3.2.2 Parameters

The model is run using a hydrodynamic timestep Δt of 12 s and a spin-up time of one tidal cycle is performed during which no morphological changes are allowed. Depending on the desired simulation timeframe, a morphological acceleration factor (MORFAC) is used for long term simulations. This factor is multiplied by the bed evolution after each time step, allowing for faster computations. Effectively, simulating a period of 100 years is done in approximately 18.3 days when using a MORFAC of 2000 and a hydrodynamic timestep Δt of 12 s. Van Gerwen et al. (2018) found that using smaller MORFAC values showed the same results quantitatively, but required longer simulation times.

The basic tidal current of the system is forced by the S_2 tidal constituent (angular frequency $\sigma_{S2} = 1.45\ x\ 10^{-4}\ rad\ s^{-1}$) so that at the lateral Riemann boundaries a depth-averaged velocity amplitude of $U_{S2} = 0.65\ ms^{-1}$ is attained. The mean water depth (H_0) is set at 25 m and sediment grain size (d_{50}) is 0.035 m. The settings for flow velocity amplitude, mean water depth and grain size resemble a typical North Sea situation for sand wave occurrence (Borsje et al., 2009). Table 2 shows an overview of parameters of the default case, the initial topography and any changes to this parameter setup will be described in the corresponding section.

*Table 2. Overview of default model settings for hydrodynamics, sand transport and numerics. Note: * is varied in later setups. ** is replaced when using VRIJN07 and Cspatial. *** is enabled when using VRIJN07.*

	Parameter	Symbol	Value	Unit
Flow	Horizontal width of domain	L	50	km
	Undisturbed water depth	H_0	25	m
	Tidal velocity amplitude	U_{s2}	0.65	$m\ s^{-1}$
	Angular frequency	σ_{s2}	$1.45 * 10^{-4}$	$rad\ s^{-1}$
Roughness	Chézy roughness coefficient**	C	75	$m^{0.5}\ s^{-1}$
	Ripple coefficient***	α_r	1	$-$
	Megaripple coefficient***	α_{mr}	1	$-$
	Ripple relaxation time***	T_r	0	min
	Megaripple relaxation time***	T_{mr}	0	min
	Roughness updating timestep***	Δt_r	1	min
Sediment	Transport model	$-$	TR1993; TR2004	$-$
	Median sediment grain size*	d_{50}	0.35	mm
	Sand density	ρ_s	2650	kgm^{-3}
	Water density	ρ_w	1000	kgm^{-3}
	Bed slope parameter	α_{bs}	3	$-$
	Bed porosity	ε	0.4	$-$
Numerics	Hydrodynamic time step	Δt	12	s
	Horizontal grid spacing	Δx	2	m
	Number of σ-layers	$-$	60	$-$
	MORFAC (initial response; long term)	$-$	$1; 500 - 2000$	$-$

3.3 Research question 1

The first research question is aimed at extending the Van Gerwen et al. (2018) model by including the roughness predictor VRIJN07 and sediment transport model TR2004. We will use a flat bottom to focus on the initial response of the system by eliminating spatial variations and only focus on the temporal behaviour of roughness and transport models. Initially, the model will be run using the default parameter values shown in table 2 for the combinations shown in table 3.

Table 3. Combinations of roughness formulation and sediment transport model that will be complemented with the default parameters to be used in research question 1.

Combination	Roughness method	Transport model
C75/TR1993	C75	TR1993
C75/TR2004	C75	TR2004
VRIJN07/TR1993	VRIJN07	TR1993
VRIJN07/TR2004	VRIJN07	TR2004

Herein, C75/TR1993 serves as the reference case since this setup is also used by Van Gerwen et al. (2018). Besides intercomparing the simulation results of these combinations, a logarithmic velocity profile is plotted against the output from Delft3D. This profile is used to measure how the model results of C75 and VRIJN07 perform against an analytical equation. The assumption that flow in a coastal environment is in the rough turbulent regime also means that the flow velocity profile will behave logarithmically (Nikuradse, 1933). The logarithmic velocity profile is determined by

$$u(z) = \frac{u_*}{\kappa} \ln\left(\frac{z}{z_0}\right) \tag{15}$$

With κ the Von Karmann constant (=0.4), z the distance from the bed, z_0 the water depth and u_* the shear velocity determined by

$$u_* = \sqrt{\frac{\tau_b}{\rho_w}} \tag{16}$$

Where τ_b the bed shear stress and ρ_w the density of water.

The next step is to see how sensitive the model results are to change in parameters, which will also show the robustness of the model. The grain size is an influential parameter as it is incorporated in VRIJN07 to determine roughness heights and directly influences sediment transport. Additional grain sizes of 0.3 and 0.4 mm along with the default 0.35mm will be modelled for the four combinations in table 3. Furthermore, VRIJN07 bedform contributions can be calibrated with a coefficient for ripples (α_r in equation 5) and megaripples (α_{mr} in equation 9). The default case has both coefficients set at 1, meaning the full contribution will be taken into account. Here, additional runs where both coefficients are set to 0 are performed to analyse the difference in bed roughness estimates.

The relaxation time of ripples (T_r in equation 12) and megaripples (T_{mr} in equation 13) can also be adjusted. For ripples and megaripples the difference in tide and morphology timescale is relatively small as compared to larger bedforms and relaxation effects are therefore less important (Herrling et al., 2019). Ripples reformation can occur within 1 min or so after flattening (Van Rijn, 2007), so the timescale at which ripples develop is so small that the relaxation time scale T_r is set to 0 min. This is also done by Wang et al. (2016), who set both the relaxation times of ripples and mega-ripples T_r, T_{mr} to 0 min. However, here we want to explore the effect of imposing a relaxation time on the larger mega-ripples. It is unclear what relaxation time is appropriate for mega-ripples, so it is

assumed that their timescale is in the order of hours. A relaxation time scale for mega-ripples of 6 hours is chosen. An overview of the additional runs by changing the discussed parameters is shown in table 4.

Table 4. Changes in default parameter for sensitivity analysis to grain size and VRIJN07 setup.

Combination	Grain size d_{50} [mm]	Ripple coefficient α_{mr} [-]	Megaripple coefficient α_{mr} [-]	Megaripple relaxation T_{mr} [min]
C75/TR1993	0.3; 0.4	-	-	-
C75/TR2004	0.3; 0.4	-	-	-
VRIJN07/TR1993	0.3; 0.4	0	0	360
VRIJN07/TR2004	0.3; 0.4	0	0	360

3.4 Research question 2

The second research question is aimed at extending the insights for a flat bed to a wavy bed with a sand wave amplitude of 0.5 meters. Besides from temporal variability, the wavy bed will introduce spatial variability to system and change the initial response of the system. However, to define the initial wavy topography, a wavelength must be known as well. Fastest growing mode (FGM) simulations will be performed for each of the combinations to find its corresponding preferred wavelength. This process is described in §3.2.2. The combinations that are considered for this research question are shown in table 5. Any parameter not listed in table 5 will set to the default parameter shown in table 2.

Table 5. Combinations of roughness formulation, sediment transport model and grain size that will be complemented with the default parameters to be used in research question 2.

Combination	Roughness method	Transport model	Grain size d_{50} [mm]
C75/TR1993	C75	TR1993	0.3; 0.35; 0.4
C75/TR2004	C75	TR2004	0.3; 0.35; 0.4
VRIJN07/TR1993	VRIJN07	TR1993	0.3; 0.35; 0.4
VRIJN07/TR2004	VRIJN07	TR2004	0.3; 0.35; 0.4

3.5 Research question 3

The third research question is aimed at gaining insight in how the roughness methods and transport models initially respond when using field observation conditions. This is because in research question 2, we observed that VRIJN07 has some deviations in bed roughness estimates as compared to field observations. For this, we increase the initial sand wave amplitude to 1.5 meters. The amplitude is increased to see whether the deviations of VRIJN07 change and give insight in the hydro-morphodynamic processes that occur in a later stage of sand wave development. Furthermore, it also suits the field conditions for the new roughness method better. The new roughness method consists of linearly interpolating a Chézy coefficient of 80 $m^{0.5}s^{-1}$ at the trough to 50 $m^{0.5}s^{-1}$ at the crest and shall be referred to as Cspatial. This method forces spatial variability in bed roughness at the cost of having no temporal variability. This Chézy coefficient range is chosen for the following reasons.

VRIJN07 roughest bed is a Chézy coefficient of approximately 56 $m^{0.5}s^{-1}$ on the crest, however, a megaripple limit of 0.2 meters roughness height is used which is reached for the majority of high tide causing a large section near the crest having the same roughness height. A Chézy coefficient of 50 $m^{0.5}s^{-1}$ at the crest implies a total roughness height of 0.5 meters and megaripples in the North Sea up to 0.4 meters have been observed by Van Dijk and Kleinhans (2005). A Chézy coefficient of 80 $m^{0.5}s^{-1}$ at the trough implies a roughness height of approximately 1.1 centimeter, which is very smooth. VRIJN07 smoothest bed in the trough is about 68 $m^{0.5}s^{-1}$, for a trough this is still relatively rough and is caused by the current-wave mobility parameter not becoming small enough to break down ripples.

Based on observations of Damveld et al. (2018), this is not the case and no bedforms were present in the sand wave trough meaning Chézy coefficients should be higher for the trough.

Similar to both previous research questions, we have to determine the initial wavelength corresponding to a wave amplitude of 1.5 meters and the roughness method and transport model combination. Since we must know the initial topography in order to linearly interpolate the Chézy coefficient from crest to trough it is not possible to perform fastest growing mode (FGM) simulations with Cspatial directly. Therefore, a uniform Chézy coefficient of 65 $m^{0.5}s^{-1}$ is used in the FGM simulation to determine a preferred wavelength as this is the average value for Cspatial. The FGM determination method is described in §3.2.2. The combinations that are considered for this research question are shown in table 6. Any parameter not listed in table 6 will set to the default parameter shown in table 2.

*Table 6. Combinations of roughness formulation and sediment transport model that will be complemented with the default parameters to be used in research question 3. * Note that for the FGM simulations Cspatial will be substituted for a uniform Chézy coefficient of 65 $m^{0.5}s^{-1}$.*

Combination	Roughness method	Transport model
C75/TR1993	C75	TR1993
Cspatial/TR1993	Cspatial*	TR1993
Cspatial/TR2004	Cspatial*	TR2004
VRIJN07/TR2004	VRIJN07	TR2004

3.6 Research question 4

The fourth research question is aimed at performing long term simulations to analyse the development towards the sand wave equilibrium stage. Previously, spatiotemporal variability was mainly achieved through the roughness method and tidal currents. Although on a far greater timescale, spatiotemporal variability will now also be implemented in the system through the evolving topography. Three cases are defined to be run on a long term based on their behavior in previous parts. The cases used are C75/TR1993, Cspatial/TR1993 and VRIJN07/TR2004. We define an initial sand wave with an amplitude of 0.5 meters and use the fastest growing mode (FGM) found in research question 2 for C75/TR1993 and VRIJN07/TR2004. Since no FGM for an amplitude of 0.5 meters is found for Cspatial/TR1993 yet, we perform a FGM simulation using a Chézy coefficient of 65 $m^{0.5}s^{-1}$ as a substitution. This process is described in §3.2.2. The FGM is used as the initial topography in order to save computation time. The combinations that are considered for this research question are shown in table 7. Any parameter not listed in table 7 will set to the default parameter shown in table 2.

*Table 7. Combinations of roughness formulation and sediment transport model that will be complemented with the default parameters to be used in research question 4. * Note that for the FGM simulations Cspatial will be substituted for a uniform Chézy coefficient of 65 $m^{0.5}s^{-1}$.*

Combination	Roughness method	Transport model	Run time [years]	MORFAC [-]
C75/TR1993	C75	TR1993	100	2000
Cspatial/TR1993	Cspatial*	TR1993	100	2000
VRIJN07/TR2004	VRIJN07	TR2004	350	500

Initially, a MORFAC of 2000 is used as Van Gerwen et al. (2018) proved that lower MORFAC values only increase the computation length rather than the equilibrium sand wave dimensions. However, Van Gerwen et al. (2018) only tested with TR1993 and we found that simulations became unstable for TR2004. A stable run for VRIJN07/TR2004 was performed using a MORFAC of 500. The initial end time was 100 years, but we found that TR2004 combinations require longer to reach an equilibrium position and 350 years is used for VRIJN07/TR2004. A MORFAC of 2000 implies that one tidal cycle is equivalent to 2.74 years while a MORFAC of 500 is equal to approximately 0.68 years.

4 Results

The results of this thesis are divided in four parts that correspond to the research questions. The first part (§4.1) will describe the effects of various roughness formulations and transport models in the initial flat bottom stage. The bottom will be perturbated in the second (§4.2) and third (§4.3) part to focus on the effects of spatial roughness variability on physical mechanisms in the initial small- to medium-amplitude stage. The fourth part (§4.4) will consist of long-term results in order to examine the effects of spatial and temporal variable roughness on the development towards the equilibrium sand wave stage.

4.1 Initial flat bottom stage

This part will focus on the effects of various roughness formulations and transport models on physical mechanisms in the initial flat bottom stage. The flat bottom will isolate the temporal variability of the roughness formulations and transport models as the topography is spatially uniform. The four base runs are analyzed that consist of a combination of a constant Chézy coefficient of 75 $m^{0.5}s^{-1}$ (C75) and the Van Rijn 2007 bedform predictor (VRIJN07) as the roughness formulations and the transport models by Van Rijn 1993 (TR1993) and Van Rijn 2004 (TR2004). Also, the sensitivity of the roughness formulations and transport models to several parameters is investigated.

4.1.1 Topography

The interaction between topography and hydrodynamics generates friction, of which the magnitude is determined by the bed roughness. Bed roughness is a highly dynamic property, as small-scale roughness elements such as ripples may appear within minutes. VRIJN07 estimates the dynamic height of these roughness elements using the current-wave mobility parameter. For a tidal amplitude of 0.65ms^{-1} and no waves, it has a range of 0 during slack tide and 46 at high tide (See appendix A). This range translates to roughness height contributions shown in figure 9.

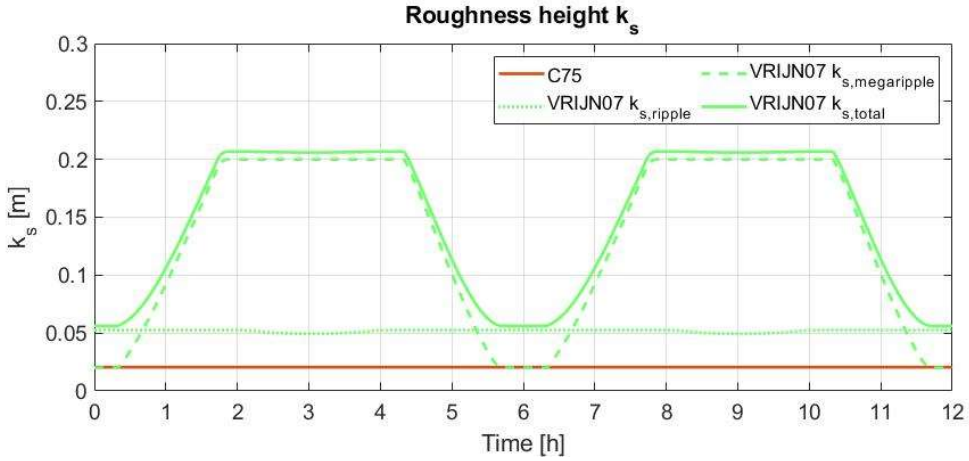

Figure 9. Roughness height k_s variability for C75 and VRIJN07 over tidal cycle. With continuous lines the total roughness height, dashed line the contribution of megaripples and dotted line the contribution of ripples.

Only the bedform roughness components are taken into consideration in figure 9 as these are dominant over the grain roughness magnitude (Nikuradse, 1933). Following figure 7, the roughness

height behavior is explained through the current-wave mobility parameter, it does not become large enough to break down ripples while the megaripple height increases rapidly. Megaripples are thus both the main dynamic property and also the main roughness source of VRIJN07. However, their roughness height is limited to 0.2m in Delft3D, causing flattened peaks. When averaging the roughness height over the tidal cycle, a total roughness height of 0.145m (Chézy coefficient = 61 $m^{1/2}s^{-1}$) emerges for VRIJN07. For C75, the corresponding total roughness height is 0.02m. So, along with high variability of VRIJN07, the magnitude of bed roughness is significantly larger than C75.

Sensitivity of the bed roughness is investigated by changing the megaripple calibration coefficient (α_{mr} in equation 9). It was found that disabling megaripple contribution only decreases the dynamic behavior of VRIJN07. Also, it effectively decreases the roughness height which leads to a situation that becomes comparable to C75. Since the focus is at the spatiotemporal variations, it is chosen to enable both ripple and megaripple contributions. Furthermore, the relaxation time of megaripples (T_{mr} in equation 13) is adjusted to include a delay in morphological development. This effect did influence the bed roughness estimates significantly but did not translate to any significant changes in the simulation results. See appendix B for more details.

4.1.2 Hydrodynamics

The structure of the flow velocity profile is determined by interaction of the flow and the topography. The friction dissipates energy from the passing flow that causes gradients to form towards the bed. This leads to a flow velocity profile over the water depth as shown in figure 10a wherein a logarithmic velocity profile is also included as a comparison based on equation 15. Furthermore, the interaction of near-bed flow velocity and bed roughness generates bed shear stresses. The generated bed shear stress during the tidal cycle is shown in figure 10b.

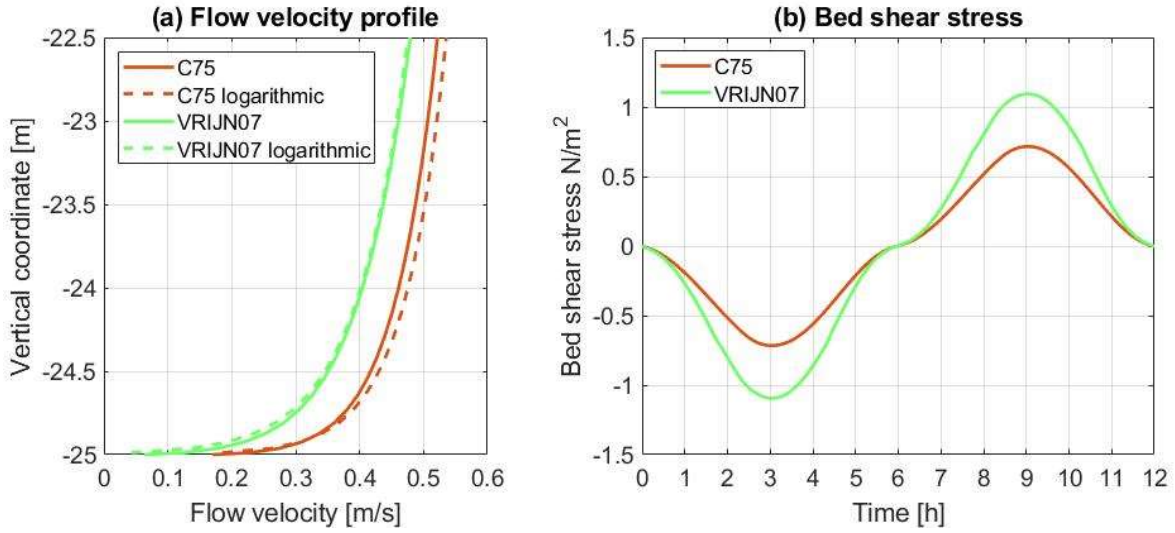

Figure 10. In (a) Near-bed flow velocity profiles (continuous lines) during slack and high tide for C75 and VRIJN07, and the corresponding logarithmic velocity profile (dashed line). Note: only 2.5 meters above the bed has been displayed. In (b) the Instantaneous bed shear stress for C75 and VRIJN07 over tidal cycle.

Figure 10 shows significant differences between C75 and VRIJN07 caused by larger bed roughness estimates of VRIJN07 leading to faster reduction of near-bed flow velocities. This difference will gradually decrease in water layers further from the bottom as the influence of the bed decreases. The modelled flow velocity profile fits the logarithmic velocity profile well, indicating that the model is robust. Small deviations exist because the logarithmic velocity profile consists of a function that is variable for distance from the bottom and bed shear stress whereas Delft3D includes more complex processes.

The steeper flow velocity profile gradient for VRIJN07 generates larger bed shear stresses than C75. At high tide, the difference is largest since VRIJN07 estimates the largest magnitude bed roughness during this time. When approaching slack tide, the bed shear stress of VRIJN07 decreases more rapidly than C75. This is because the bed roughness estimates decrease with a falling tide while C75 remains constant. Maximum values are 1.1 nm^{-2} for VRIJN07 and 0.72 nm^{-2} for C75. These differences have implications for the sediment transport as the threshold of motion of larger grains is exceeded for VRIJN07. These larger grains will predominantly be transported in the bedload regime. Therefore, the sediment transport mode ratios will be altered and could affect sand wave development.

4.1.3 Sediment transport

Two different sediment transport models have been applied, the default TR1993 and TR2004. Although the bed shear stresses for both transport models are equal when considering the same roughness method, the translation to sediment transport varies significantly. This is visible in the results for the bedload and suspended load regime shown in figure 11.

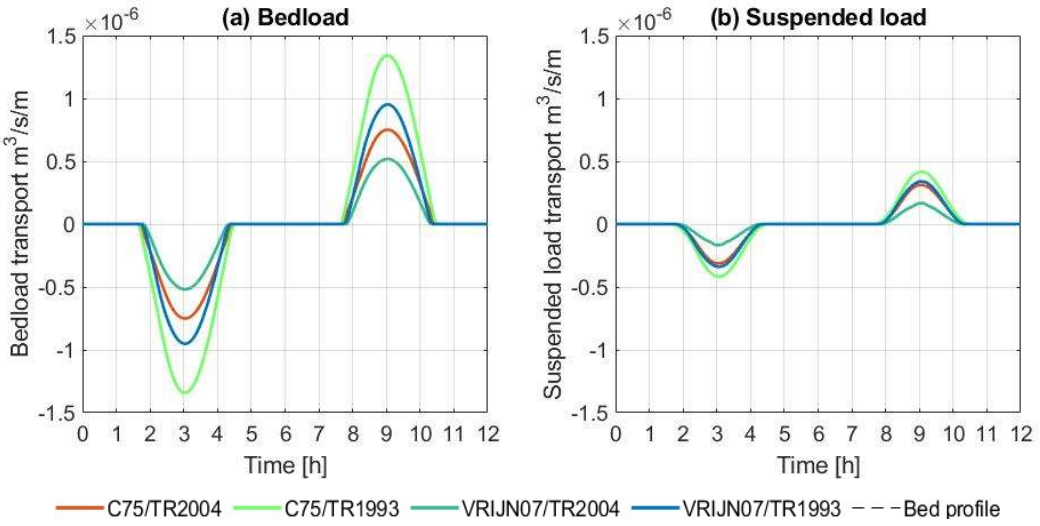

Figure 11. Bedload (a) and suspended load (b) transport variability for C75 and VRIJN07 combined with TR1993 and TR2004 over tidal cycle.

Figure 11 shows that during slack tide, the hydrodynamic action is not sufficient to exceed the threshold of motion of the sediment particles and no transport occurs. As high tide approaches, sediment transport begins to initiate while bedload is the dominant transport regime. While VRIJN07 produces larger magnitude bed shear stresses, C75 leads to larger sediment transport rates in both the bedload and suspended load regime than VRIJN07. Furthermore, TR1993 estimates significantly higher transport rates than TR2004. The sensitivity of sediment transport to grain sizes is available in appendix C.

4.1.4 Highlights

Here, the most important results are summarized from this part.

- VRIJN07 estimates bed roughness that is significantly rougher than C75. The main source of bed roughness in VRIJN07 is the megaripple roughness height. It is also the most dynamic component during a tidal cycle and is limited to values lower than 0.2 meters.
- A rougher bed results in a steeper gradient in the flow velocity profile and leads to larger bed shear stresses. Surprisingly, VRIJN07 leads to lower sediment transport rates than C75.
- TR1993 estimates significantly larger sediment transport rates than TR2004, wherein the bedload regime is dominant over the suspended load regime.

4.2 Initial low amplitude sand wave stage

This part will focus on the effects of various roughness formulations and transport models on physical mechanisms in the initial wavy bottom stage. The wavy bottom will cause spatial variability of the roughness formulations along with the temporal variability we have seen in §4.1. This part focusses on a 0.5m amplitude sand wave.

First, we find the fastest growing mode of all runs to model the correct wavelength of the bottom perturbation. Secondly, we analyze four base runs that consist of a combination of a constant Chézy coefficient of 75 $m^{0.5}s^{-1}$ (C75) and the Van Rijn 2007 bedform predictor (VRIJN07) as the roughness formulations and the transport models by Van Rijn 1993 (TR1993) and Van Rijn 2004 (TR2004). Thirdly, the sensitivity analysis from part 1 will be extended with the slope parameter and the effect of grain size for a wavy bottom.

4.2.1 Fastest growing mode

The fastest growing mode (FGM) describes the wavelength with the largest growth rate and is therefore most likely to emerge over time. Figure 12 shows the FGM categorized for C75 and VRIJN07 combined with TR1993 and TR2004. Table 8 shows the preferred wavelength for these combinations, along with variations in grain size and bed slope parameter.

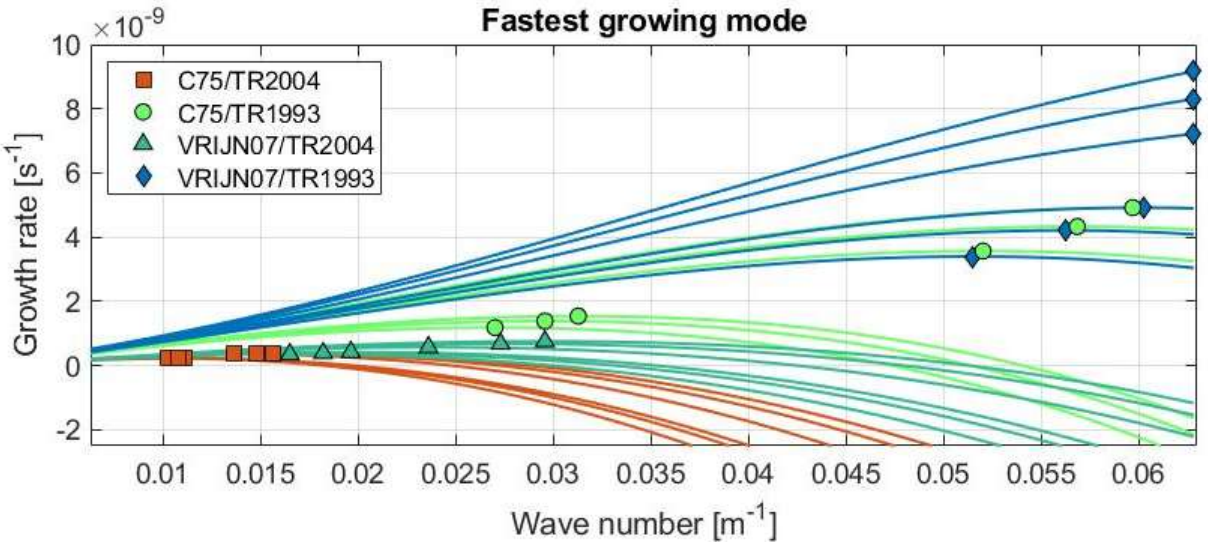

Figure 12. FGM categorized on roughness formulation and transport model based on wave number and growth rate.

Table 8. Preferred wavelengths in meters for C75 and VRIJN07 combined with TR1993 and TR2004. Grain size and bed slope parameter variations are also included for sensitivity purposes.

	Bed slope α [-]	3			1,5**		
Roughness	Grain size [mm] / Transport	0,3	0,35	0,4	0,3	0,35	0,4
C75	TR1993	232	212	201	121	110	105*
	TR2004	612	580	565	460	424	401
Vrijn07	TR1993	122	112	104*	100*	100*	100*
	TR2004	380	345	320	266	230	212

* These runs have smaller wavelengths than noted here, the shortest wavelength used in the FGM determination was 100 meters. It is arguable whether bedforms with these wavelengths can be classified as sand waves and this is therefore ignored.
** The effect of the bed slope parameter is large and displayed here with the purpose of showing the variability in preferred wavelength. It has not been considered further in this work due its ability to significantly affect the results.

Figure 12 shows that clusters occur for the roughness formulation and transport model combinations. Combinations with TR2004 tend to prefer large wavelengths with small growth rates, while TR1993 favors the short wavelengths with large growth rates. This behavior is already observed in part 1 where TR2004 generally estimates smaller sediment transport rates than the TR1993 counterpart. This can be explained by the bedload to suspended load transport ratio found in part 1. There, it was found that the bedload transport rates for TR1993 are nearly double the bedload rates of TR2004. This while the suspended load transport rate remains relatively even. It is known that the main growth mechanism of sand waves are circulation cells which transport sediment mostly in the bedload regime to the crests. So, this effect is enhanced due to the larger bedload transport rates, causing large growth rates for TR1993 as compared to TR2004.

Lastly, it is notable that the growth rate trend from the clusters in figure 12 is reversed from the sediment transport rates found in part 1. Where C75 has larger sediment transport rates for both transport models in a flat bottom case, VRIJN07 has larger growth rates for both transport models in a wavy bottom case. This is caused by the effect that the wavy topography has on the hydrodynamics and is elaborated further in §4.2.3.

4.2.2 Topography

In the previous part, VRIJN07 estimated a dynamic roughness based on the time-varying hydrodynamics through the current-wave mobility parameter. Since the bed was flat, hydrodynamics were uniform in space causing the bed roughness estimates to only vary temporally. The wavy bed leads to areas that are sheltered from the flow which cause decreased flow velocities and corresponding spatial variations in the current-wave mobility parameter. In the sand wave trough, the current-wave mobility parameter reaches approximately 44 during high tide while reaching approximately 48 at the crest as opposed to 46 for a flat bed.

When averaging the roughness height over the tidal cycle, a total roughness height estimated by VRIJN07 emerges of approximately 0.142m for the trough and 0.148m for the crest (Chézy coefficient = 60.65 $m^{1/2}s^{-1}$ and 60.5 $m^{1/2}s^{-1}$ respectively). So, during the tidal cycle a subtle roughness height gradient forms towards the crest, which likely occurs under periods with smaller flow velocities. However, these spatial variations are small and are caused by the fact that the megaripple roughness height limit of 0.2m is still reached for the lower values of the current-wave mobility parameter in the trough. So, although there is a high temporal variability in roughness height of VRIJN07, there is little to no spatial variability in roughness height caused by the small-amplitude sand wave. See appendix A for figures.

4.2.3 Hydrodynamics

A wavy bed will lead to variations in the flow velocity over the sand wave that is due to flow contraction and expansion when it passes. When considering flow in one direction, the sand wave shape initially causes flow contraction and inherently increases the flow velocity. Once the flow has passed the crest the water depth increases and the flow will expand, lowering the flow velocity. So, the backside of the sand wave is always sheltered and over the tidal cycle and both sides of the sand wave experience higher flow velocities and lower flow velocities once. This phenomenon generates circulation cells that is described by Hulscher (1996) and causes growth of the sand wave. Figure 13 shows these tide-averaged circulation cells over the sand wave for the various roughness formulation and transport model combinations.

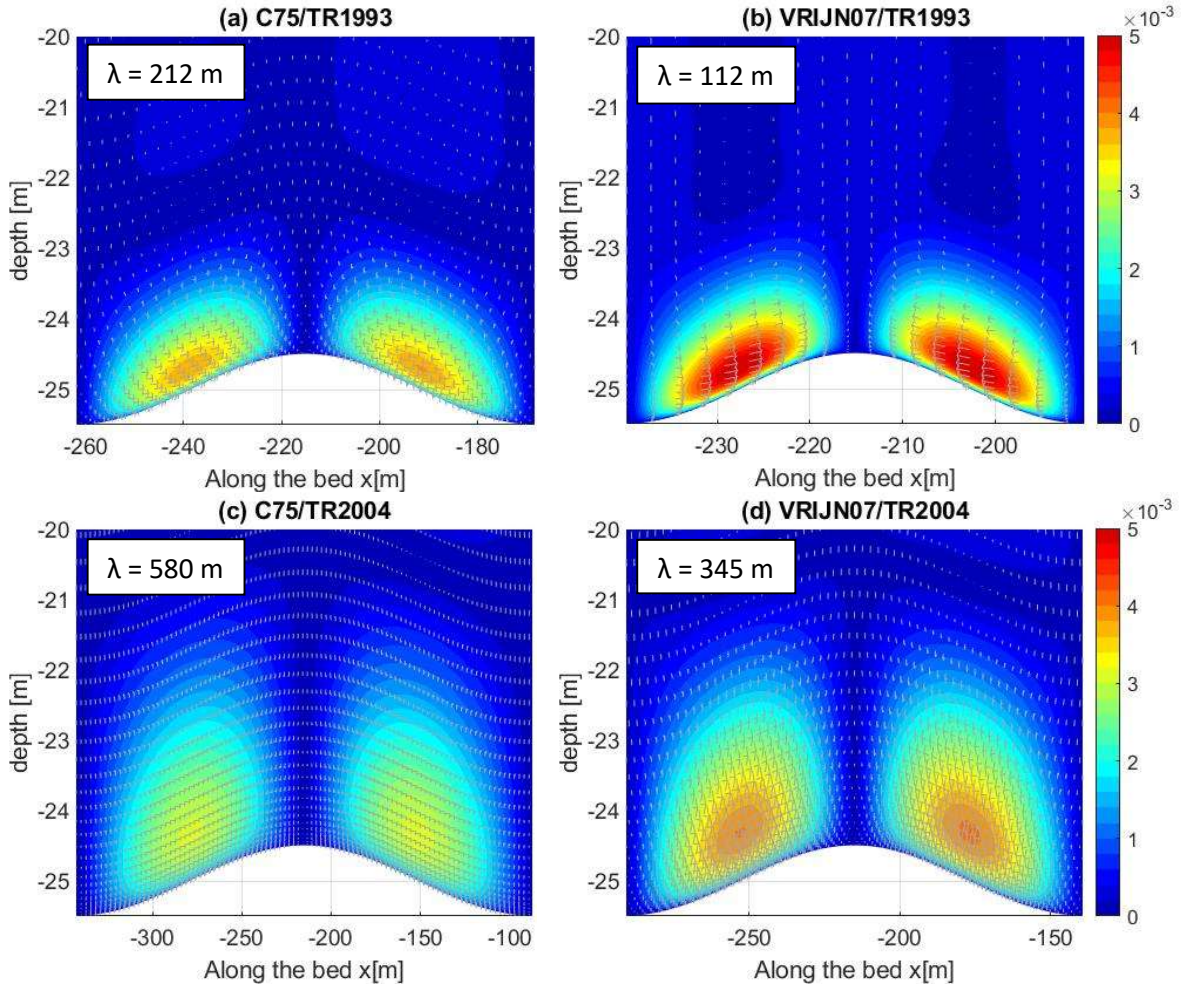

Figure 13. Tide-averaged flow velocity magnitude and circulation cells for C75(a,c) and VRIJN07(b,d) combined with TR1993(a,b) and TR2004(c,d). Note that the flow velocity on the right part of the sand wave represents negative flow velocities and convergence towards the crest occurs and that the x-axis have different scales.

Figure 13 shows that there are differences in tide-averaged flow velocities for both transport models. The fact that differences exist while the roughness magnitude is the same for both transport models and the transport model does not directly affect the flow velocities leads to the observation that the topography must cause differences. While the sand wave height is equal for all runs, the wavelength varies greatly when using the FGM from table 8. This means that the steepness of the slope is responsible for variations in the tide-averaged circulation cells. Generally, it was observed that TR1993 favors shorter wavelengths than TR2004 and thus have steeper slopes. Figure 13 shows that the TR1993 combinations indeed have stronger tide-averaged circulation cell velocities than TR2004, which also matches the larger growth rates observed in figure 12. While the milder slopes have lower tide-averaged circulation cell velocities, the circulation cell extends higher into the water column. Due to the longer wavelength that corresponds with milder slopes, the flow adapts more gradually and affect layers higher in the water column. The flow needs to adjust more rapidly for short and steep slopes, then a certain lag between water layers prevents the extension higher in the water column.

Since the wavelength seems to influence the tide-averaged circulation cells greatly, the combinations in figure 13 have been simulated with a fixed wavelength as well. The value for the fixed wavelength is chosen to be 312 m as this is the average FGM of the four combinations. By doing this, the variable wavelength influence is eliminated and the differences between the roughness formulations is isolated.

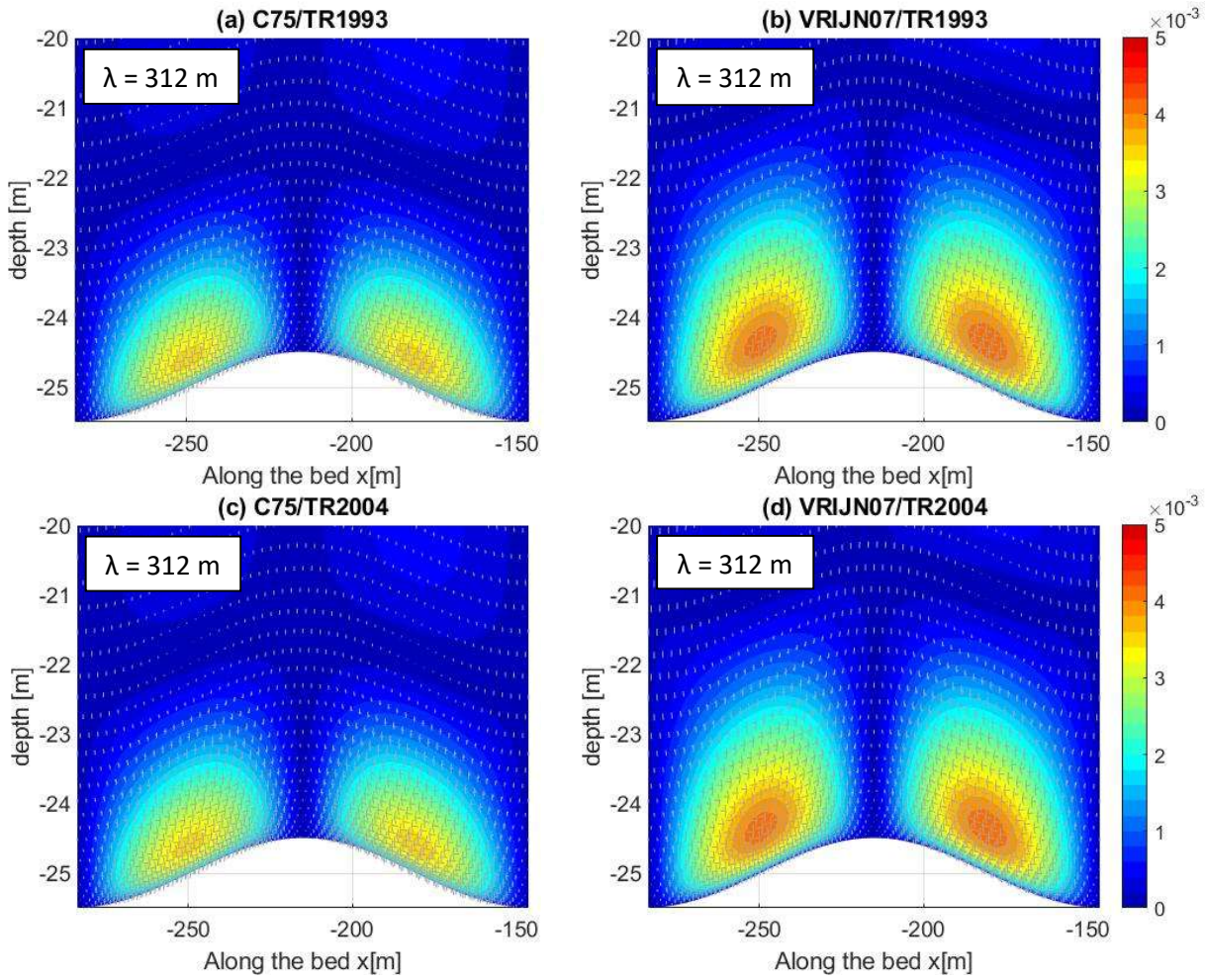

Figure 14. Tide-averaged flow velocity magnitude and circulation cells for C75(a,c) and VRIJN07(b,d) combined with TR1993(a,b) and TR2004(c,d) on a fixed wavelength of 312 meters. Note that the flow velocity on the right part of the sand wave represents negative flow velocities and convergence towards the crest occurs.

Figure 14 shows that once the wavelength is fixed for all runs, only the bed roughness influences the circulation cells and the effect of the transport model vanishes. C75 is confined near the bed while VRIJN07's influence spreads further into layers above and VRIJN07 shows more intense tide-averaged circulation cell velocities. Aside from flow expansion and contraction affecting flow velocities, a larger roughness decreases the flow velocity more as the flow passes over the sand wave. Effectively, this increases the difference between flow velocities on both slopes of the sand wave when considering one flow direction. Tide-averaged, this leads to more intense circulation cells. The observation that VRIJN07 extends higher into the water column is because a rougher bed affects water layers further away from the bed.

The variability in circulation cell strength is largest when the sand wave is given its corresponding preferred wavelength and the difference in roughness method mainly seems to have effect on the circulation cell shape. This implies that the effect of the sand wave shape has a dominant effect over the bed roughness magnitude.

4.2.3.1 Bed shear stress

Part 1 consisted of a flat bed and averaging the bed shear stress over a tidal cycle would result in a net zero bed shear stress due to the symmetrical flow velocities. However, the circulation cells shown in figure 13 imply asymmetrical tide-averaged flow velocities and result in non-zero tide-averaged bed

shear stresses. The resulting tide-averaged and maximum bed shear stresses over the sand wave are shown in figure 15.

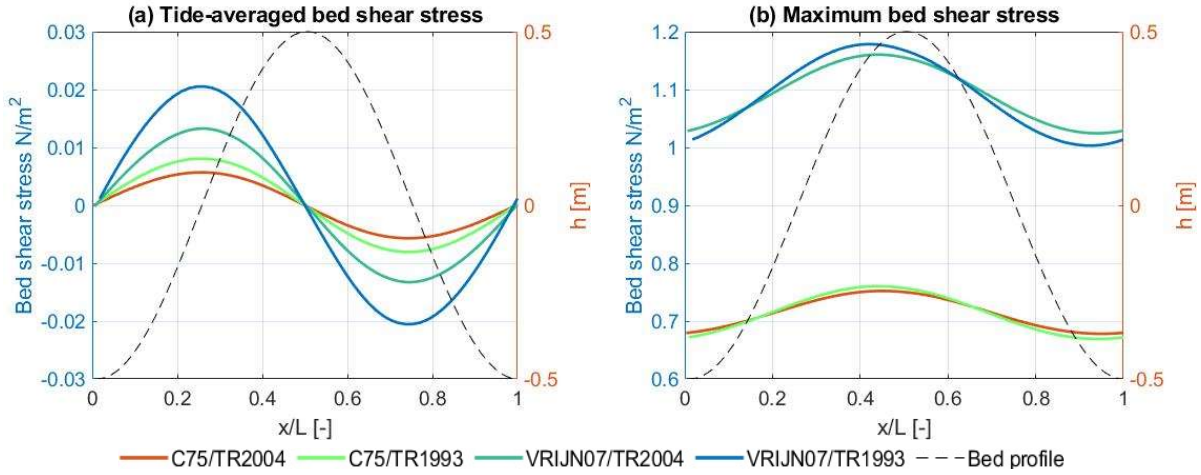

Figure 15. Tide-averaged bed shear stress (a) and maximum bed shear stress (b) during flow in positive x-direction for C75 and VRIJN07 combined with combined with TR1993 and TR2004. Note that positive values imply bed shear stress directed towards the right while negative values imply a direction towards the left.

Figure 15 shows variations in bed shear stress that are caused by the difference in tide-averaged flow velocity from the circulation cells. Given that VRIJN07 estimates a rougher bed, a larger magnitude bed shear stress is generated. The maximum bed shear stress is generated on the upper slope of the sand wave as the crest has the largest bed roughness magnitude and is subjected to the highest flow velocities. The spatial variation in maximum bed shear stress means that a sediment particle of the same size may be mobilized on the sand wave crest while the threshold of motion is not exceeded in the trough. Furthermore, the large difference between C75 and VRIJN07 means that larger sediment fractions may be mobilized by VRIJN07 and changes in the sediment transport mode ratios may occur.

4.2.4 Sediment transport

The wavy bottom gives rise to circulation cells and will lead to non-zero sediment transport rates at the slopes. Herein, a larger circulation cell intensity will inherently lead to larger transport rates as the tide-averaged flow velocity towards the crest is larger. Furthermore, the distinction between TR1993 and TR2004 is made which will both translate the hydrodynamics differently and thus estimate different sediment transport rates. The tide-averaged bedload and suspended load transports for the roughness and transport model combinations are shown in figure 16a,c. To eliminate the effect of topography on sediment transport rates, the wavelength has also been fixed at 312 m in figure 16b,d, this is the average FGM of the four combinations.

Tide-averaged, the bedload and suspended load transports show convergence of sediment towards the crest which lead to sand wave growth. This behavior is expected as the initial perturbation only has an amplitude of 0.5 meters and the equilibrium amplitude of sand waves is generally far greater. Figure 16a and c also illustrates the reason why TR1993 showed the largest growth rates in figure 12. The combination of intense circulation cells, favoring bedload regime and generally larger sediment transport rates for TR1993 leads to significantly larger growth rates than TR2004. The bedload transport rates for TR2004 are lower but shows a more balanced ratio between bedload and suspended load transport. When looking at the roughness formulation, it appears that the bedload transport rate for VRIJN07 is larger than C75, while having lower suspended loads than C75. This does not correspond to the behavior observed for a flat bed, where C75 had both larger bedload and suspended load transport rates. This is likely caused by the fact that the preferred wavelength for

VRIJN07 is lower than C75, which leads to more intense circulation cells and thus transport in the bedload regime.

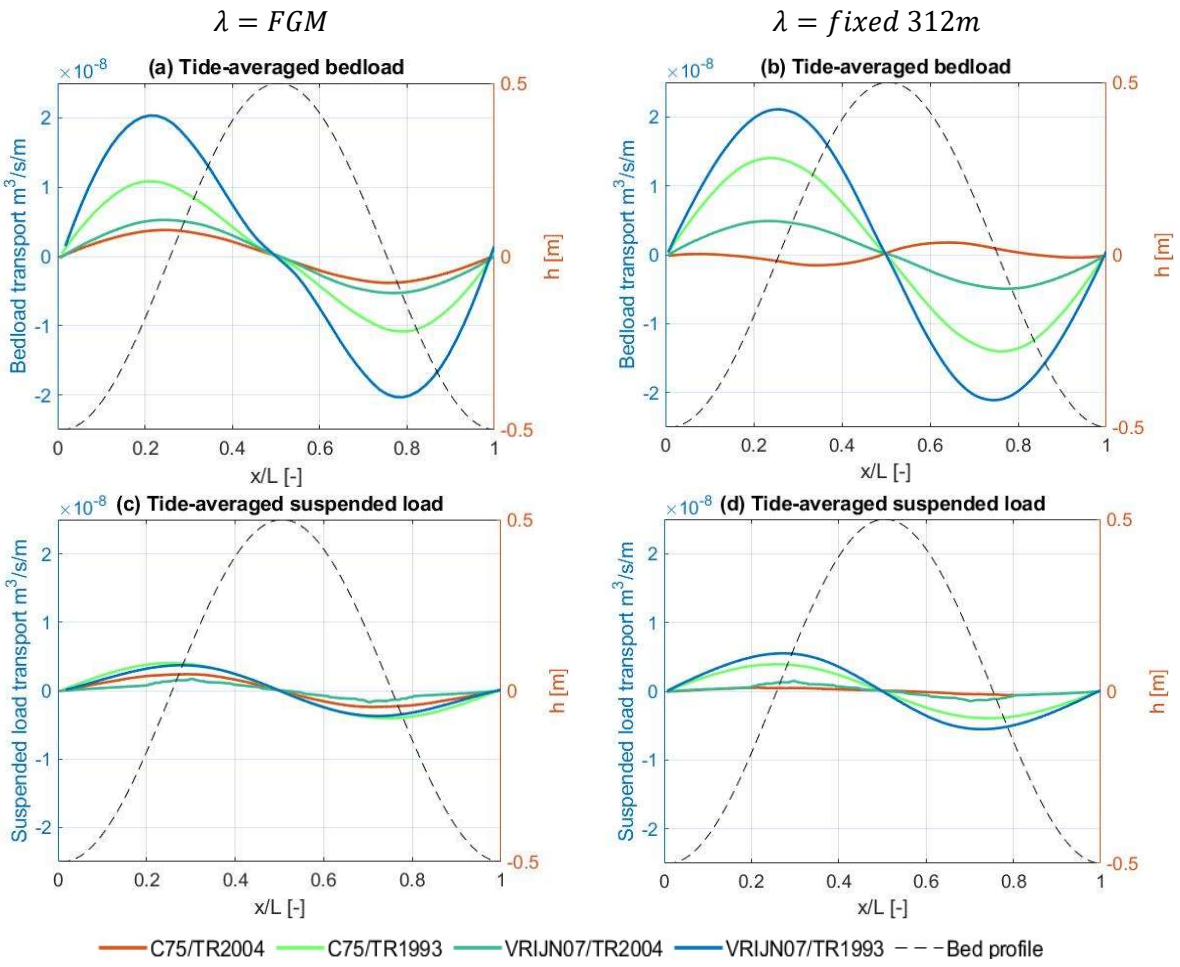

Figure 16. Tide-averaged bedload (a) and suspended load (c) transport for C75 and VRIJN07 combined with TR1993 and TR2004 for the preferred wavelength, and (b,d) respectively for a fixed wavelength of 312m. Positive values imply transport to the in the positive x-direction.

Figure 16b and d show that using a fixed wavelength of 312m mainly affects the C75/TR2004 combination. The bedload transport diverges from the sand wave crest which implies decay of the sand wave and the suspended load transport decreases to near zero. This is likely caused by the fact that the FGM of this combination is 580m, which leads to compensation effects during the initial response phase. Both TR1993 combinations seem to slightly increase the bedload and suspended load transport rates and the bedload transport peak is concentrated slightly more towards the crest. In this case, these combinations attempt to reach their preferred smaller wavelength by transporting more sediment towards the crest. The observation that this is compensation behavior is supported by the fact that the FGM of VRIJN07/TR2004 is close to the fixed wavelength and this combination shows equal bedload and suspended load transport rates for both wavelengths.

It is noteworthy that TR2004 produces 'wiggles' in the suspended load transport. However, it is unclear what causes these irregularities. This will be elaborated in chapter 5.

4.2.5 Highlights

Here, the most important results are summarized from this part.

- The preferred wavelength shows clusters with C75 favoring larger wavelengths and slower growth rates than VRIJN07. TR1993 shows larger growth rates and shorter wavelengths than TR2004.
- The small amplitude sand wave does not have a significant effect on the bed roughness estimates of VRIJN07. This is caused by the megaripple roughness height limit of 0.2 meters.
- Bed roughness increases the difference in flow velocity over the sand wave. Tide-averaged, this leads to more intense circulation cells. However, this effect is overshadowed by the circulation cell sensitivity to the topography. Steep slopes increase the circulation cell strength considerably.
- VRIJN07 generally has stronger circulation cells than C75. This generates larger bed shear stresses which cause more sediment transport towards the crest.
- The transport rates are heavily affected by the transport model as TR1993 estimates far greater transport than TR2004. Furthermore, the bedload regime is dominant for TR1993 while TR2004 shows a balanced bedload to suspended load ratio.

4.3 Initial large amplitude sand wave stage

The low amplitude sand wave results showed some observations that could be investigated further. This mainly aims at the fact that very little spatial variation in bed roughness was estimated by the Van Rijn 2007 bedform predictor (VRIJN07). Therefore, the initial sand wave amplitude is increased to 1.5m in order to see whether VRIJN07 estimates spatial variation. This is done as field observations by Damveld et al. (2018) show distinct variations between the crest and trough of sand waves. Small-scale bedforms are present at the crest, while these are absent in the trough. Furthermore, we try to imitate this observation by manually defining a spatially variable Chézy coefficient (Cspatial) ranging from rough (50 $m^{0.5}s^{-1}$) at the crest to smooth (80 $m^{0.5}s^{-1}$) at the trough.

The considered combinations will consist of C75/TR1993, Cspatial/TR1993, Cspatial/TR2004 and VRIJN07/TR2004. In this, C75/TR1993 is regarded as the default setup and VRIJN07/TR1993 is excluded based on the results from the low amplitude sand wave. This is because this combination already estimates significantly higher bedload transport than the other combinations as well as a wavelength of 112 meters. It is arguable whether such wavelength still classifies as a sand wave. Furthermore, when tripling the wave height, the wavelength remains similar. This means that the bed slope becomes even steeper, generating stronger circulation cells, even faster growth rates and shorter wavelengths.

4.3.1 Fastest growing mode

The fastest growing mode (FGM) describes the preferred wavelength of the model setup and is used to define the initial topography. Figure 17 shows the FGM categorized for C65 combined with TR1993 and TR2004, C75/TR1993 and VRIJN07/TR2004. Herein, C65 is used as a substitution for the reasons described in §3.5. As a comparison to the low amplitude sand wave, the FGM and growth rates for C75/TR1993 and VRIJN07/TR2004 have been added in table 9.

Table 9. Preferred wavelengths and growth rates comparison for 0.5- and 1.5-meter sand wave amplitude with combinations C75/TR1993 and VRIJN07/TR2004.

	Sand wave amplitude 0.5m		Sand wave amplitude 1.5m	
Combination	FGM [m]	Growth rate [s^{-1}]	FGM [m]	Growth rate [s^{-1}]
C75/TR1993	212	$1.36*10^{-9}$	219	$2.69*10^{-9}$
VRIJN07/TR2004	345	$3.86*10^{-10}$	350	$3.80*10^{-10}$

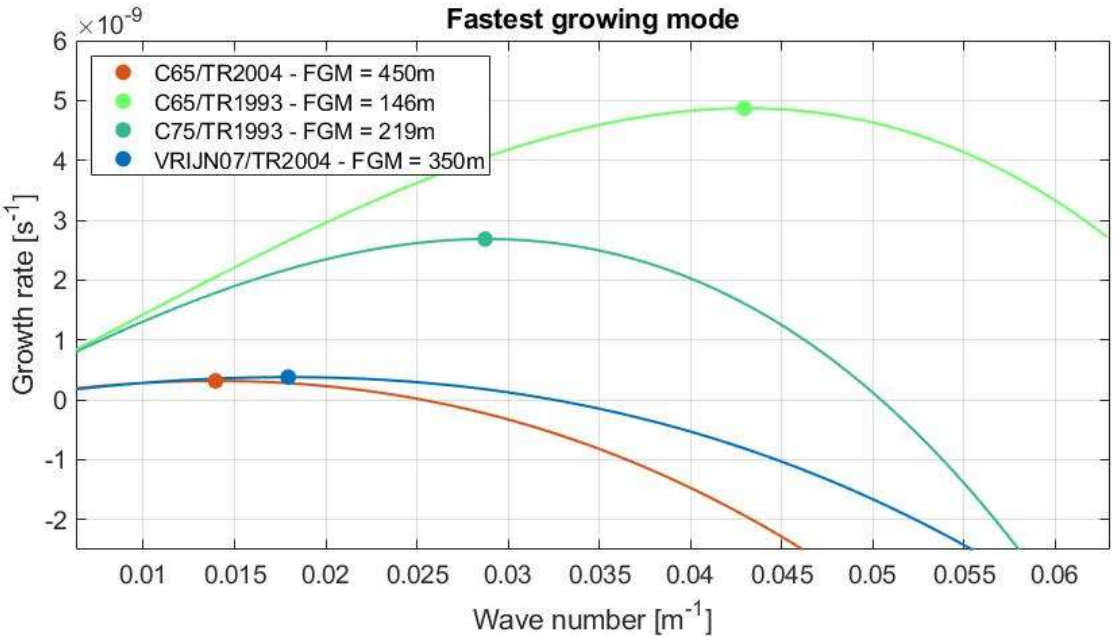

Figure 17. FGM categorized on roughness formulation and transport model based on wave number and growth rate, with the FGM shown in the legend in meters.

Figure 17 shows that the trend found in the low amplitude sand wave also occurs for larger amplitude sand waves. TR1993 estimates the largest growth rates and smallest wavelengths while TR2004 has small growth rates but long wavelengths. Table 9 compares the FGM and growth rate of the two runs that also have been considered for the low amplitude sand wave. It shows that the wavelength remains relatively unchanged for a significant increase in sand wave amplitude. However, the growth rate for C75/TR1993 has doubled while the growth rate of VRIJN07/TR2004 as remained equal. An increase in growth rate is expected, the wavelength is similar while the sand wave amplitude tripled. This increases the steepness of the slope which then leads to stronger circulation cells moving more sediment towards the crest. The fact that VRIJN07/TR2004 does not show this behavior is likely caused due to the larger suspended sediment component that was observed for the low amplitude case, which dampens the sand wave and reduces growth rate.

4.3.2 Topography

Similar to the low amplitude case, the current-wave mobility parameter is used in VRIJN07 to estimate the bed roughness over the sand wave. The increase in sand wave amplitude leads to more sheltering of the trough which cause decreased flow velocities and corresponding spatial variations in the current-wave mobility parameter. In the sand wave trough, the current-wave mobility parameter reaches approximately 39 during high tide while reaching approximately 53 at the crest as opposed to 44 and 48 correspondingly for the 0.5m amplitude case. However, the current-wave mobility parameter is still large enough to reach the maximum megaripple roughness height of 0.2m for both the crest and trough. Effectively, this means that the spatial variability of VRIJN07 is hardly increased for the larger sand wave amplitude compared to both the low amplitude and the flat bottom case. See appendix A for figures. Figure 18 shows the tide averaged Chézy coefficient wherein the total roughness height estimated by VRIJN07 is inserted in equation 3 to obtain the Chézy coefficient.

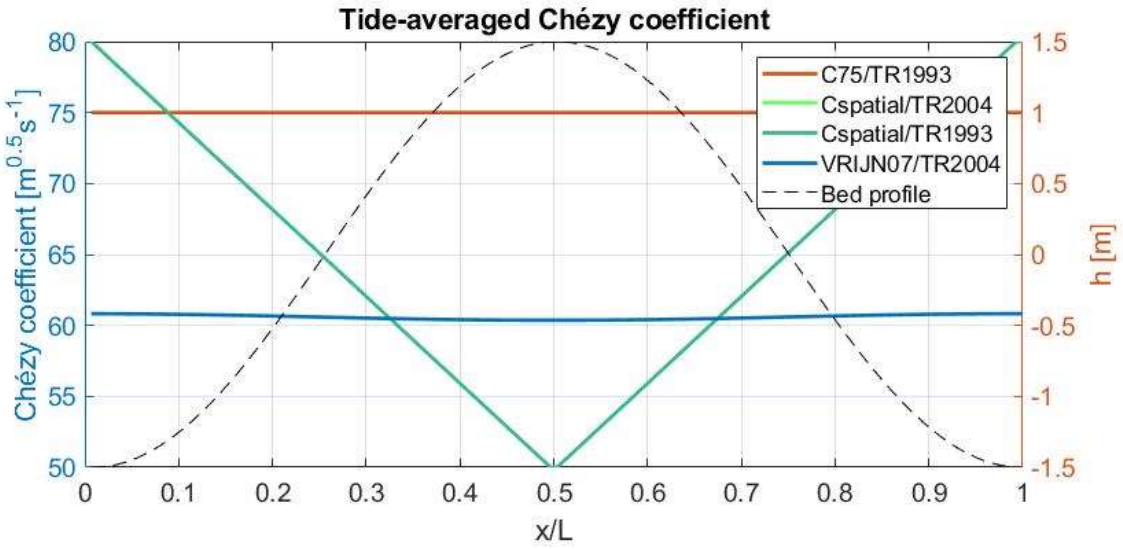

Figure 18. Tide averaged Chézy coefficient for C75/TR1993, VRIJN07/TR2004 and Cspatial combined with TR1993 and TR2004 for large amplitude sand wave.

4.3.3 Hydrodynamics

A larger amplitude sand wave will have a larger impact on the circulation cells as we previously saw that the shape of the sand wave is very influential for the circulation cells strength. The circulation cells for a 1.5-meter amplitude sand wave with the preferred wavelengths from figure 17 are shown in figure 19.

When comparing the circulation cell strength of the low-amplitude and large amplitude sand wave, it shows that the strength has increased significantly. This is due to the fact that the sand wave amplitude has tripled while the preferred wavelength has only change by some meters. This means that the slope is even steeper, enhancing the circulation cell strength.

Figure 19d shows that Cspatial/TR2004 has significantly stronger circulation cells than C75/TR1993 and VRIJN07/TR2004. This does not follow the previously observed pattern that shorter wavelengths lead to more intense circulation cells as the wavelength for Cspatial/TR2004 is larger. In §4.2.3, it was observed that a larger bed roughness magnitude leads to stronger circulation cells. However, this effect could not be observed when defining the wavelength as the FGM as the topography was found to be dominant over bed roughness on the circulation cell strength. So, in this case Cspatial/TR2004 overcomes this topography dominance for large wavelengths. For Cspatial/TR1993, the strong circulation cells are enhanced further by the large magnitude of bed roughness. For this reason, fixing the wavelength (291m in this case) to isolate the behavior of bed roughness does not result in significantly different behavior of Cspatial. The difference with a fixed wavelength is largest for Cspatial/TR1993 since the enhancement with the topography is removed. Effectively, the increase of wavelength leads to slightly larger circulation cells that are less intense. For Cspatial/TR2004, the fixed wavelength is shorter and leads to slightly smaller and more intense circulation cells. Both results are consistent with previous observations that shorter wavelengths lead to intenser circulation cells. This comparison is shown in appendix E.

It is important to note that the Cspatial results will show some form of compensating effects due to the roughness being interpolated on a preferred wavelength for a simulation with a Chézy coefficient of 65 $m^{0.5}s^{-1}$ which means that the used wavelength deviates from the preferred wavelength.

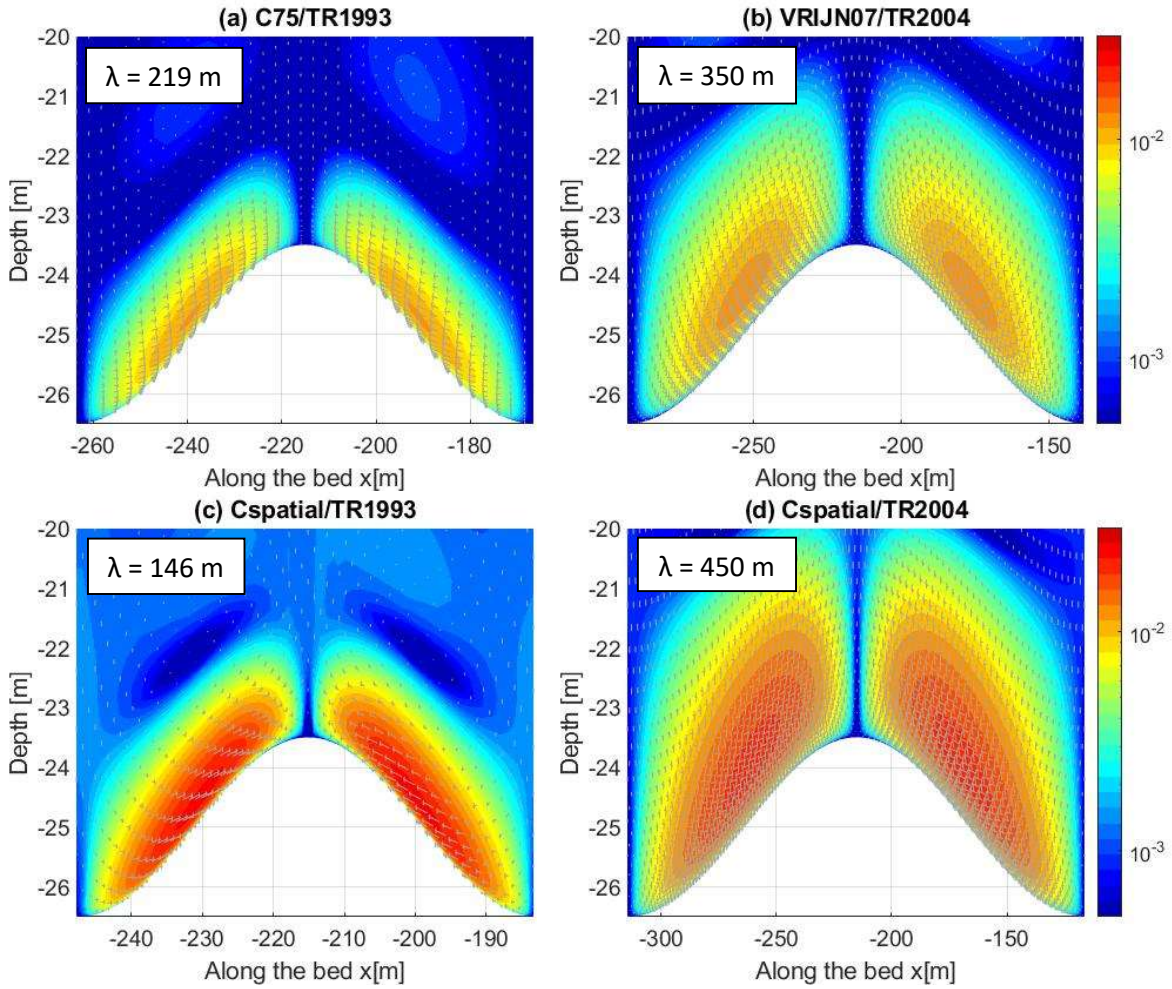

Figure 19. Tide-averaged flow velocity magnitude and circulation cells for C75/TR1993 (a), VRIJN07/TR2004 (b) and Cspatial combined with TR1993 (c) and TR2004 (d) for large amplitude sand wave.

4.3.3.1 Bed shear stress

The increase in circulation cell strength due to the increase in sand wave amplitude leads to an increase in bed shear stress as well. The tide-averaged and maximum bed shear stresses over the sand wave are shown in figure 20.

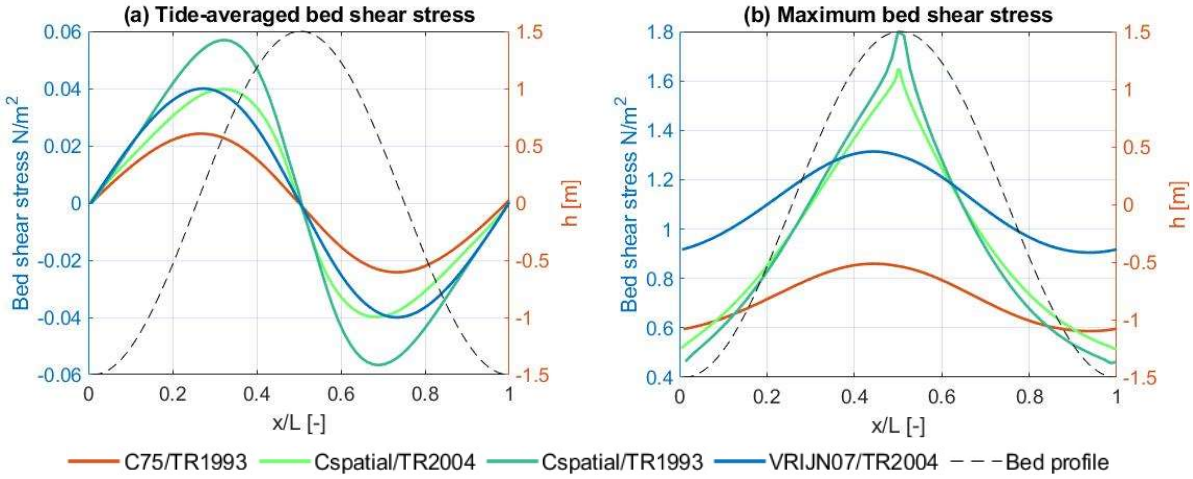

Figure 20. Tide-averaged bed shear stress (a) and maximum bed shear stress (b) during flow from left to right for C75/TR1993, VRIJN07/TR2004 and Cspatial combined with TR1993 and TR2004 for large amplitude sand wave. Note that positive values imply bed shear stress directed towards the right while negative values imply a direction towards the left.

When comparing figure 20 with the low-amplitude case in figure 15, it shows that the tide-averaged bed shear stresses have increased by approximately threefold while the maximum bed shear stresses only increased by 0.1 Nm^{-2}. This implies that the maximum hydrodynamic forces have not necessarily have increased in strength but show larger flow velocities during a longer period of the tidal cycle. The fact that the maximum bed shear stress has only increased relatively little is because the flow velocity forced on the system boundaries is still equal and the bed roughness for the considered runs has not increased. As these are the two main components of bed shear stress, the maximum bed shear stress cannot significantly increase.

The Cspatial combinations show skewed peaks towards the crest, this is because the bed roughness increases linearly towards the crest, while the flow velocity increases as well due to flow contraction. Furthermore, the maximum bed shear stress for the Cspatial is shaped triangularly as bed shear stress is generated by the interaction of bed roughness and flow velocity. When both are largest, the largest bed shear stress will be generated. Since the bed roughness does not vary temporally, the maximum bed shear stress is generated during high tide. There is a slight gradient in both slopes due to the differences in flow velocity at the stoss and lee slope that is caused by decreasing flow velocities due to the bed roughness. The triangular shape means that there might be significant variation in local sediment transport once different sediment fractions are implemented.

4.3.4 Sediment transport

A larger amplitude sand wave affects the hydrodynamics and significantly increases the tide-averaged bed shear stresses while only slightly increasing the maximum bed shear stresses. This implies that the duration of relatively large bed shear stresses increases during the tidal cycle. Consequently, this leads to longer durations wherein sediment is mobile and inherently more sediment transport. Furthermore, the locations on the sand wave where bed shear stresses are largest change, meaning a change in sediment transport location will occur as well. Figure 21 shows the tide-averaged bedload and suspended load transport rates.

Comparing figure 21 with figure 16a,c shows a significant increase in transport rates, which is a consequence of the increased bed shear stresses. C75/TR1993 continues to show sand wave growth for a 1.5-meter amplitude sand wave. However, while convergence of sediment in both transport regimes occurs at the lower sand wave slopes, the crest shows slight divergence in bedload transport from the crest. For the total transport rate this results in sand wave growth on the lower slopes while the crest has neutral transport rates. This means that the initial response of the sand wave is not to grow in height, but rather increase the wavelength. VRIJN07/TR2004 shows convergence towards the crest for both bedload and suspended load transport. Although the transport rate is relatively small, the 1.5-meter amplitude sand wave will continue to grow at a slow rate.

Cspatial/TR1993 shows large bedload transport convergence towards the crest. This is the result of intense circulation cells and bed shear stresses causing large transport in the bedload regime. Additionally, TR1993 enhances the bedload transport rates as this transport model heavily emphasizes the bedload regime. The suspended load transport rate large decay of the sand wave crest. This is because the bed roughness and thus bed shear stress on the crest is largest which leads large quantities of sediment being suspended. Since the flow velocity is also largest near the crest, suspended particles are transported away from the crest rapidly by the currents. The initial response of the 1.5-meter amplitude sand wave is to decrease the sand wave height rapidly. Note that this effect is likely caused by compensation of the wavelength, as the used wavelength for Cspatial is the fastest growing mode of a Chézy coefficient of $65 m^{0.5} s^{-1}$.

Cspatial/TR2004 shows convergence of bedload towards the crest that is skewed towards the upper slope. The bedload transport of Cspatial/TR2004 wants to increase the sand wave height while sustaining the wavelength. The suspended load transport shows a massive peak in transport rate towards the crest on the middle slope. It is uncertain what causes this peak in transport and not physically explainable. Therefore, this combination will not be used for following simulations.

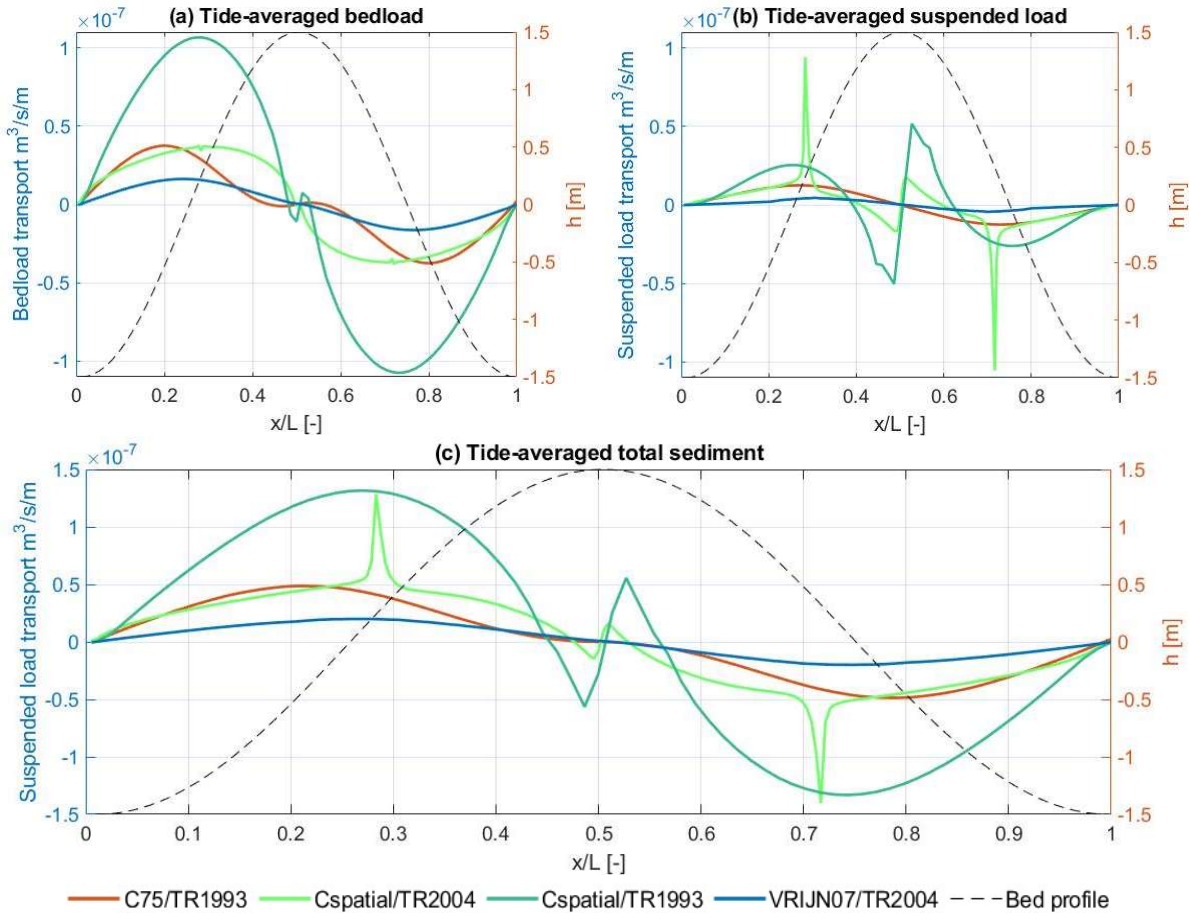

Figure 21. Tide-averaged bedload (a), suspended load (b) and total transport (c) for C75/TR1993, VRIJN07/TR2004 and Cspatial combined with TR1993 and TR2004 for large amplitude sand wave. Positive values imply transport to the right and negative values to the left.

4.3.5 Highlights

Here, the most important results are summarized from this part.

- Increasing the sand wave amplitude to 1.5 meters shows only a small change in preferred wavelength leading to significantly steeper slopes and more intense circulation cells than the 0.5m amplitude case.
- The large amplitude sand wave does not have a significant effect on the bed roughness estimates of VRIJN07. This is caused by the megaripple roughness height limit of 0.2 meters.
- When forcing spatial variability with Cspatial, the bed roughness magnitude becomes large enough to exceed the influence of the topography on the circulation cells.
- The tide-averaged bed shear stress becomes larger rather than the maximum bed shear stress. So, bed shear stress magnitudes from a low-amplitude sand wave are generated for a longer duration of the tidal cycle, rather than stronger circulation cells leading to larger magnitude bed shear stresses. For sediment transport, this means that a larger quantity of sediment is transported during the tidal cycle instead of coarser material becoming mobile.
- Generally, the total transport rates are still towards the crest which implies sand wave growth.

4.4 Long term equilibrium stage

The initial response showed quite different behavior between the roughness method and transport model combinations. In this part, it is investigated how the initial response develops further towards the equilibrium stage for C75/TR1993, Cspatial/TR1993 and VRIJN07/TR2004.

4.4.1 Case I: C75/TR1993

Case I consists of the combination C75 and TR1993, with an initial sand wave amplitude of 0.5 meters and the FGM of 212 meters. This combination has been analyzed for the low- and large amplitude case where the following observations were made. The growth rate for a 0.5-meter amplitude sand wave was $1.36*10^{-9}$ s^{-1} while it doubled to $2.69*10^{-9}$ s^{-1} for the 1.5-meter amplitude sand wave case. Compared to other combinations, the circulation cell strength was relatively weak while the tide-averaged flow velocity for the 1.5-meter amplitude case was triple that of the 0.5-meter amplitude case. Bedload regime was dominant for both amplitudes, large transport rates were observed towards the crest for the 0.5-meter amplitude case. The 1.5-meter amplitude case showed relatively large transport rates towards the crest on the slopes, while sediment transport on the crest was neutral. To see how these initial responses translate to a longer timeframe, the morphological bed profile development over 100 years is shown in figure 22.

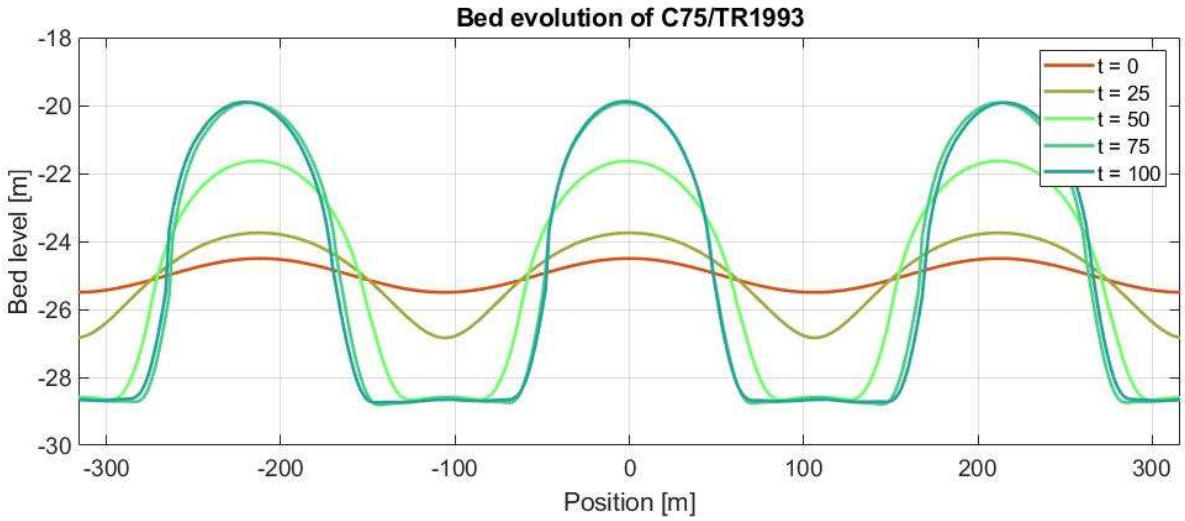

Figure 22. Bed evolution of C75/TR1993 over time in years.

C75/TR1993 serves as the reference case to compare Cspatial/TR1993 and VRIJN07/TR2004 to. The default case of Van Gerwen et al. (2018) is used, the bed profile evolution in figure 22 shows a match of bed profile after 100 years of simulating. Therefore, for elaboration of the morphological development towards this equilibrium position we refer to Van Gerwen et al. (2018).

4.4.2 Case II: Cspatial/TR1993

Case II consists of the combination Cspatial and TR1993, with an initial sand wave amplitude of 0.5 meters and the FGM of C65 which is 141 meters. This combination has been analyzed for the large amplitude case only and the following observations were made. The growth rate for a 1.5-meter amplitude sand wave was $4.87*10^{-9}$ s^{-1}, which is the fastest growth rate of the considered combinations. This fast growth rate is caused by strong circulation cells and leads to more than double the sediment transport rate on the slopes as any other combination. Although the bedload regime is dominant, relatively large suspended sediment transport divergence occurs at the sand wave crest. Total transport rates show growth of the slopes and decay of the sand wave crest. To see how these

initial responses translate to a longer timeframe, the morphological bed profile development over 100 years is shown in figure 23.

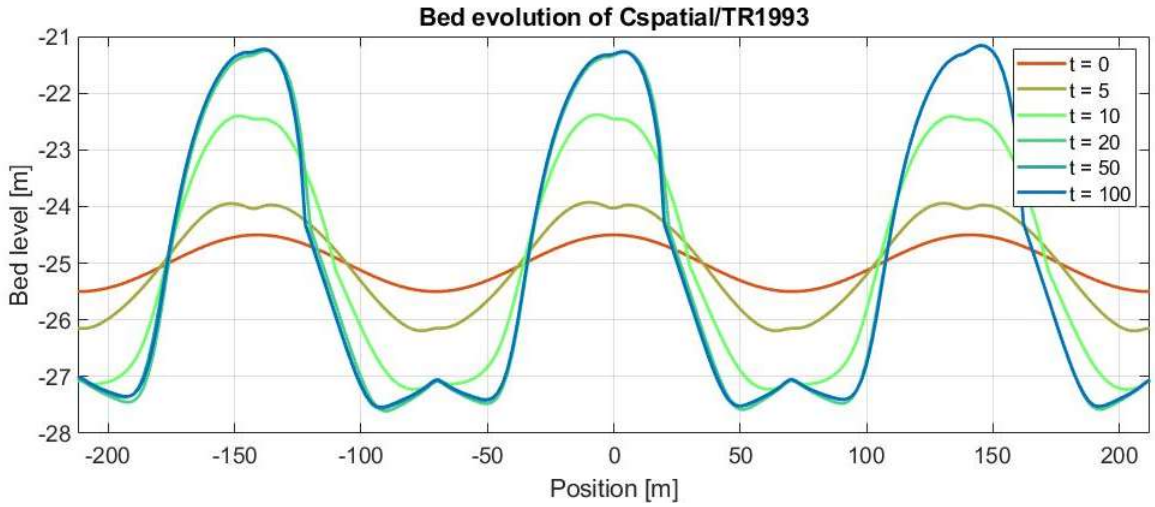

Figure 23. Bed evolution of Cspatial/TR1993 over time in years.

With the largest growth rate of all three combinations, it is expected that Cspatial/TR1993 reaches its equilibrium position in the shortest timespan. Although the linear behavior of the bed roughness from trough to crest is quite artificial, it depicts that bed roughness can be a very influential parameter on a long term when comparing figure 23 and figure 22. Between case I and II only the bed roughness is changed, which leads to shorter wavelengths, stronger circulation cells and thus faster growth.

In the first years of bed evolution the bed profile shows that erosion occurs at the crest which causes a deformation. This is a result of the strong suspended sediment divergence from the crest discussed and observed in §4.3.4 and is likely caused by compensation for the initial wavelength. As time progresses, the crest deformation becomes less pronounced.

On a longer term the same behavior as C75/TR1993 is observed for the sand wave trough. Once the troughs have reached their equilibrium depth, coarser sediment particles begin to accumulate here and create a hump. This process is enhanced as compared to case I because of the spatially varying bed roughness. Firstly, the way the spatially varying bed roughness is defined is that the roughness is largest at the crest while being lowest at the trough. Furthermore, since the bed roughness is temporally uniform, only the flow velocity magnitude will affect the bed shear stresses. This means that the maximum bed shear stresses at the crest are always larger than any other place of the sand wave. So, this leads to larger sediment fractions being mobile at the crest and once they settle at the slopes or trough, hydrodynamic action is likely not sufficient anymore to overcome the threshold of motion. Coarse sediment deposited on the slopes could become mobile through slope-induced transport, but become immobile once at the trough.

This process is also the reason for the limited sand wave equilibrium height. As there is always more bed shear stress at the top, more sediment is eroded here. At the trough, the bed shear stress likely does not exceed the critical bed shear stress of the coarser troughs. Furthermore, although this combination has strong circulation cells able to move relatively coarse material from the slopes to the crest, this material likely remains mobile once it has reached the crest for a longer period of the tidal cycle. The growing sand wave leads to steeper slopes and at a certain point the still mobile particles will go into the slope-induced regime adding to the decaying mechanism of more erosion at the crest. This combination severely limits the height that the sand wave can attain.

4.4.3 Case III: VRIJN07/TR2004

Case III consists of the combination VRIJN07 and TR2004, with an initial sand wave amplitude of 0.5 meters and the FGM of 345 meters. This combination has been analyzed for the low- and large amplitude case where the following observations were made. The growth rate for a 0.5-meter amplitude sand wave was $3.86*10^{-10}$ s^{-1} and remained equal for the 1.5-meter amplitude case with $3.80*10^{-10}$ s^{-1}. Compared to other combinations, the circulation cell strength was slightly stronger than C75/TR1993 but significantly weaker than Cspatial/TR1993. VRIJN07/TR2004 shows a balanced bedload to suspended load ratio and an increase in tide averaged sediment transport rate of approximately 3 times from the 0.5-meter amplitude case to the 1.5-meter amplitude case, directed towards the crest. To see how these initial responses translate to a longer timeframe, the morphological bed profile development over 350 years is shown in figure 24.

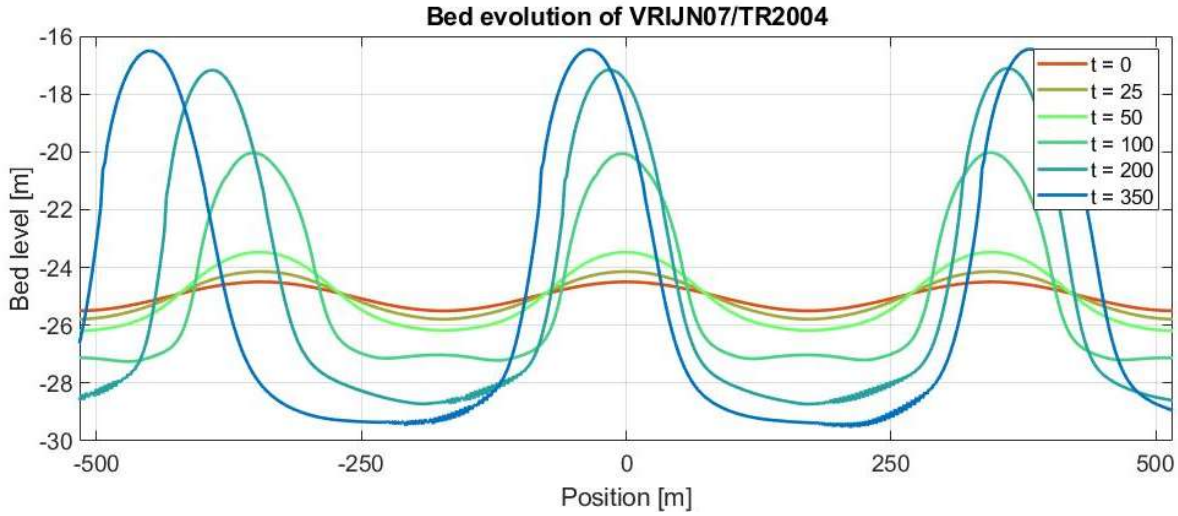

Figure 24. Bed evolution of VRIJN07/TR2004 over time years.

Previously we observed that VRIJN07/TR2004 shows very slow growth rates and this translates to requiring over 350 years to reach an equilibrium position. This is because TR2004 is a more conservative model, leading to lower sediment transport rates. Also, the dynamics in temporal roughness causes the roughness to decrease with lower tides as well. This causes both flow velocity and the bed shear stress to decrease when slack tide is approaching. This likely leads to insufficient bed shear stress for the transport of sediment. During high tide, because of the megaripple roughness height limitation, there is little to no spatial variation over the sand wave. This means that VRIJN07 is reduced to temporal variability only and therefore governed by the change in flow velocity. Since a large portion of the tidal cycle consists of low flow velocities, less sediment transport will occur during slack tide and the majority of sediment transport will occur during high tide.

Due to the low spatial variability in bed roughness and relatively small variation in flow velocity over a low amplitude sand wave, this means that the sediment transport over the sand wave is quite similar during early stages. This leads to a relatively small net sediment transport towards the crest and somewhat balanced growth of the crest and decay of the trough in the first 50 years. However, as the sand wave increases in height it is possible that the spatial variability in bed roughness increases and the sheltering effect of the troughs increases as well. Larger differences of bed roughness, flow velocity and thus bed shear stress will occur for larger amplitudes leading to different erosion and accretion rates. For example, at 100 years the lower sand wave slopes have been eroded at a faster rate than the trough. This is due to a combination of the trough being slightly more sheltered causing grains to become immobile and increasing slope-induced transport as a result of steeper bed slopes.

There seems to be some migration of the sand waves which is caused by influence from the boundaries. Because the wavelength is relatively long, less sand waves fit in the domain causing the center sand wave to be affected by the boundary conditions. Over time, the sand wave troughs become quite wide. This is partly caused by the outward migration of sand waves because of interference from the boundary conditions. Although this can be fixed by increasing the computational domain, it will increase the simulation duration even more.

Finally, it is noteworthy that some noise develops in the bed of the lower stoss slope later in the simulation. It is unknown what causes this and is possibly caused by some numeric error, but does not seem to affect the simulation significantly.

4.4.4 Comparison

From the previous figures we already got an insight in how the individual cases develop towards the equilibrium position. In this section, a comparison of the morphological development over time will be made for the three cases. Figure 21 shows the sand wave height development over time and figure 26 shows the crest and trough evolution over time.

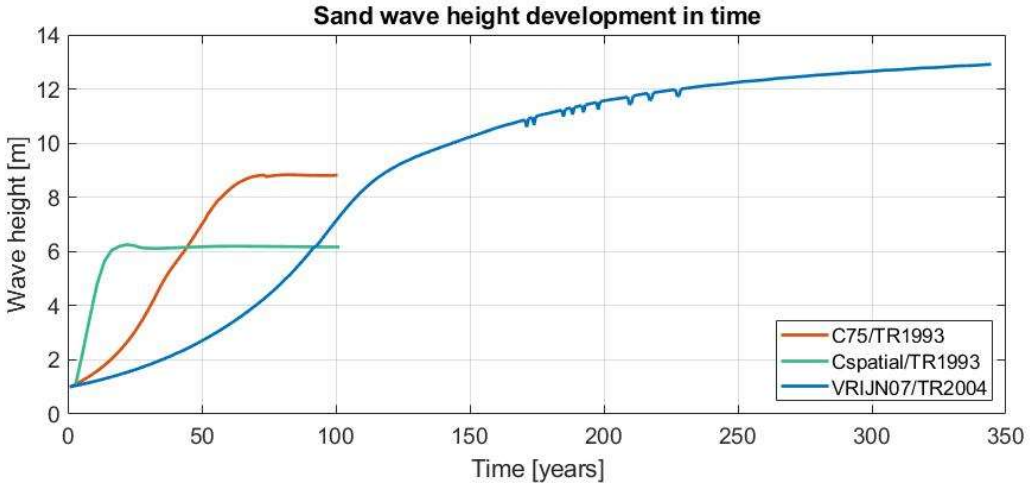

Figure 25. Development of the sand wave height over time in years for C75/TR1993, Cspatial/TR1993 and VRIJN07/TR2004.

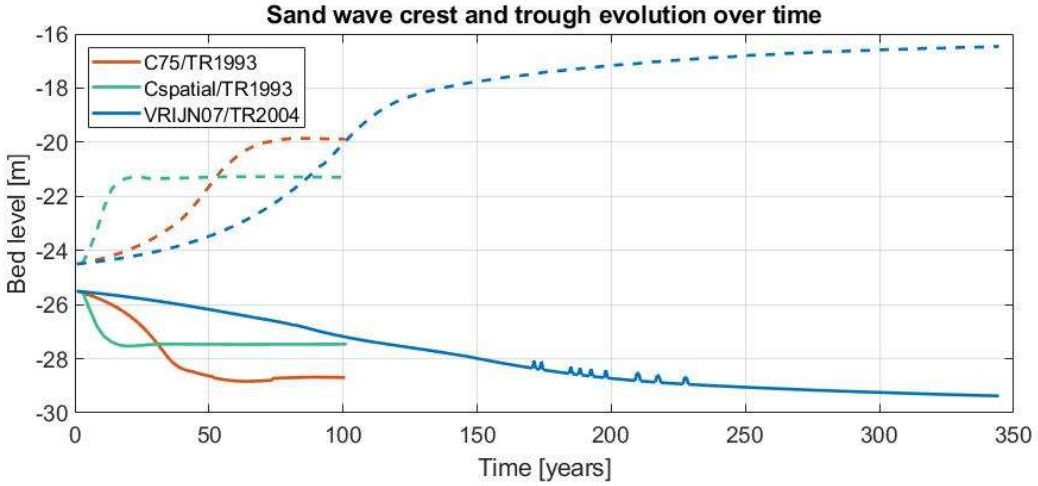

Figure 26. Sand wave crest (dashed line) and trough (solid line) development over time in years for C75/TR1993, Cspatial/TR1993 and VRIJN07/TR2004.

Figure 25 shows that a large difference in equilibrium height and morphological development rate exists between the three cases. The reference case C75/TR1993 grows towards a stable equilibrium

height of approximately 8.8 meters after approximately 80 years. The stable equilibrium sand wave height for Cspatial/TR1993 is significantly lower than the reference case and is 6.2 meters after approximately 30 years. The VRIJN07/TR2004 case has a much larger equilibrium sand wave height than the reference case and is approaching 13 meters. However, it seems that after approximately 350 years, VRIJN07/TR2004 has not yet reached its equilibrium position.

Figure 26 shows that the trough bed level of C75/TR1993 and VRIJN07/TR2004 are quite similar while the crest of VRIJN07/TR2004 grows significantly higher than C75/TR1993. This can be explained by the effect of slope-induced transport. Firstly, VRIJN07/TR2004 has a much larger wavelength than C75/TR1993 causing the slopes to be less steep. This means that C75/TR1993 will experience more slope-induced transport that counteracts the growth mechanism and reducing the potential sand wave height. Secondly, TR1993 emphasizes transport in the bedload regime significantly more than TR2004. Slope-induced transport is a component of the bedload regime, which means that TR1993 potentially also models higher slope-induced transport rates than TR2004. However, this may be partially counteracted by the higher suspended transport rates of TR2004 over TR1993 which also cause dampening of the sand wave.

The same behavior in the trough is observed for Cspatial/TR1993 and C75/TR1993. Sediment begins to accumulate once a certain bed level of the trough is reached and a sort of hump is created. This behavior is not visible in VRIJN07/TR2004 meaning that either the equilibrium position is not yet reached, or this difference is caused by the transport model. If it is caused by the transport model it could also be the result of more slope-induced transport for TR1993 due to larger bedload contributions. However, it seems more likely that the equilibrium position is not yet reached after 350 years for VRIJN07/TR2004.

Furthermore, the shape of the sand wave is also important to consider. The shape of the sand wave at different stages of the development is shown in figure 27. Herein, the x-axis is normalized due to the difference in wavelength and the time is normalized due to the difference in simulation times.

Figure 27 shows the rapid morphological development of Cspatial/TR1993 and reaching the stable equilibrium position within 15 years. Given the growth rate, it is quite difficult to compare the shape of the sand wave with the other combination at the same phases of the morphological development.

C75/TR1993 has a relatively lower crest height, but wider slopes up until t*=0.25. Furthermore, the trough erodes at a quicker rate that the growth of the crest between t*=0.15 and t*=0.25. Between t*=0.25 and t*=0.5, the slopes erode to their equilibrium depth while also showing a growth of approximately 2 meters for the crest. Between t*=0.5 and t*=1, the crest increases another 2 meters in height while decreasing the width of the sand wave. In this period, the trough remains unchanged as it has already reached the equilibrium position before.

Comparing VRIJN07/TR2004 to C75/TR1993, it shows a reversed pattern. The sand wave crest grows more rapidly while the slopes erode quicker up until t*=0.15. Between t*=0.15 and t*=0.25, the sand wave crest grows and the trough erodes at a relatively fast rate. From t*=0.25 and t*=0.5 the crest grows by approximately 3 meters while decreasing the width of the sand wave and eroding the trough until it has nearly reached an equilibrium bed level and is relatively stable up to t*=1. The growth rate of the sand wave slows down between t*=0.5 and t*=1 where the crest only increases about 1.5 meters in height and the sand wave seems to have become wider. Especially in the last phase the influence of the boundary conditions become apparent. We mentioned prior that the boundary conditions affect the sand waves due to the domain width and this shows in some migration of the sand wave towards the left boundary.

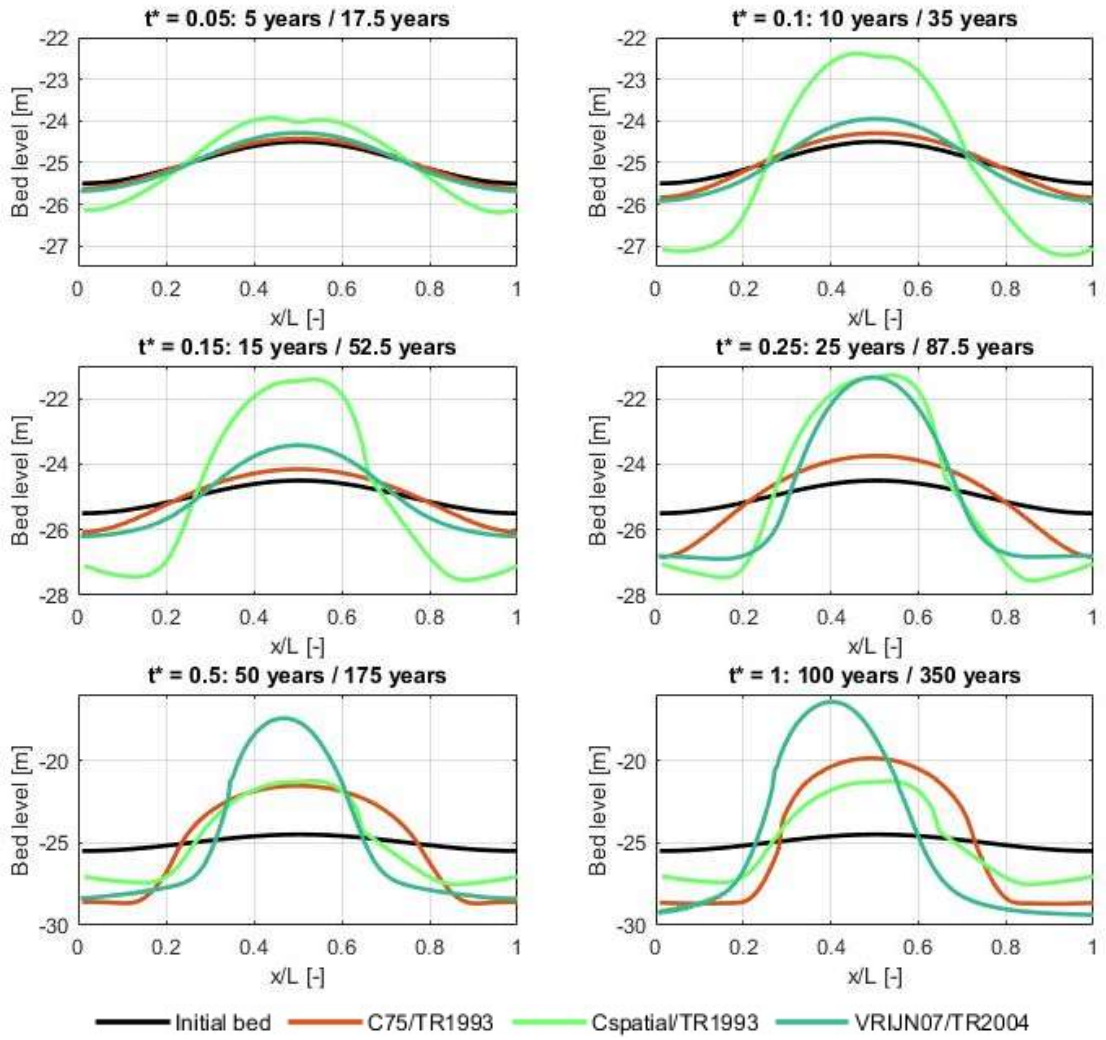

Figure 27. Sand wave shape development for a normalized x-axis for C75/TR1993, Cspatial/TR1993 and VRIJN07/TR2004 with t being the normalized time. Furthermore, the time passed in years corresponds to C75/TR1993 and Cspatial/TR1993 having an end time of 100 years and VRIJN07/TR2004 of 350 years respectively.*

The difference between C75/TR1993 and VRIJN07/TR2004 is caused by the strength of the circulation cells. The larger roughness for VRIJN07/TR2004 causes a larger difference in flow velocity of the sand wave leading to stronger circulation cells. This means that more sediment transport takes place from the slopes towards the crest leading to lower slopes but a higher crest. We previously observed that a steeper bed slope enhances the circulation cell strength, increasing the sediment transport towards the crest while the sand wave grows. Therefore VRIJN07/TR2004 starts growing more rapidly than C75/TR1993 beyond t*=0.15. At some sand wave steepness, the slope-induced transport will counter the sediment transport towards the crest leading to the decreased growth rates in later stages of the sand wave development. This is also the cause of the rapid growth of Cspatial/TR1993, the relatively large roughness causes much stronger circulation cells. The relatively short wavelength for this combination leads to a rapid increase in slope steepness and increase in slope-induced transport. This leads to a quick development towards the equilibrium stage, but also to a significantly lower sand wave equilibrium height.

4.4.5 Highlights

Here, the most important results are summarized from this part.

- Generally, the growth rate of the sand waves increase as the amplitude increases. This is because the wavelength remains similar throughout their development while the slope becomes steeper and thereby increasing circulation cell strength.
- The reference C75/TR1993 case matches with Van Gerwen et al. (2018). In the initial stages, the constant bed roughness and small spatial differences in flow velocity causes the growth and accretion rates to be balanced. The equilibrium sand wave height of 8.8 meters is reached after approximately 80 years.
- Cspatial/TR1993 grows very rapidly due to the intensity of circulation cells caused by the large roughness and short wavelength. The equilibrium sand wave height of 6.2 meters is reached in approximately 30 years. This decrease of equilibrium height compared to the reference case is caused by the roughness distribution as it causes the largest shear stresses at the crest throughout the entire tidal cycle. Therefore, the crest always erodes at a faster rate than the trough. Ultimately, this limits the equilibrium height of the sand wave.
- VRIJN07/TR2004 shows very slow growth rates and is unable to reach the equilibrium sand wave height after 350 years, it appears that it is approaching 13 meters. This slow growth rate is caused by a combination of long wavelengths, low intensity circulation cells, TR2004 being a more conservative transport model and a limitation of sediment transport during low tide. Decreasing flow velocities when approaching slack tide cause a decrease in bed roughness, this combination leads to insufficient bed shear stresses during slack tide to transport sediment. The long wavelength is likely also the cause of the large equilibrium height, as the sand wave decaying slope-induced transport rates are lower due to the mild slope in comparison to other combinations.

5 Discussion

In this work the influence of modelling spatiotemporal bed roughness is investigated on the effect of sand wave morphology. This chapter discusses the results that were found in §5.1, mainly focusing on the sand wave shape and the behavior observed of both roughness methods and transport models. §5.2 discusses the methods that were used to obtain the results and describes some major assumptions, limitations, and applicability of Van Rijn's 2007 bedform predictor and transport model. Finally, the relevance of this work is discussed.

5.1 Results

5.1.1 Influence initial topography

In this thesis we rely on the determination of the fastest growing mode (FGM) to define the initial wavelength as described in §3.2.2. It was found that there is substantial variation in FGM for the various bed roughness methods and transport models. This is mainly caused by the fact that larger bed roughness increases the difference of flow velocity over the sand wave, leading to stronger circulation cells. Consequently, the transport model is very influential on the translation of the hydrodynamics to a sand wave growth rate meaning that stronger circulation cells does not guarantee higher growth rates with shorter wavelengths. Sediment transport cannot directly influence the hydrodynamics as it is a result of sufficient hydrodynamic action. However, with the FGM simulations the sediment transport rates ultimately determine the growth rate and consequently the wavelength. After implementing the FGM as the initial topography, the steepness of the slope is very influential on the strength of the circulation cells. This means that the FGM causes an indirect influence of the sediment transport on the initial hydrodynamic response.

To eliminate the difference in wavelength between runs with the same transport model a fixed average wavelength was used. However, the FGM is only true for the simulation setup that it was determined for. This means that the initial response of the fixed wavelength system is to compensate and rearrange to the preferred wavelength. This compensation effect is especially noticeable when using Cspatial because it is difficult to define the bed roughness over the sand wave whilst the wavelength is unknown. Using the FGM of Chézy coefficient of 65 $m^{0.5}s^{-1}$ as a substitute means that the initial wavelength is not the preferred wavelength of Cspatial. Interpolating the bed roughness over every wavelength considered in the FGM simulation possibly solves this issue but could have implications on the outcome.

5.1.2 The spatiotemporal behavior of VRIJN07

The estimation of roughness height by VRIJN07 is mainly done by using the current-wave mobility parameter, which is based on the intensity of tidal currents and wave orbital motion. The determination of ripple roughness height is only dependent on the grain size and the current-wave mobility parameter as shown in equations 5 and 6. This means that any spatial variation in ripple roughness height is caused by flow velocity differences over the sand wave, or variability of grain size over the sand wave wherein the latter is not included in this work. For the 0.5- and 1.5-meter sand wave amplitudes that we consider, the flow velocity difference over the sand wave was too small to cause ripples to break down according to figure 7. Figure 7 also shows that the current-wave mobility parameter needs to reach a certain level before ripple roughness height starts to significantly decrease,

however, our tidal velocity amplitude was insufficient to reach this stage. Therefore, spatiotemporal variation in ripple roughness height estimated by VRIJN07 can be neglected.

This is especially the case when megaripples are present as their roughness height is significantly larger. Unlike ripples, the megaripple roughness height is also dependent on the water depth for the current-wave mobility parameter range in this work as shown in equation 9 and 10. Furthermore, megaripple roughness height increases as the hydrodynamic action increases as shown in figure 7. Due to the oscillatory tide, this means that significant temporal variation is estimated in megaripple roughness height by VRIJN07. A maximum roughness height is set at 0.2 meters which is attained for a significant period during the tidal cycle. The 0.5-meter amplitude sand wave did not provide significant spatial variation in the roughness heights, this is expected as this amplitude is still relatively small in comparison to the water depth. However, VRIJN07 still showed no significant spatial variation for the 1.5-meter amplitude case. This means that the maximum attainable roughness height for megaripples is used over the entire sand wave during most of the tidal cycle, which contrasts to field observations by Damveld et al. (2018). So, combining both the ripple and megaripple roughness height, this means that VRIJN07 is in fact only temporally variable while its spatial component is neglectable up to a 1.5-meter amplitude. Davies and Robins (2017) used VRIJN07 on a tidal channel and also found that spatial differences in roughness height were small in relation to using a more traditional fixed roughness height. However, more spatial variation likely occurs in later stages of morphological development, but whether it becomes significant is uncertain.

The fact that VRIJN07 can only be considered temporally variable is arguably not beneficial for long term simulations. Slower flow velocities and consequently bed shear stress and sediment transport occur naturally whilst the tide approaches slack tide. However, when bed roughness decreases as well, even less bed shear stress is generated causing the period wherein hydrodynamic action is sufficient to transport sediment to be shorter. Since VRIJN07 is mainly designed for fluvial environments, this would be less of an issue as all sediment is transported downstream. However, in an oscillatory tide this effectively means that the time required for the sand wave to reach an equilibrium position is increased significantly.

5.1.3 The difference in behavior of TR1993 and TR2004

Compared to TR1993, TR2004 has recalibrated a coefficient and exponent in the simplified formula for bedload transport in current only conditions. These recalibrated values increase the performance of bed-load transport prediction of flow velocities > 0.6 m/s with all computed values being within factor 2 of the measured values. However, the inaccuracies remain largest (underprediction compared to measurements) for relatively low velocities (< 0.5 m/s) close to initiation of motion (Van Rijn, 2007).

The TR2004-model results (total sand transport rates) are based on predicted bed roughness and suspended sediment size values, whereas the TR1993 model results are based on prescribed values for roughness height in the range of 0.02 to 0.1 m and suspended sediment size between 0.17 to 0.25 mm. Model results show that the TR2004 results are quite close to the TR1993 results when waves are enabled. However, the TR2004 model yields smaller transport rates for the current-alone case. This effect is caused by smaller bed roughness values when using the TR2004-model. The TR2004 results are in good agreement with the current-alone measured data points, whereas the TR1993-model seems to over predict the measured transport rates (Van Rijn and Walstra, 2004). So, Van Rijn's validation of both transport models concluded that TR1993 estimates larger sediment transport, which is also observed in this work. It is uncertain why TR1993 heavily emphasizes the bedload regime over the suspended load regime and such observations are not described by Van Rijn. The validation cases primarily consist of river based setups, meaning that coastal conditions with larger depths and lower flow velocities are not thoroughly analyzed.

Although TR2004 was used in combinations without the roughness predictor VRIJN07, it was initially unclear how fundamental VRIJN07 was in the sediment transport estimates. Consequently, by combining TR2004 with C75 and Cspatial, relations between VRIJN07 and TR2004 were not valid anymore and show behavior that cannot be physically explained occurs. For example, figure 37c in appendix D showed suspended sediment concentrations up to four times as large as any other combination. This while using TR2004 with defaults values (e.g. no scaling of transports) and settings (e.g. using the suspended sediment diameter predictor). Furthermore, a spike in suspended sediment transport and concentrations is estimated at the sand wave slope in figure 21. Physically, such a peak in transport rate cannot be explained logically and no further attention was given to it.

Furthermore, TR2004 showed some numerical artifacts in suspended transport. 'Wiggles' in the tide averaged suspended transport are estimated and are visible in the figure 16c,d, it is interesting that the wiggle amplitude increases when using VRIJN07 as opposed to C75. Some investigating was made whether the instantaneous flow velocities showed this behavior by plotting five neighboring grid cells, but no irregular behavior was found. Secondly, the most recent Delft3D version was used to check if this problem also occurred here, which it did. More interestingly however, the newer Delft3D version predicted completely different tide averaged suspended load transports as shown in figure 28. It is noteworthy that this was only the case for TR2004, TR1993 transports were identical.

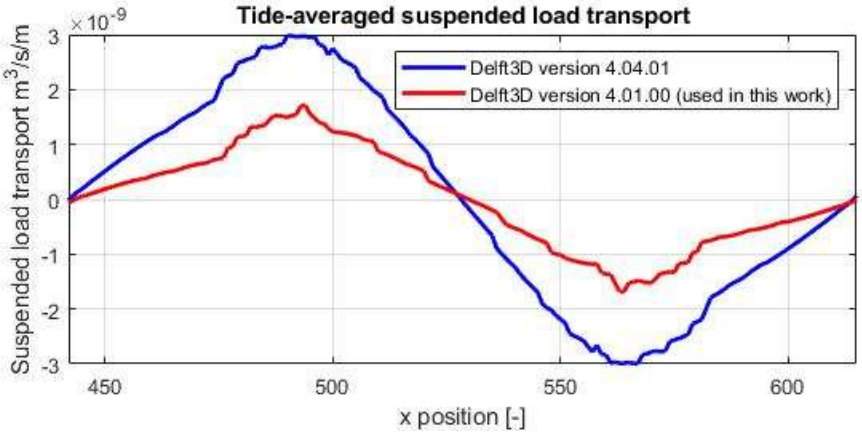

Figure 28. Comparison tide averaged suspended load transports for used Delft3D version in this work (4.01.00) and most recent one at the time of writing (4.04.01).

Furthermore, the long term simulation of VRIJN07/TR2004 in figure 24, 25 and 26 show a noise developing in the bed profile of the trough. It is unclear what causes this behavior but is assumed to be numerical as well. Finally, when running long term simulations, TR2004 provided more issues by crashing under large MORFAC values. Where TR1993 has no problems in completing a stable simulation for MORFAC values of 2000 as Van Gerwen et al. (2018) showed, VRIJN07/TR2004 only remained stable for a MORFAC of 500. The instability could be caused by the wiggles in suspended sediment transports or perhaps the noise in the bed profile becoming too large under high MORFAC values. Concluding, physically unexplainable behavior of TR2004, differences in transport rates between Delft3D versions and presumably numerical artifacts raises questions about using VRIJN07/TR2004.

5.1.4 Comparison of the equilibrium positions

In this work we found that the equilibrium position of the various roughness methods and transport models vary significantly. Generally, it was found that larger bed roughness causes faster growth rates but shorter wavelengths. Herein, TR1993 enhances the growth rates due to large bedload transports and TR2004 dampens the growth rates and increases the wavelength due to conservative modelling

of sediment transport rates. Shorter wavelengths then lead to lower equilibrium sand wave heights as the slope-induced transport increases, countering the growth mechanism. This causes TR1993 to reach its equilibrium position within 100 years of morphological development while TR2004 requires over 350 years. Despite simulating the VRIJN07/TR2004 combination for 5 days on an external computing facility, it has not reached a stable equilibrium yet. However, it appears to be approaching a sand wave height of 13 meters. This value is far greater than the C75/TR1993 and Cspatial/TR1993 combinations, with C75 being at a stable equilibrium of 8.8 meters and Cspatial of 6.2 meters.

When comparing these values to the work of Van Gerwen (2016), after which the model in this work was setup, the equilibrium height shows similar behavior in regards to sensitivity to bed roughness and initial wavelength. This sensitivity is shown in figure 29.

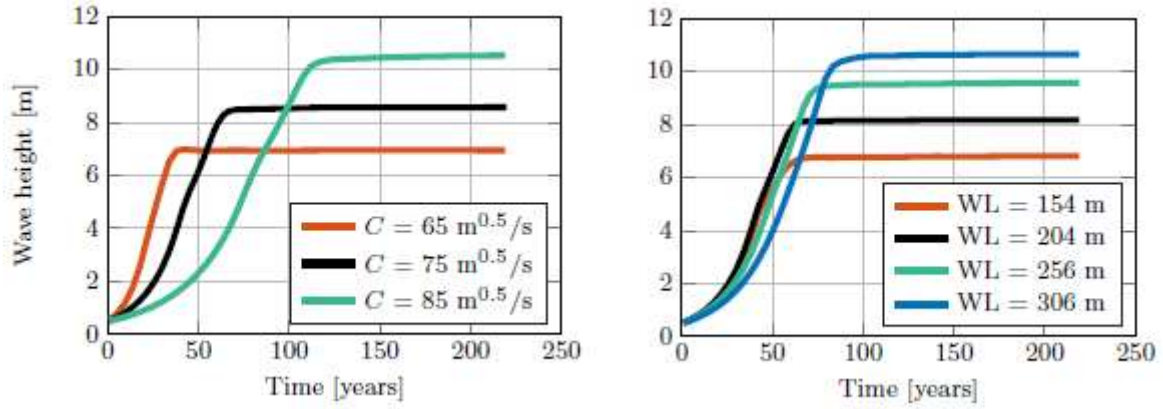

Figure 29. Sensitivity of the equilibrium roughness height to variation in the Chézy coefficient (left) and initial wavelength (right) (Van Gerwen, 2016).

Since the reference case C75/TR1993 uses the same setup as Van Gerwen (2016) the results are identical. VRIJN07/TR2004 has a larger magnitude bed roughness as the reference case which would decrease the equilibrium wave height. However, is also has an initial wavelength of 345 meters, meaning an equilibrium wave height larger than shown in figure 29. With an assumed equilibrium wave height around 13 meters, this implies that the sensitivity to initial wavelength is stronger than the bed roughness. Nevertheless, looking at figure 29 (right), an equilibrium wave height of 13 meters is in agreement with previous simulation results for an initial wavelength of 345 meters. The fact that it requires a significantly longer time to reach that position is the effect of the low transport rates of VRIJN07/TR2004 while constant Chézy coefficients and TR1993 is used by Van Gerwen (2016). The equilibrium position of Cspatial/TR1993 also matches with the behavior shown in 39, it has a spatially average Chézy coefficient of 65 $m^{0.5}s^{-1}$ and an initial wavelength of 146 meters. This means that it would be an almost perfect match for the line in orange in figure 29. In our work, the equilibrium height is significantly lower and is due to the fact that we have spatially varying bed roughness in Cspatial. This means that the crests are rougher and the troughs are smoother than the orange line, effectively causing more erosion at the crest and less erosion at the trough that leads to lower equilibrium wave heights.

The model is setup with parameters representative of North Sea conditions, so we will compare our simulation results with field observations of the North Sea. Terwindt (1971) found sand waves below a water depth of 17 meters and measured sand wave dimensions at 21 locations in the southern part of the North Sea. The average wave height was 6.8 meters, with values ranging from 2.9 - 9.1 meters. The average wavelength was 314 meters, with values ranging from 125 – 1250 meters. More recently, Damen et al. (2018) performed an analysis for sand wave characteristics of all sand waves of the Dutch Continental Shelf at a 25x25m resolution. A dataset of 1.5 million points containing sand wave heights

and length was used to analyze patterns in spatial variations of sand wave characteristics. It was found that sand waves occur only outside the coastal zone at water depths of more than 15 meters. Sand waves are highest in the southwestern area (>7 m) and decrease in height toward the north as well as in areas near the coast (to 1–2 m). Sand waves are longer at the northern edge of the main sand wave field and near the coast (500–1,000 m). Sand wavelengths in the south are between 200 and 300 meters.

The analysis of Damen et al. (2018) shows a relation between wave height and wavelength that is different to our simulation results. Longer sand waves correspond with lower wave heights while the area with the largest sand waves have relatively short wavelengths. In our case, the larger roughness causes shorter wavelength by increasing the circulation cell strength. Furthermore, spatial difference in the tidal current strength can also cause differences, wherein weaker tidal amplitudes cause larger wavelengths. We did not investigate the influence of tidal velocity amplitude and used an average value of the North Sea. Therefore, our results correspond to sand wave dimensions somewhere in the average sand wave dimensions found by Damen et al. (2018).

So, in comparison to our results, VRIJN07/TR2004 greatly increases the overestimation of the equilibrium height of sand waves under North Sea conditions (from 8.8 to approximately 13 meters), while the larger wavelengths are more comparable to field observations. Cspatial/TR1993 greatly increases the accuracy of the equilibrium height (from 8.8 meters to 6.2 meters), at the cost of underestimating the wavelength of sand waves.

5.2 Methods

5.2.1 Applicability of VRIJN07/TR2004 in a coastal environment

VRIJN07 is classified as a fluvial bedform predictor by Deltares (2014) capable of estimating ripple, megaripple and dune dimension. This means that VRIJN07, and particularly it's dune component, have primarily been developed for riverine conditions. However, in Van Rijn (2007) the combination of VRIJN07 and TR2004 does extend the prediction of bed-load transport to coastal flow. To verify the new bed-load transport rate equation of TR2004, 48 field data sets have been used for steady river flow while only two were used for tidal flow and one for coastal flow (Van Rijn, 2007). Nevertheless, the scheme has already been applied in a few large-scale coastal area models and appears to be robust (Davies and Robins, 2017; Herrling et al., 2017; Villaret et al., 2011; Wang et al., 2016) (Herrling et al., 2019).

Davies and Robins (2017) applied VRIJN07 on a tidal channel and considered that subtle spatial differences estimated by VRIJN07 could have the potential to alter long-term morphodynamic outcomes. Herrling et al. (2017) apply VRIJN07 on an estuary and found the results to be satisfactory in comparison to field observations, no further emphasis on the influence of VRIJN07 on these results was given though. Villaret et al. 2011 used VRIJN07 as a method of feedback for a friction coefficient which avoided inconsistencies between flow and sediment transport model. It proved to give physically realistic as well as stable numerical results for an estuarine environment. The bed friction predictor can therefore be viewed as a way to guide a time-consuming trial and error procedure, on physically sound basis. However, using VRIJN07 was found to produce slightly smaller tidal amplitudes than measurements which was likely caused by overestimation of friction due to neglecting waves. Wang et al. (2016) used VRIJN07 on a sandy tidal inlet system and found the bedform roughness height predictor to be a useful tool for determining spatial and temporal bed frictions. The model results were found to be consistent with the observations.

5.2.2 Limitations

One of the main limitations in coastal modelling is the scarcity of reliable datasets. This does not only affect the verification of predictors used such as VRIJN07 and transport models, but also the ability to calibrate the model to field observations. Examples in this work include the relaxation timescale of ripples T_r and megaripples T_{mr} and their coefficients for varying their contribution α_r and α_{mr} in equations 5 and 9 respectively. Although including relaxation effects of these small-scale bedforms did not affect the results significantly, the used relaxation time for megaripples is arguably arbitrary as there is no general agreement in literature on their relaxation timescale.

Furthermore, the ripple and megaripple coefficients can be altered to reduce the contribution of these bedforms in the estimated bed roughness. This work does not focus on a specific study site and both coefficients are therefore set to one. However, field data is required for site specific studies to calibrate the roughness predictor. This is because while most sand waves are covered in megaripples (Van Santen et al., 2011), their dimensions vary significantly. Van Dijk and Kleinhans (2005) observed megaripples heights up to 0.4 meters while even larger megaripples between 0.2 and 2 meters were observed by Terwindt (1971). VRIJN07 is unable to estimate these megaripple sizes due to its megaripple roughness height cap of 0.2 meters, it is also unable to estimate the absence of megaripples unless the hydrodynamic action is either near zero or very large (see figure 7). Since megaripple roughness is dominant in VRIJN07, reliable datasets or field observations are required to determine suitable coefficient values to not overestimate the bed roughness.

Finally, the scarcity of datasets prevents the quantitative comparison of our model results to field conditions as a dataset with both topography and small-scale bedform data is required. Effectively, this means that only the equilibrium sand wave height and wavelength can be compared qualitatively.

5.3 Relevance

It is known that the seabed is a complex dynamic region where bed roughness has a crucial effect in the near-bed hydrodynamics. However, generally these complex near-bed processes are avoided by parameterizing the bed roughness. Bed roughness then becomes some sort of calibration parameter which yields reasonable results compared to field observations when simulating sand waves.

We implemented Van Rijn's 2007 bedform predictor (VRIJN07) to model the dynamic complex near-bed processes in an attempt to increase the accuracy of simulation results compared to field observations. Although VRIJN07 has been extended for oscillatory flow, its foundation remains based on riverine environments. Limited studies exist where VRIJN07 is applied in a coastal environment, so its performance and effect on sand waves is not yet fully investigated. This makes this work relevant in the sense that we apply VRIJN07 in sand wave modelling, analyze its effect of the physics governing sand wave morphodynamics and see whether it improves accuracy compared to field observations. By implementing VRIJN07 and its corresponding TR2004, the relevance of this work is also practical. Since this combination is not frequently used in sand wave modelling, some limitations have been found of which future researchers are made aware and can thus be avoided.

We have dived deeper into the effects of spatiotemporal bed roughness on sand wave behavior and found how bed roughness has a significant effect on the preferred wavelength and inherently wave height of sand waves. Furthermore, bed roughness has a large effect of the bedload and suspended load transport ratio, effectively leading to changing growth rates of sand waves. Roughness can be used to obtain simulation results closer to field observations. However, more long term sensitivity research should be conducted in order to see if it matches more specific field conditions.

6 Conclusions

In this chapter, answering the sub-questions will give a conclusion to the main research question:

"What is the effect of modelling spatiotemporal variations of bed roughness in process-based morphodynamic models, on sand wave morphology, and how do the results compare to field observations?"

6.1 Initial response of a flat bed

"What is the initial response of hydro-morphodynamic processes on a flat bed using constant bed roughness, a roughness predictor and different sediment transport models, and how sensitive are the results to changing parameters?"

The Van Rijn 2007 predictor (VRIJN07) estimates dynamic behavior of megaripples, while ripples are nearly constant. The roughness height estimates are larger than the constant Chézy coefficient of 75 $m^{0.5}s^{-1}$ (C75) during the entire tidal cycle. VRIJN07 results in a velocity profile that is smaller in magnitude, but shear stresses that are larger than C75. Surprisingly, sediment transport rates appear to be smaller for VRIJN07 with bedload being the dominant transport mode. The sediment transport models differ greatly from each other as Van Rijn 1993 (TR1993) estimates significantly larger transport rates than the Van Rijn 2004 transport model (TR2004). Bedload transport is relatively insensitive to changes in grain size, while suspended load decreases for larger grain sizes. This changes the bedload-suspended load ratio, and it is known that suspended load has a dampening effect on sand waves. Using a relaxation time bedforms changes the roughness height but has no significant effect on sediment transport rates.

6.2 Initial response of low-amplitude wavy bed

"How does the bed roughness estimate of the roughness predictor vary, based on initial morphodynamic response over a low-amplitude wavy bed, and how do these spatial and temporal bed roughness variations affect hydrodynamics and morphodynamics?"

- **Spatiotemporal variation of roughness predictor**

The low-amplitude sand wave does not cause significant spatial variation in VRIJN07's bed roughness estimates which is mainly caused by a maximum attainable megaripple roughness height which is reached for both crest and trough. The low-amplitude sand wave does not change the temporal variation in bed roughness significantly. Effectively, this leads to a near-constant tide-averaged bed roughness for VRIJN07 that is rougher than C75.

- **Effect spatiotemporal bed roughness variation**

Flow over the sand wave causes circulation cells that are sensitive to the shape of the sand wave. Larger bed roughness increases the difference in flow velocity over the sand wave and averaged over the tide, leads to larger flow velocities towards the crest, i.e. stronger circulation cells. This leads to faster growth rates that correspond to shorter wavelengths. Since VRIJN07 estimates a rougher bed, it leads to shorter wavelengths, stronger circulation cells, larger bed shear stresses and therefore faster growth than C75.

- **Effect of the transport model**

The transport rates are heavily affected by the transport model, TR1993 estimates far greater transport rates than TR2004. Furthermore, the bedload regime is dominant for TR1993 while TR2004 shows a balanced bedload to suspended load ratio. Due to the bedload dominance in TR1993, this enhances growth rates for VRIJN07 due to the rougher bed. Due to the lower transport rates of TR2004 and large suspended load component, the growth rate of sand waves is decreased significantly as less sediment is transported towards the crest and suspended load transport is known to dampen sand wave growth.

6.3 Initial response of large-amplitude wavy bed

"How does the roughness predictor perform against field-observation based bed roughness as an initial morphodynamic response over a large-amplitude wavy bed, and how do these spatial and temporal variations affect the morphodynamics of sand waves?"

- **Differences in low- and large-amplitude case**

Increasing the sand wave amplitude to 1.5 meters shows little change in preferred wavelength, this causes the slope to be significantly steeper. C75/TR1993 shows a large increase in sand wave growth rate when increasing the sand wave amplitude, while the growth rate of VRIJN07/TR2004 remained equal to the 0.5-meters amplitude case. This is likely caused by TR2004 having a higher suspended load transport component and possibly accounting for more slope-induced transport, both decreasing sand wave growth rate. The larger sand wave amplitude increases the difference in current-wave mobility parameter between trough and crest slightly. However, the maximum attainable megaripple roughness height prevents this difference from translating to spatially varying bed roughness. Changes in spatiotemporal VRIJN07 roughness estimates from the 0.5-meter amplitude case are thus considered to be insignificant.

- **Comparison of uniform- and field-observation based bed roughness and a roughness predictor**

Forcing spatial variability with Cspatial causes lower flow velocities at the sand wave crest than at the trough due to linear interpolation of the Chézy coefficient. This effect increases the difference in flow velocity between the stoss and lee slope, leading to more intense circulation cells, bed shear stresses and transport rates for Cspatial. Generally, it is the tide-averaged bed shear stress that becomes larger rather than the maximum bed shear stress for larger amplitudes. So, similar magnitude bed shear stresses are generated for a longer duration of the tidal cycle, rather than stronger circulation cells leading to larger magnitude bed shear stresses. For sediment transport, this means that a larger quantity of sediment is transported during the tidal cycle instead of larger sediment fractions becoming mobile or traveling in another transport mode. Overall, the total transport rates are still towards the crest which implies sand wave growth. For Cspatial, large erosion rates are estimated at the crest that is caused by very high local bed roughness magnitudes leading to significantly larger bed shear stresses and sediment transport.

6.4 Long term equilibrium stage

"How does the roughness predictor perform against uniform and field-observation based bed roughness, in long term morphodynamic simulations, and what are the causes for any differences or similarities?"

Generally, the growth rate of the sand waves increase as the amplitude increases until an equilibrium with the slope-induced transport decaying mechanism is reached. This is because the wavelength remains similar throughout their development while the slope becomes steeper and thereby increasing circulation cell strength, while simultaneously increasing slope-induced transport.

- **Long term results with uniform bed roughness C75**

In the initial stages, the constant bed roughness and small spatial differences in flow velocity causes the growth and accretion rates to be balanced. In a later stage, the sheltering of the trough and smooth bed causes bed shear stresses to be insufficient to erode the trough. Slope-induced transport enhances the transport rate towards the trough, creating a local relatively flat bed. The equilibrium sand wave height of 8.8 meters is reached after approximately 80 years.

- **Long term results with field-observation based bed roughness Cspatial**

Cspatial/TR1993 grows very rapidly due to the intensity of circulation cells caused by the large roughness and short wavelength. The equilibrium sand wave height of 6.2 meters is reached in approximately 30 years. The relatively small equilibrium height is caused by the roughness distribution of Cspatial as the erosion rates of the crest are always larger than other parts of the sand wave. However, besides the smaller wavelength and faster growth rate for Cspatial/TR1993, the behavior of C75/TR1993 and Cspatial/TR1993 towards the equilibrium stage is similar.

- **Long term results with roughness predictor VRIJN07**

The growth rate of VRIJN07/TR2004 is very slow requires over 350 years to reach the equilibrium sand wave height which appears to be approaching 13 meters. This slow growth rate is caused by a combination of long wavelengths, low intensity circulation cells, TR2004 being a more conservative transport model and a limitation of sediment transport during low tide. The long wavelength also contributes to the large equilibrium height, as the sand wave decaying slope-induced transport rates are lower due to the mild slope in comparison to other combinations.

- **Effect spatiotemporal bed roughness variations on long term sand wave dynamics**

Since bed roughness affects the fastest growing mode significantly, it plays a large role in the definition of the initial topography. Larger magnitude bed roughness decreases the flow velocity over the sand wave, leading to larger differences between the stoss and lee slope. This gives rise to stronger circulation cells that increase the growth rate of sand waves. Herein, the temporal variability of bed roughness mainly causes slower growth rates, induced by shorter periods of sediment transport as slack tide approaches. Spatial variability of bed roughness mainly causes local variation in erosion rates, having a large effect on long term sand wave equilibrium dimensions.

Comparison of simulation results to North Sea sand wave characteristic data analysis shows that VRIJN07/TR2004 greatly increases the overestimation of the equilibrium height of sand waves, while the larger wavelengths are more comparable to field observations. Cspatial/TR1993 greatly increases the accuracy of the equilibrium height meters, at the cost of underestimating the wavelength of sand waves.

7 Recommendations

This chapter gives recommendations on the modelling of spatiotemporal variability in bed roughness and future research. These are based on the discussion and conclusions found in this work.

7.1 Modelling bed roughness

Although the VRIJN07 captures more near-bed processes to estimate a bed roughness that is arguably more physically correct, it shows a large deviation from observations made in the North Sea. Ultimately, the aim of this work was to investigate whether roughness predictors could improve the accuracy of simulation results in comparison to field conditions. Unfortunately, we have to conclude that VRIJN07 is unable to do so for North Sea conditions. Physically unexplainable behavior does not give confidence either. Furthermore, the practicality of modelling sand waves has to be considered as well. By itself low transport rates are not a bad sign. However, the combination of VRIJN07/TR2004 having low sediment transport rates and performing unstable simulations for large MORFAC values leads to very long simulation times (> 5 days) required to study the equilibrium stage. Therefore, we recommend to not use VRIJN07/TR2004 in North Sea conditions that were used in this work without further calibration. Furthermore, TR2004 should only be used in combination with VRIJN07.

C75/TR1993 has proven itself to give simulation results with reasonable agreement to field observations by parameterizing complex near-bed processes. Using a constant Chézy coefficient also eliminates complex and elaborate feedback mechanisms in Delft3D, reducing uncertainty in the simulation results. Therefore, modelling bed roughness with a constant Chézy coefficient is a solid method to study sand wave morphodynamics.

Cspatial/TR1993 was introduced to force spatial variation in bed roughness as this lacked in VRIJN07. Although the method is arguably artificial, it provided a significant improvement of modelling equilibrium sand wave heights under North Sea conditions. It is recommended to further explore this method of modelling bed roughness. Furthermore, both C75/TR1993 and Cspatial/TR1993 are recommended from a practical viewing point as they reach their equilibrium position well within 100 years of morphological development and remain stable for MORFAC values of 2000. Simulation results of the equilibrium position can be obtained within 4-5 hours. That being said, Cspatial does need some additional attention when tidal asymmetry is imposed. Migration of the sand wave and asymmetry of the sand wave shape require frequent updating of the Chézy coefficient interpolation in long term simulations. The sand wave shape causes asymmetric Chézy coefficient distribution which possibly has interesting hydro-morphodynamic behavior as the bed roughness increases rapidly on the much shorter lee slope.

7.2 Further research

The next step in the topic of spatiotemporal bed roughness modelling is to extend the model with an asymmetrical tide, wind-currents and -waves, grain sorting and the influence of bio-organisms. The extension of VRIJN07/TR2004 to be applicable in a coastal environment consisted of also modelling the effect of waves. Since we have disabled waves, a large component in the determination of bed roughness and sediment transport vanishes. VRIJN07/TR2004 has a relatively large suspended sediment contribution. This could cause this combination to favor sand wave migration, rather than

rapid growth as opposed to TR1993. The combination of residual currents and waves may therefore significantly improve the accuracy of VRIJN07/TR2004 in the predictor of sand wave development. Furthermore, grain sorting and bio-organisms both influence bed roughness directly and implementation possibly increases the simulation accuracy.

References

Amos, Carl & Kassem, Hachem & Friend, Patrick. (2019). Ripple Marks. 10.1007/978-3-319-48657-4_262-2.

Besio, Giovanni & Blondeaux, Paolo & FRISINA , P. . (2003). A note on tidally generated sand waves. Journal of Fluid Mechanics. 485. 171 - 190. 10.1017/S0022112003004415.

Besio, Giovanni & Blondeaux, Paolo & Brocchini, Maurizio & Vittori, Giovanna. (2004). On the modeling of sand wave migration. Journal of Geophysical Research C: Oceans. 109. C04018 1-13 . 10.1029/2002JC001622.

Besio, G., Blondeaux, P., Brocchini, M., Hulscher, S. J. M. H., Idier, D., Knaapen, M., Nemeth, A., Roos, P. C., & Vittori, G. (2008). The morphodynamics of tidal sand waves: A model overview. Coastal engineering, 55(7-8), 657-670. https://doi.org/10.1016/j.coastaleng.2007.11.004

Borsje, B.W. & de Vries, Mindert & Bouma, Tjeerd & Besio, Giovanni & Hulscher, Suzanne & Herman, Peter. (2009). Modeling bio-geomorphological influences for offshore sandwaves. Continental Shelf Research 2009. 29. 1289-1301. 10.1016/j.csr.2009.02.008.

Borsje, B. W. (2012). Biogeomorphology of coastal seas. How benthic organisms, hydrodynamics and sediment dynamic shape tidal sand waves. University of Twente. https://doi.org/10.3990/1.9789036534345

Borsje, B. W., Roos, P. C., Kranenburg, W., & Hulscher, S. J. M. H. (2013). Modeling tidal sand wave formation in a numerical shallow water model: the role of turbulence formulation. Continental shelf research, 60, 17-27. https://doi.org/10.1016/j.csr.2013.04.023

Borsje, B. W., Kranenburg, W. M., Roos, P. C., Matthieu, J., & Hulscher, S. J. M. H. (2014). The role of suspended load transport in the occurrence of tidal sand waves. Journal of geophysical research. Earth surface, 119(4), 701-716. https://doi.org/10.1002/2013JF002828

Brakenhoff, Laura & Schrijvershof, Reinier & van der Werf, Jebbe & Grasmeijer, Bart & Ruessink, Gerben & van der Vegt, Maarten. (2020). From Ripples to Large-Scale Sand Transport: The Effects of Bedform-Related Roughness on Hydrodynamics and Sediment Transport Patterns in Delft3D. Journal of Marine Science and Engineering. 8. 10.3390/jmse8110892.

Campmans, G. H. P., Roos, P. C., Schrijen, E. P. W. J., & Hulscher, S. J. M. H. (2018a). Modeling wave and wind climate effects on tidal sand wave dynamics: A North Sea case study. Estuarine, coastal and shelf science, 213, 137-147. https://doi.org/10.1016/j.ecss.2018.08.015

Campmans, G. H. P., Roos, P. C., de Vriend, H. J., & Hulscher, S. J. M. H. (2018b). The influence of storms on sand wave evolution: a nonlinear idealized modeling approach. Journal of geophysical research. Earth surface, 123(9), 2070-2086. https://doi.org/10.1029/2018JF004616

Cataño-Lopera, Y. A., & García, M. H. (2006). Geometry and migration characteristics of bedforms under waves and currents. Part 1: Sandwave morphodynamics. Coastal Engineering, 53(9), 767-780. https://doi.org/10.1016/j.coastaleng.2006.03.007

Cataño-Lopera, Y.A., & Garcia, M. (2006). Geometry and migration characteristics of bedforms under waves and currents: Part 2: Ripples superimposed on sandwaves. Coastal Engineering, 53, 781-792.

Chriss, T., & Caldwell, D. (1984). Turbulence spectra from the viscous sublayer and buffer layer at the ocean floor. Journal of Fluid Mechanics, 142, 39-55. doi:10.1017/S0022112084000987

Damen, J. M., van Dijk, T. A. G. P., & Hulscher, S. J. M. H. (2018). Spatially varying environmental properties controlling observed sand wave morphology. Journal of Geophysical Research: Earth Surface, 123, 262–280. https://doi.org/10.1002/2017JF004322

Damveld, J. H., Van Der Reijden, K. J., Cheng, C., Koop, L., Haaksma, L. R., Walsh, C. A. J., Soetaert, K., Borsje, B. W., Govers, L. L., Roos, P. C., Olff, H., & Hulscher, S. J. M. H. (2018). Video Transects Reveal That Tidal Sand Waves Affect the Spatial Distribution of Benthic Organisms and Sand Ripples. Geophysical research letters, 45(21), 11.837-11.846. https://doi.org/10.1029/2018GL079858

Damveld, Johan & Roos, Pieter & Borsje, B.W. & Hulscher, Suzanne. (2019). Modelling the two-way coupling of tidal sand waves and benthic organisms: a linear stability approach. Environmental Fluid Mechanics. 19. 1-31. 10.1007/s10652-019-09673-1.

Damveld, J. H., Borsje, B. W., Roos, P. C., & Hulscher, S. J. M. H. (2020). Horizontal and vertical sediment sorting in tidal sand waves: modeling the finite-amplitude stage. Journal of Geophysical Research: Earth Surface, 125(10), [e2019JF005430]. https://doi.org/10.1029/2019JF005430

Davies, A., Robins, P., 2017. Residual flow, bedforms and sediment transport in a tidal channel modelled with variable bed roughness. Geomorphology 295, 855–872.

Deltares (2014), User manual Delft3D FLOW, Deltares (www.deltares.nl), Delft, The Netherlands.

Dodd, Nicholas & Blondeaux, Paolo & Calvete Manrique, Daniel & Falqués, Albert & de Swart, Huib & Hulscher, Suzanne & Różyński, Grzegorz & Vittori, Giovanna. (2003). Understanding Coastal Morphodynamics Using Stability Methods. Journal of Coastal Research. 19.

Flemming, B. W. (2000). The role of grain size, water depth and flow velocity as scaling factors controlling the size of subaqueous dunes. In A. Trentesaux, & T. Garlan (Eds.), Proceedings of the Marine Sandwave Dynamics International Workshop (pp. 23– 24). France: University of Lille 1.

Fredsøe, J., and R. Deigaard (1992), Mechanics of coastal sediment transport, World Scientific.

Glenn, S. M., and Grant, W. D. (1987), A suspended sediment stratification correction for combined wave and current flows, J. Geophys. Res., 92(C8), 8244– 8264, doi:10.1029/JC092iC08p08244.

Grant WD, Madsen OS (1982) Moveable bed roughness in unsteady flow. J Geophys Res 87(C1):469–481

Grant, W. D., , and O. S. Madsen, 1986: The continental-shelf bottom boundary layer. Annu. Rev. Fluid Mech., 18 , 265–305.

Herrling, Gerald & Benninghoff, Markus & Zorndt, Anna & Winter, Christian. (2017). Drivers of channel-shoal morphodynamics at the Outer Weser estuary.

Herrling, Gerald & Becker, Marius & Krämer, Knut & Lefebvre, Alice & Winter, Christian. (2019). Parametrization of bedform induced hydraulic flow resistance in coastal-scale numerical models – an evaluation of Van Rijn's empirical bedform roughness predictors.

Houwman, K., & Rijn, L. (1999). Flow resistance in the coastal zone. Coastal Engineering, 38, 261-273.

Hulscher, S. J. M. H., & van den Brink, G. M. (2001). Comparison between predicted and observed sand waves and sand banks in the North Sea. Journal of geophysical research : Oceans, 106(C5), 9327-9338. https://doi.org/10.1029/2001JC900003

Hulscher, S. J. M. H. (1996), Tidal-induced large-scale regular bed form patterns in a three-dimensional shallow water model, J. Geophys. Res., 101(C9), 20727– 20744, doi:10.1029/96JC01662.

Idier, D., Astruc, D., & Hulscher, S. J. M. H. (2004). Influence of bed roughness on dune and megaripple generation. Geophysical research letters, 31(13), [L13214]. https://doi.org/10.1029/2004GL019969

Le Bot, Sophie & Alain, Trentesaux. (2004). Architecture of very large submarine dunes influenced by tide-and wind-generated processes (Dover Strait, northern France).

Lesser, G.R., Roelvink, J.A., van Kester, J.A.T.M., Stelling, G.S., 2004. Development and validation of a three-dimensional morphological model. Coastal Eng. 51, 883–915.

Li MZ, Amos CL (1998) Predicting ripple geometry and bed roughness under combined waves and currents in a continental shelf environment. Cont Shelf Res 18:941–970

McCave, I. N. (1971), Sand waves in the North Sea off the coast of Holland, Mar. Geol., 10, 199–225

Németh, A., Hulscher, S. J. M. H., & de Vriend, H. J. (2002). Modelling sand wave migration in shallow shelf seas. Continental shelf research, 22(18-19), 2795-2806. https://doi.org/10.1016/S0278-4343(02)00127-9

Nikuradse, J. 1933. "Tech. Rep. NACA Technical Memorandum 1292". In Stromungsgesetz in rauhren rohren, vDI Forschungshefte 361 (English translation: Laws of flow in rough pipes), Washington, DC, , USA: National Advisory Commission for Aeronautics. (1950)

Nittrouer, C. A., and Wright, L. D. (1994), Transport of particles across continental shelves, Rev. Geophys., 32(1), 85– 113, doi:10.1029/93RG02603.

Rijksoverheid (2015). Beleidsnota Noordzee 2016-2021.

Rijksoverheid (2019). Klimaatakkoord.

Roos, P. C. (2019). On the crest of sandwave modelling: Achievements from the past, directions for the future. . 197-202. Abstract from MARID VI, Marine and River Dune Dynamics 2019, Bremen, Germany. https://www.marum.de/Binaries/Binary18538/MARIDVI-Roos-Pieter-KEYNOTE.pdf

Salon, Stefano & Crise, Alessandro. (2008). Chapter 6 Dynamics of the Bottom Boundary Layer. Developments in Sedimentology. 60. 10.1016/S0070-4571(08)10006-1.

Smith, J. D., and McLean, S. R. (1977), Spatially averaged flow over a wavy surface, J. Geophys. Res., 82(12), 1735– 1746, doi:10.1029/JC082i012p01735.

Soulsby, R.L., and Whitehouse, R., 2005. Prediction of ripple properties in shelf seas. HR Wallingford, Internal Report, Report TR 154, pp. 99.

Soulsby, R.L., 1983. The bottom boundary layer of shelf seas. Physical Oceanography of coastal and Shelf seas. B. Johns. Amsterdam, Elsevier: 189-266.

Terwindt, J.H.J., 1971. Sand waves in the Southern Bight of the North Sea. Mar. Geol. 10, 51–67.

Tonnon, P.K. & Rijn, L.C. & Walstra, Dirk-Jan. (2006). The morphodynamic modelling of tidal sand waves on the shoreface. Coastal Engineering. 54. 279-296. 10.1016/j.coastaleng.2006.08.005.

Toodesh, Reenu and Verhagen, Sandra. "Adaptive, variable resolution grids for bathymetric applications using a quadtree approach" Journal of Applied Geodesy, vol. 12, no. 4, 2018, pp. 311-322. https://doi.org/10.1515/jag-2017-0043

Van Rijn, L.C. & Walstra, D.J.R., 2004 Description of TRANSPOR2004 and implementation in Delft3D-ONLINE: interim report. Deltares (WL)

Veen, Hennie & Hulscher, Suzanne & Knaapen, Michiel. (2006). Grain size dependency in the occurrence of sand waves. Ocean Dynamics. 56. 228-234. 10.1007/s10236-005-0049-7.

Van Dijk, T. A. G. P., and Kleinhans, M. G. (2005), Processes controlling the dynamics of compound sand waves in the North Sea, Netherlands, J. Geophys. Res., 110, F04S10, doi:10.1029/2004JF000173.

Van Gerwen, W. (2016). Modelling the equilibrium height of offshore sand waves (MSc Thesis, University of Twente, Enschede, The Netherlands). Retrieved from https://www.utwente.nl/en/et/wem/education/msc-thesis/2016/gerwen.pdf

Van Gerwen, W., Borsje, B. W., Damveld, J. H., & Hulscher, S. J. M. H. (2018). Modelling the effect of suspended load transport and tidal asymmetry on the equilibrium tidal sand wave height [Journal Article]. Coastal Engineering, 136, 56-64. doi: 10.1016/j.coastaleng.2018.01.006

Van Rijn, L.C. (1984). Sediment Transport, Part III: Bed forms and alluvial roughness. Journal of Hydraulic Engineering, ASCE, Vol. 110, No. 12, p. 1733-1755.

Van Rijn, L. C. (1993). Principles of sediment transport in rivers, estuaries and coastal seas (Vol. 1006, pp. 11-3). Amsterdam: Aqua publications.

Van Rijn, L. C. (2007). Principles of sediment transport in rivers, estuaries, and coastal seas (Update/supplement), Aqua, Blokzijl, The Netherlands, www.aquapublications.nl

Van Santen, R. B., de Swart, H. E., & van Dijk, T. A. G. P. (2011). Sensitivity of tidal sand wavelength to environmental parameters: a combined data analysis and modelling approach. Continental shelf research, 31(9), 966-978. https://doi.org/10.1016/j.csr.2011.03.003

Villaret, C. and Huybrechts, N. and Davies, A.G. (2012) A large scale morphodynamic process-based model of the Gironde estuary. In: NCK-days 2012 : Crossing borders in coastal research., 13 March 2012 - 16 March 2012, Enschede, the Netherlands.

Wang, Yunwei & Yu, Qian & Jiao, Jian & Tonnon, Pieter & Wang, Zheng Bing & Gao, Shu. (2016). Coupling bedform roughness and sediment grain-size sorting in modelling of tidal inlet incision. Marine Geology. 381. 10.1016/j.margeo.2016.09.004.

Wright, J., Colling, A., Park, D., & Open University. (1999). Waves, tides, and shallow-water processes. Oxford: Butterworth-Heinemann, in association with the Open University.

Appendix

A. Effect of a wavy bed on the bed roughness

Figure 30 shows that the current-wave mobility parameter range increases for increasing sand wave amplitudes. This is because the topography shelters the troughs while the crest remains exposed, leading to lower flow velocities in the trough and consequently variation in current-wave mobility parameter.

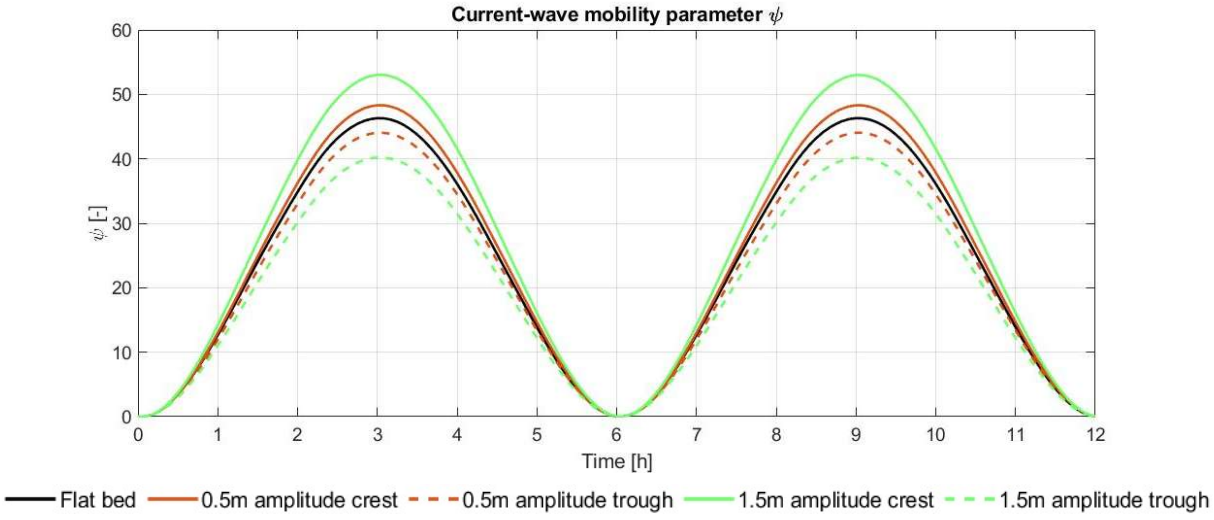

Figure 30. Variability current-wave mobility parameter ψ by Van Rijn 2007 bedform predictor over tidal cycle for the sand wave crest and trough for various topographies.

Although there is variation in the current-wave mobility parameter, figure 31 shows that this is not translated to the roughness height. This is due to the megaripple roughness height limitation at 0.2m, that is reached for both crest and through during high tide. So, when the variability in current-wave mobility parameter is largest, this mechanism leads to the disappearance of any significant spatial variation in roughness height.

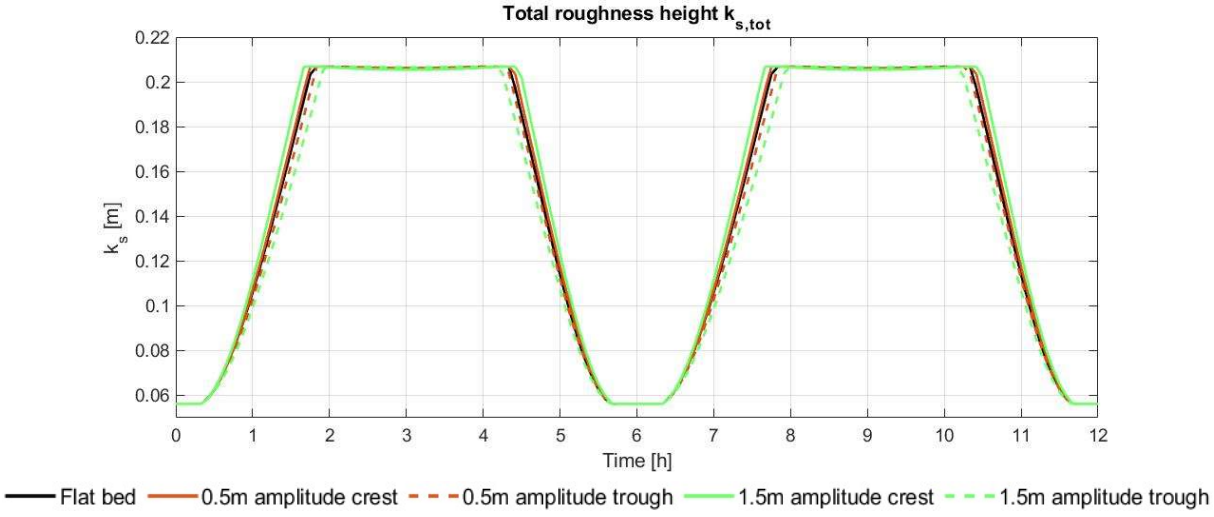

Figure 31. Variability current-wave mobility parameter ψ by Van Rijn 2007 bedform predictor over tidal cycle for the sand wave crest and trough for various topographies.

B. Effect of relaxation time on bed roughness

Including relaxation time on the bedform height estimates implies that there is a delay in the morphological development. When using no relaxation, this means that bedforms dimensions instantaneously develop to the equilibrium form under the present hydrodynamic conditions. Six hour relaxation time means that it takes six hours to completely adjust to the equilibrium form based on the present hydrodynamic conditions. However, since the hydrodynamic conditions vary, the equilibrium roughness height (no relaxation runs) is not reached for the six hour megaripple relaxation runs. This leads to lower maximum, but higher minimum megaripple roughness heights during the tidal cycle as shown in figure 32.

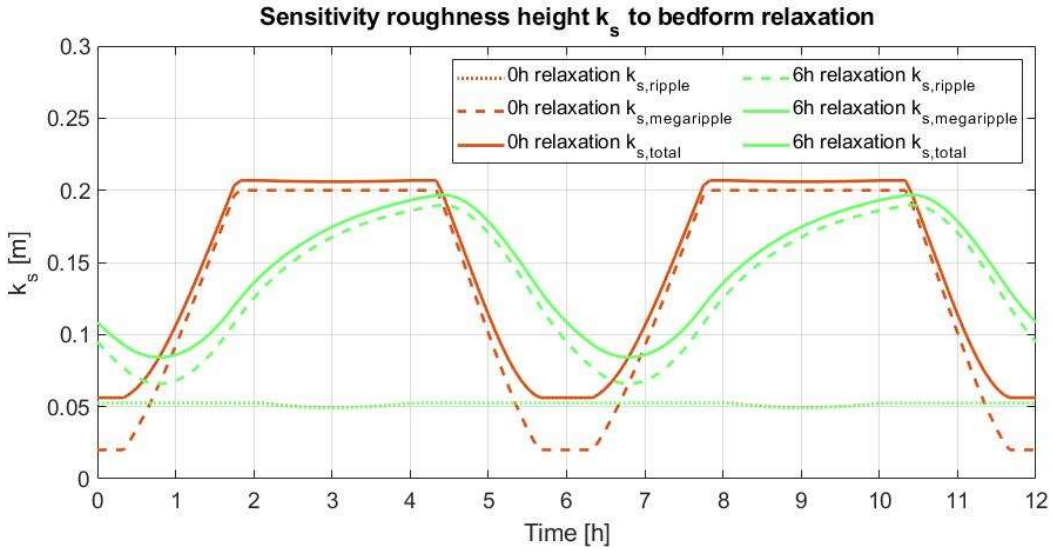

Figure 32. Sensitivity of the roughness height to relaxation time for VRIJN07 over tidal cycle. With continuous lines the total roughness height, dashed line the contribution of megaripples and dotted line the contribution of ripples.

Although there is significant difference in megaripple roughness height in both runs over the tidal cycle, differences in sediment transports are minimal. This is because the high tides are smoother while the slack tides are rougher for the run that includes relaxation. On average, the roughness height for both the run with and without relaxation are similar. Tide averaged, there is only a 1% difference in sediment transports during the high tides, when the difference is largest, for runs with the same sediment transport model. This difference is negligible when comparing the differences in sediment transport rates of using different transport models. Hence, relaxation times of both ripples and megaripples are kept at 0 minutes in this work.

C. Sensitivity to grain size

As equations 5-10 show, grain size plays a large role in estimating the roughness height by VRIJN07. Therefore, grain sizes of 0. 3mm and 0.4mm have been used to complement the default 0.35mm grain size. For a flat bed, averaging sediment transport values over time would result in zero transports due to symmetrical currents. Therefore, the total transport rate during one half of the tidal cycle is used and the total transport in one direction is used to compare the transport rates of the various runs in figure 33.

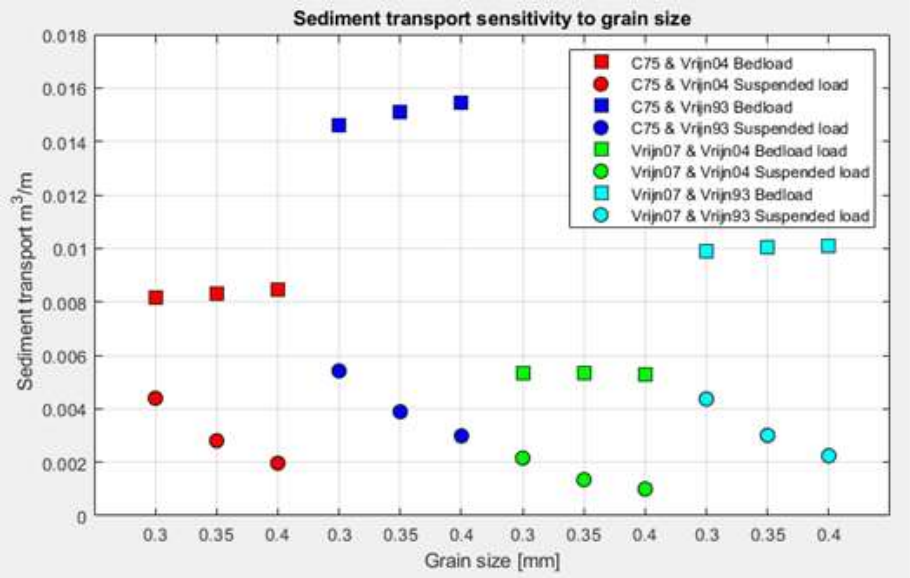

Figure 33. Sensitivity of the sediment transport rate in the bedload and suspended load regime to grain size during half a tidal cycle for C75 and VRIJN07 combined with TR1993 and TR2004.

Most of the sensitivity in the transport rates is composed of the suspended load regime with larger grain sizes leading to less suspended load transport. This is due to the relation of particle surface area to volume. The gravitational forces pulling the particles down increase to the power three as the volume and thus weight increase with a cubic relation. The forces keeping the particle suspended work on the surface area of the sediment particle, which increases to the power two as the particle becomes larger and increases the area with a square relation. The forces responsible for suspension will therefore rapidly be exceeded by the gravitational forces which will lead to settlement of the suspended particles.

For a wavy bed additional simulations have been performed with grain sizes of 0.3mm and 0.4mm as a comparison to the default 0.35mm grain size. Using various grain sizes inherently comes with different FGM's, as table 8 and figure 12 suggest, coarser grains lead to shorter wavelengths. By increasing the grain size, consequently the bed shear stress is also increased trough the increase in slope steepness. So, this leads to an increase in both bed shear stress as critical bed shear stress, which partly counteracts the effect of the increased grain size on sediment transport rates. With this in mind, we first look at figure 34 which shows the results for C75 and VRIJN07 combined with TR1993.

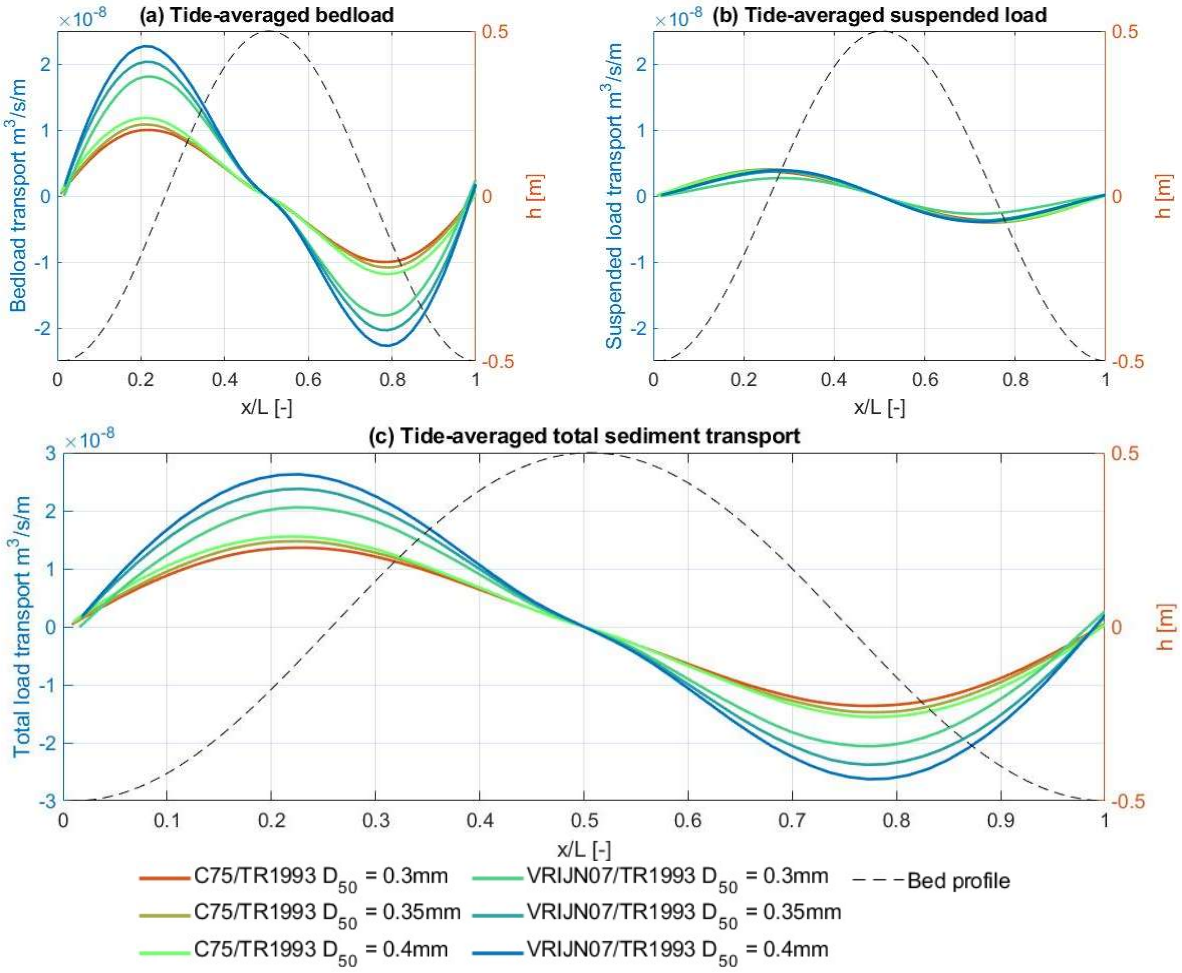

Figure 34. Tide-averaged bedload (a), suspended load (b) and total transport (c) for C75 and VRIJN07 combined with TR1993 for grain sizes 0.3, 0.35 and 0.4mm. Positive values imply transport to the right and negative values to the left.

It was already observed that TR1993 favors transport in the bedload regime which figure 34 reinforces. VRIJN07 estimates higher roughness and thus bed shear stresses than C75. This means that the bedload transport rate is larger due to the threshold of motion of more particle sizes being exceeded. However, since it appears that the bedload transport rate increases for larger grain sizes, this leads to believe that the increase in bed shear stress due to shorter wavelengths and more intense circulation cells exceeds the increase in critical shear stress. Overall, TR1993 estimates larger sediment transport rates than TR2004 which are shown in figure 35.

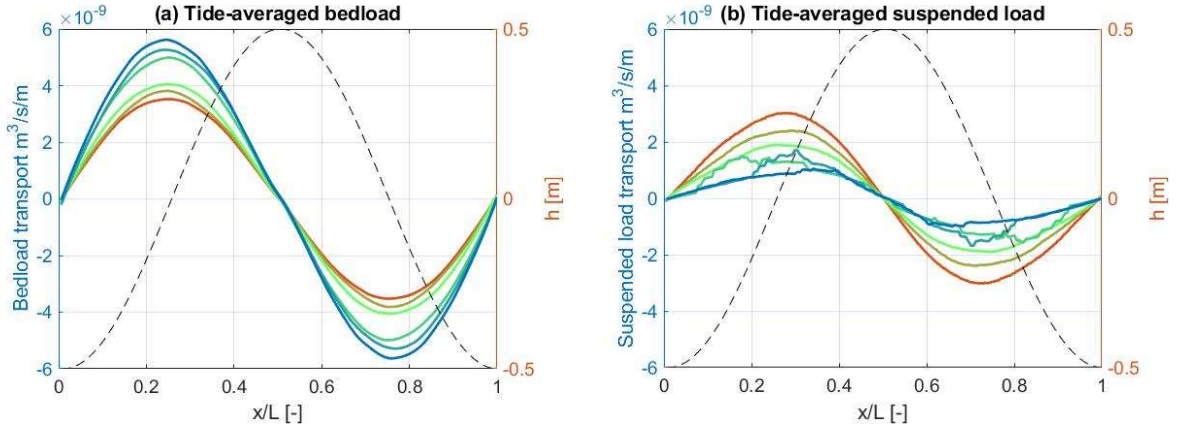

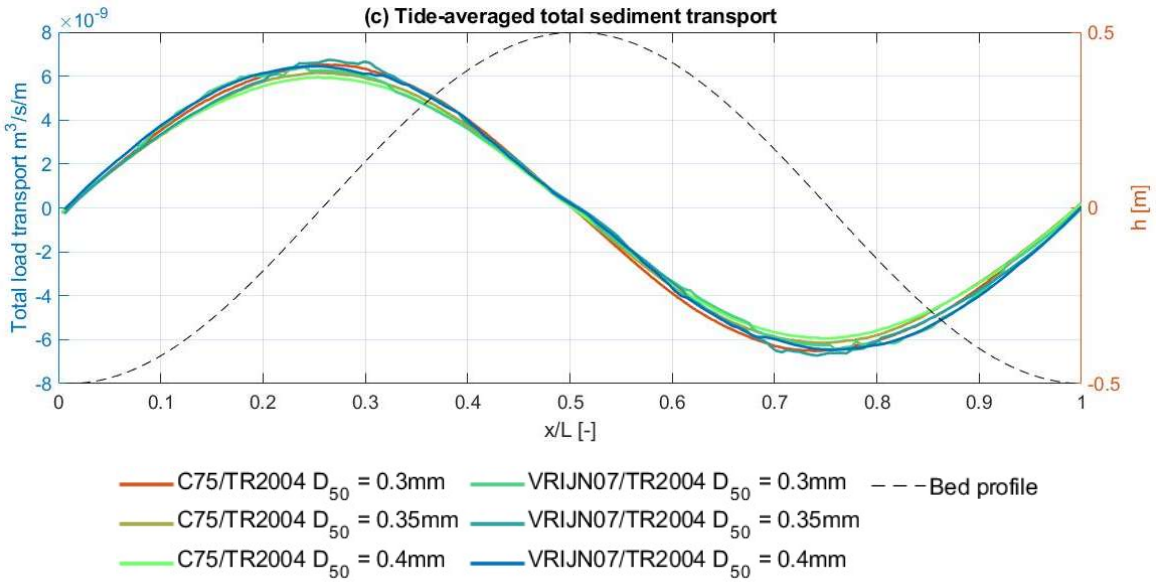

Figure 35. Tide-averaged bedload (a), suspended load (b) and total transport (c) for C75 and VRIJN07 combined with TR2004 for grain sizes 0.3, 0.35 and 0.4mm. Positive values imply transport to the right and negative values to the left.

Figure 35 shows that the same trend of TR1993 is observable for TR2004, the coarser the grains and rougher bed, the more bedload transport. However, the opposite pattern is visible for the suspended load transport where finer grains and a smoother bed leads to more suspended load transport. With these trends, the total sediment transport is roughly equal for all combinations.

D. Suspended sediment concentration profiles

Figure 36 shows the suspended concentration profile for a flat bed during high tide.

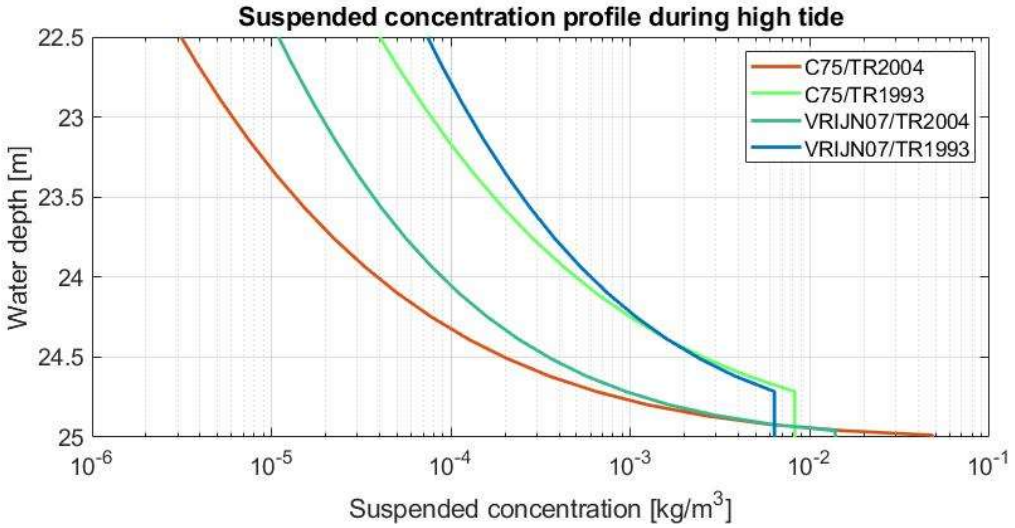

Figure 36. Suspended sediment concentrations for C75 and VRIJN07 combined with TR1993 and TR2004 during high tide.

Figure *36* shows that the sediment transport model has a larger influence on the suspended sediment concentration profile than the roughness formulations. The suspended sediment concentration for C75 appears to decrease more rapidly with increasing distance from the bed than the results of VRIJN07. This can be explained by turbulence, the mechanism that counteracts fall velocities of the suspended particles, keeping them suspended longer. The smooth bed with C75 generates little turbulence. The rough bed estimated by VRIJN07 generates more turbulence and sustains the suspended sediment particles in the water column instead of settling. Furthermore, the suspended sediment concentration profile becomes vertical at some point above the bed. This is caused by the way Van Rijn made the sediment transport models. A reference level at some distance above the bed marks the equilibrium suspended sediment concentration. Below this reference level, sediment is transported in the bedload regime while it is transported in the suspended load regime above it. TR2004 has changed the reference height calculation, effectively making it thinner. This is also clearly visible in figure *37*, where the suspended concentrations are shown for a 0.5m amplitude wavy bed.

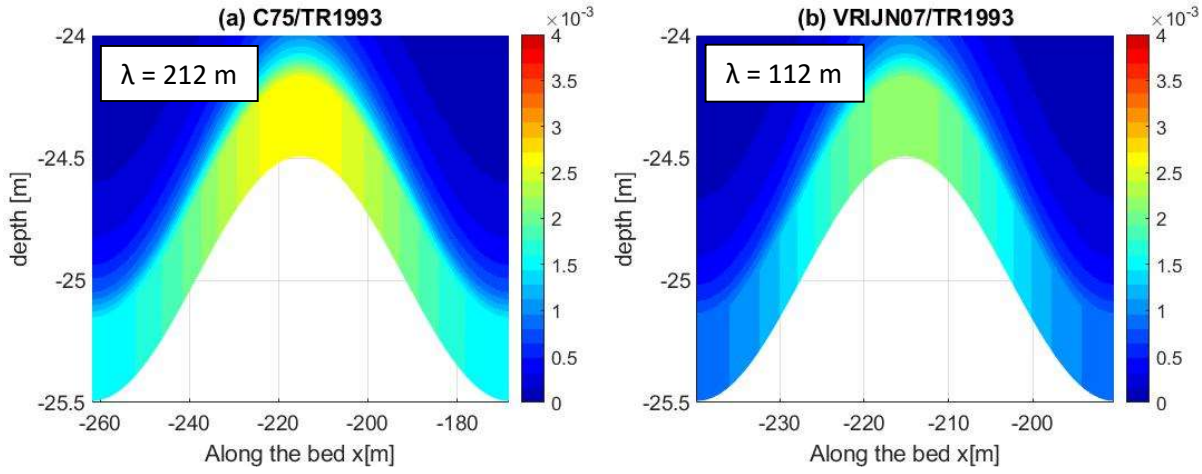

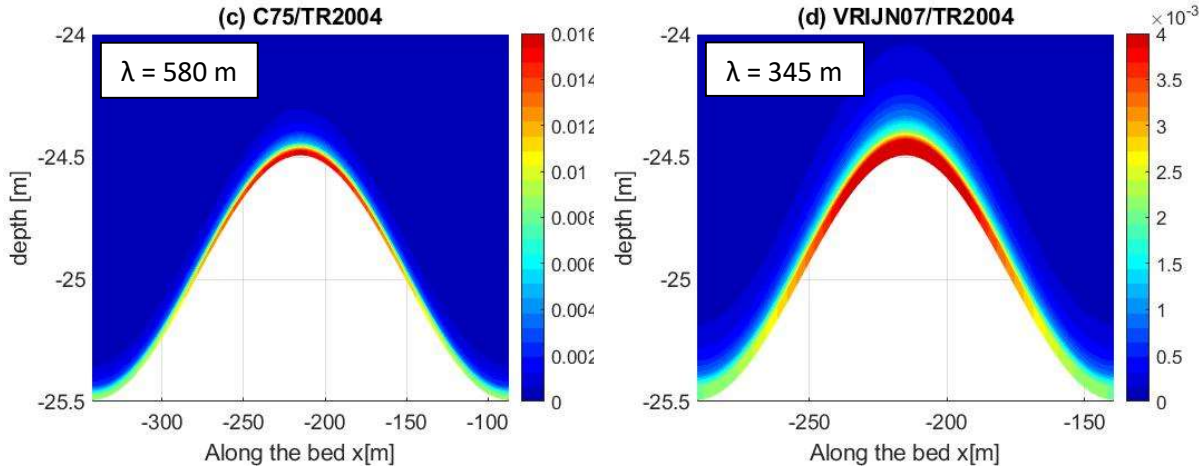

Figure 37. Tide-averaged suspended concentration [kg/m³] for C75 (a,c) and VRIJN07 (b,d) combined with TR1993 (a,b) and TR2004 (c,d). Note the difference in magnitude of the C75/TR2004 plot.

Figure 37 also shows a gradient in suspended concentration near the sand wave crest. This is because turbulence is generated here that counteracts the fall velocity of the suspended particles and keeps the particles suspended. Furthermore, it is noteworthy that fixing the wavelengths does not have any significant effect on the tide-averaged suspended concentration compared to using the FGM wavelength. This is caused by the fact that the turbulence is more governed by the bed roughness magnitude than the wavelength. Since the fall velocity of the sediment particles is equal for all runs as they are setup with the same grain size, the suspended concentrations are unaffected.

Also, for the 1.5m amplitude case, the suspended concentrations of C75/TR1993 and VRIJN07/TR2004 shows qualitative similar behavior as the low amplitude case and are only larger in magnitude due to the increased sand wave height. Cspatial/TR1993 shows the same quantitative behaviour as C75/TR1993 but has a more triangular shape near the crest as the bed roughness increases linearly instead of being constant.

E. Fixed wavelength for 1.5m amplitude case

The wavelength is also fixed for the 1.5m amplitude case to eliminate the effect of different topographies. The resulting tide-averaged circulation cells are shown in figure 38, elaboration of the limited effect on the hydrodynamics is already provided in §4.3.3 and will not be repeated here. The corresponding tide-averaged sediment transport rates in figure 39.

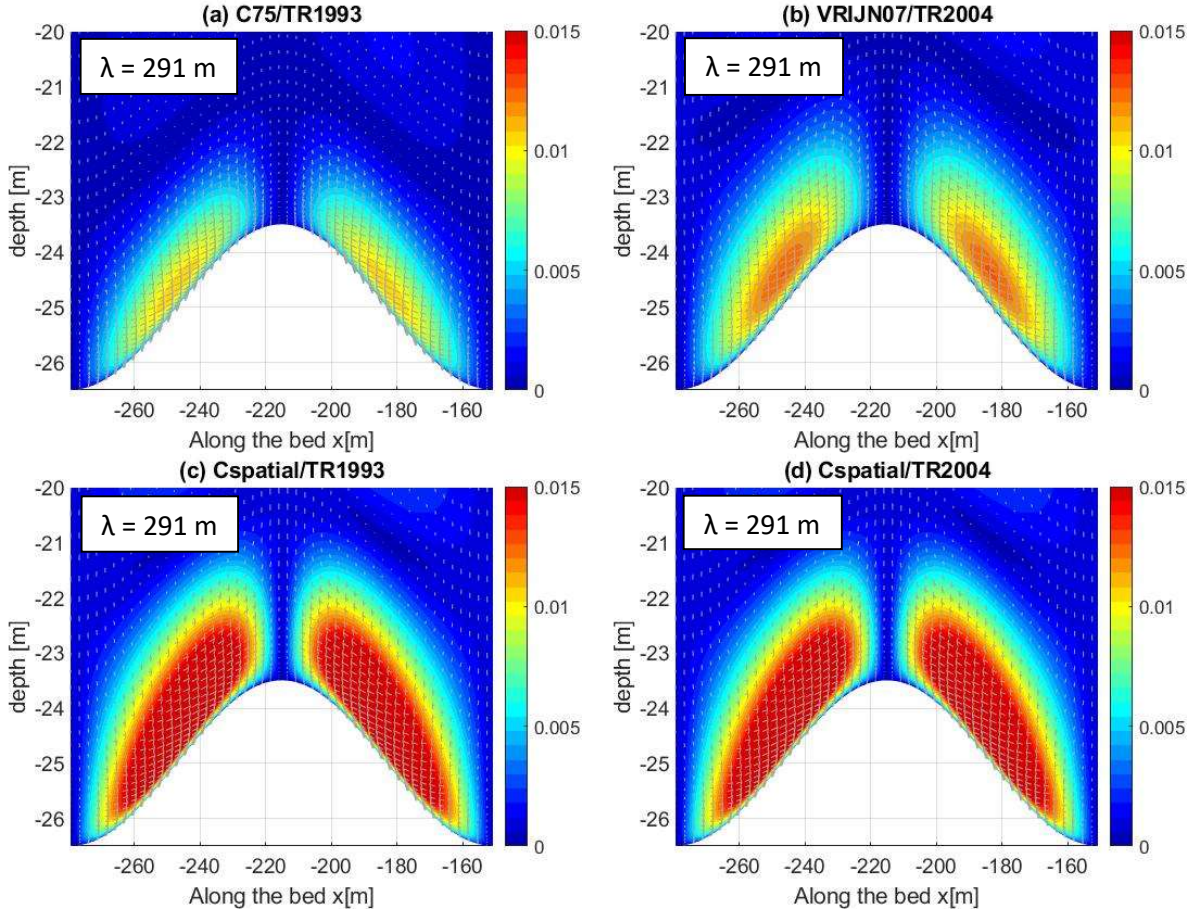

Figure 38. Tide-averaged flow velocity magnitude and circulation for C75/TR1993 (a), VRIJN07/TR2004 (b) and Cspatial combined with TR1993 (c) and TR2004 (d) for large amplitude sand wave with a fixed wavelength of 291 meters. Note that the flow velocity on the right part of the sand wave represents negative flow velocities and convergence towards the crest occurs.

Cspatial/TR1993 is the only combination where the circulation cell is significantly affected when fixing the wavelength. So, to see how this combination responds, the transport rates with a fixed wavelength of 291m is shown in figure 39. Comparing figure 39 to figure 21 shows that both the bedload and suspended load decrease. It changes from rapid crest decay somewhat indecisiveness on the crest, generally the sediment will convergence towards the crest causing sand wave growth. This means that instead of decreasing the crest to adjust the wavelength, it wants to grow the sand wave height. This implies that the fixed wavelength is closer to the preferred wavelength of Cspatial/TR1993 than C65/TR1993.

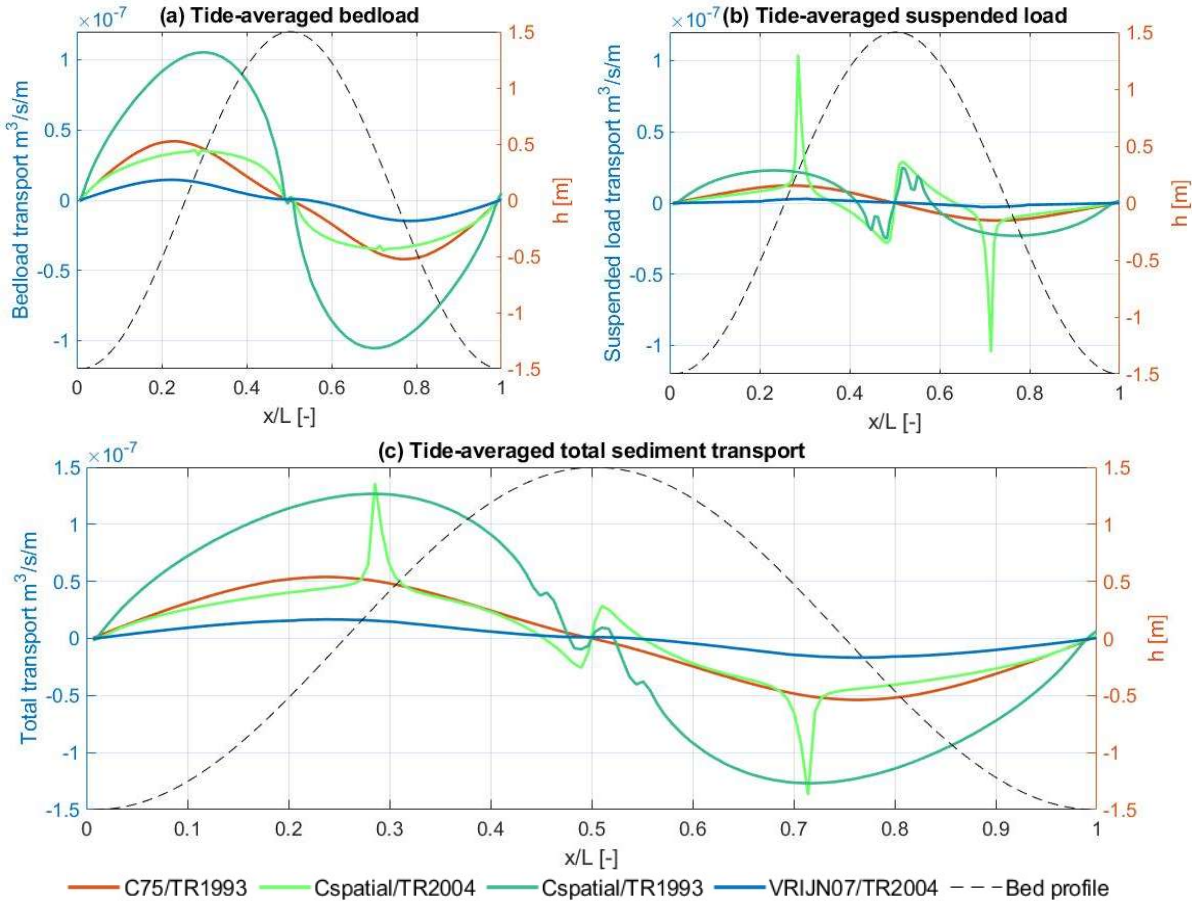

Figure 39. Tide-averaged bedload (a), suspended load (b) and total transport (c) for C75/TR1993, VRIJN07/TR2004 and Cspatial combined with TR1993 and TR2004 for large amplitude sand wave with a fixed wavelength of 291 meters. Positive values imply transport to the right and negative values to the left.